TECHNISCHE UNIVERSITÄT WIEN
Vienna University of Technology

D I P L O M A R B E I T

Calculation of Spin-Spiral States from First Principles

ausgeführt am Institut für
Angewandte Physik E134
der Technischen Universität Wien

unter der Anleitung von
Ao. Univ. Prof. Dipl.-Ing. Dr. techn. Peter Mohn

durch

Stefan Danner
0525717
Urlweg 12, A-3362 Mauer

Wien, am 10.02.2012

Kurzfassung

Diese Diplomarbeit beschäftigt sich mit der Untersuchung von Spin Spiral Strukturen im Rahmen der Dichtefunktionaltheorie unter Verwendung des *Vienna Ab-initio Simulation Package*, VASP.
Das Ziel dieser Arbeit ist es zu zeigen, dass Spin Spiral Rechnungen, die bisher von der VASP Gruppe nicht offiziell dokumentiert sind, zu konsistenten Resultaten führen.
In dieser Arbeit werden die theoretischen Konzepte, auf denen Spin Spiral Rechnungen basieren, zusammengefasst. Darüber hinaus wird gezeigt wie derartige Spin Spiral Rechnungen aufgesetzt werden müssen. Ein Softwarepaket, das künftigen Anwendern von derartigen Rechnungen als Unterstützung dienen soll, wurde entwickelt.
Es werden Beispiele für Spin Spiral Rechnungen in verschiedenen Materialien, wie bcc Fe, fcc Fe, hcp Co, MnO und FM $LaMnO_3$ in verschiedene Kristallrichtungen vorgestellt.
Die Ergebnisse dieser Rechnungen werden zur Bestimmung der entsprechenden magnetischen Strukturen herangezogen. Zusätzlich wird gezeigt wie kritische Temperaturen und experimentell nachweisbare Spinwellen-Steifigkeitskonstanten von diesen Rechnungen abgeleitet werden können.

Abstract

This thesis deals with the investigation of spin spiral structures in the context of density functional theory using the *Vienna Ab-Initio Simulation Package*, VASP.
The aim is to show that spin spiral calculations, which are not documented officially by the VASP group up to now, lead to consistent results.
The thesis summarizes the theoretical concepts spin spiral calculations are based on. Moreover it is shown how spin spiral calculations have to be set up. A software package that should support future users of these kind of calculations has been developed.
Examples for spin spiral calculations in different materials, i.e. bcc Fe, fcc Fe, hcp Co, MnO and FM $LaMnO_3$, into different crystallographic directions are given.
The results of these calculations are used to determine the respective magnetic structures. In addition it is shown how critical temperatures and experimentally verifiable spin wave stiffness constants can be derived from these calculations.

Contents

1 Motivation

When talking about magnetic materials one usually thinks of collinearily ordered systems. Basic courses on solid state physics deal with collinear ferro- and antiferromagnetic materials as well as ferrimagnetism. In this context antiferomagnetic systems are treated as two separate sublattices with opposite magnetic order, which lead to a vanishing average magnetic moment of the respective material. Nevertheless many alloys, compounds, and even elements show non-collinear magnetic order. This thesis is going to deal with a special class of non-collinear magnetic ordering which is known as spin spiral ordering. In such a magnetic structure the magnetic moments rotate periodically about a global quantization axis. The magnetic moments can thus be characterized by spherical coordinates using their modulus and two angles φ and θ. In bcc Eu a so called flat spin spiral, $\theta = \frac{\pi}{2}$, has been verified [1], see figure 1.1,

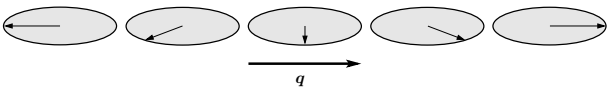

Figure 1.1: Flat spin spiral.

while in $LaMn_2Ge_2$ a conical spin spiral, $0 < \theta < \frac{\pi}{2}$, has been found [2].

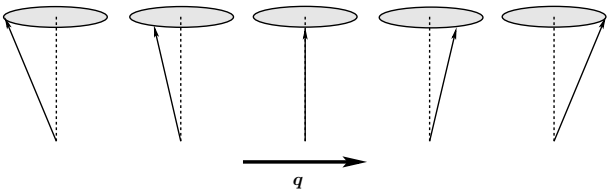

Figure 1.2: Conical spin spiral.

It has been shown that in the multiferroic material $Eu_{0.75}Y_{0.25}MnO_3$ ferroelectricity, which is a synonym for large electric polarizability, is caused by a spin spiral state [3]. As a consequence the vector of polarization $\boldsymbol{P}$ is proportional to the spin spiral wave vector $\boldsymbol{q}$ in this case. This is illustrated in figure 1.3.
The ab-initio treatment of spin spirals is of interest because they offer an insight to the magnonspectra of materials. If the dispersion gained this way is mapped onto a Heisenberg model the material's exchange constants J as well as its critical temperature T_C can be estimated.
Spin spiral calculations have been implemented in the *Vienna Ab-initio Simulation*

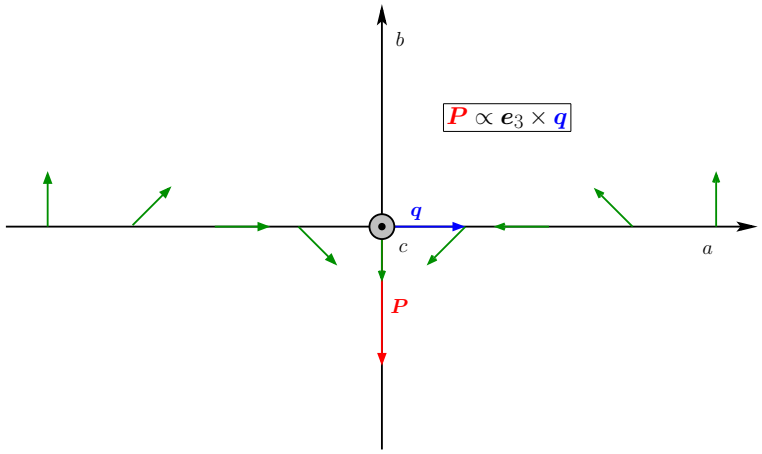

Figure 1.3: Large electric polarizability in $Eu_{0.75}Y_{0.25}MnO_3$.

Package VASP, which is used by the CMS group for theoretical investigations of material properties, in 2002 [4].

As mentioned above, spin spiral states may be important in the description of multiferroic properties, which are of the CMS group's field of interest. The aim of this work is to learn as much as possible about how such calculations have to be set up and to formulate the conditions where these calculations can be applied.

During the course of my work at the Center for Computational Materials Science a vast amount of tests has been performed for different compounds and elements. In order to keep things clear this thesis contains only some of the respective results.

The first few chapters provide the theoretical basis of electronic structure calculations within density functional theory. The following chapters will give an introduction to the treatment of non-collinear magnetic structures and spin spirals. Subsequent to these chapters the Heisenberg model and its mean field approximation are discussed. After this theoretical part an introduction to spin spiral calculations using VASP is given. The last part of the thesis is a discussion of spin spiral calculations for different materials such as bcc Fe, hcp Co, MnO and ferromagnetic $LaMnO_3$.

2 Electronic Structure

The aim of this chapter is to motivate some basics of solid state theory such as the Bloch theorem, the reciprocal lattice and the Brillouin zone. The derivations given below follow Ref. [5].

2.1 Bloch Functions

This summary of basic elements of solid state physics starts with a crystal of some symmetry and a single electron moving in it. The potential in which the electron moves shall be an effective potential, so that it is not necessary to care about any interaction terms besides the effective potential $V(\boldsymbol{r})$.
The electron's motion is then defined by the single particle Schrödinger equation

$$\left[-\frac{\hbar^2}{2m_e}\triangle + V(\boldsymbol{r})\right]\psi_i(\boldsymbol{r}) = \varepsilon_i\psi_i(\boldsymbol{r}) \ , \tag{2.1}$$

where $\psi_i(\boldsymbol{r})$ is the electron's wave function, ε_i is the respective energy-eigenvalue and

$$\mathbf{H} = -\frac{\hbar^2}{2m_e}\triangle + V(\boldsymbol{r}) \tag{2.2}$$

is the Hamiltonian of the system.
Due to the fact that the effective potential $V(\boldsymbol{r})$ is of equivalent symmetry to the crystal lattice, which is spanned by the Bravais lattice vectors $\boldsymbol{a_1}$, $\boldsymbol{a_2}$, and $\boldsymbol{a_3}$, the potential is periodic with a lattice vector $\boldsymbol{R_j}$,

$$V(\boldsymbol{r} + \boldsymbol{R}_j) = V(\boldsymbol{r}) \ , \tag{2.3}$$

where

$$\boldsymbol{R}_j = n_{1j}\boldsymbol{a_1} + n_{2j}\boldsymbol{a_2} + n_{3j}\boldsymbol{a_3} \ . \tag{2.4}$$

It is possible to define an operator $\mathbf{T}_j$ acting as

$$\mathbf{T}_j \ (f(\boldsymbol{r})) = f(\boldsymbol{r} + \boldsymbol{R}_j) \ , \tag{2.5}$$

which performs translations through the lattice. It can be shown that the operators $\mathbf{T}_j$ form a group and commute with each other

$$[\,\mathbf{T}_j, \mathbf{T}_i\,] = 0\ . \tag{2.6}$$

Due to the potential's periodicity $\mathbf{T}_j$ moreover commmutes with the Hamiltonian (2.2)

$$[\,\mathbf{T}_j, \mathbf{H}\,] = 0\ . \tag{2.7}$$

As a consequence energy eigenstates stay unchanged for any translation. The eigenvalue problem belonging to the translation operator $\mathbf{T}_j$ can therefore be written as

$$\mathbf{T}_j\,\psi_i(\boldsymbol{r}) = \psi_i(\boldsymbol{r} + \boldsymbol{R}_j) = \lambda_j \psi_i(\boldsymbol{r})\ , \tag{2.8}$$

where $\psi_i(\boldsymbol{r})$ is still an eigenfunction of the Hamiltonian (2.2) and λ_j describes the effect of the operator $\mathbf{T}_j$ on the function ψ_i. Due to the fact that the norm of ψ_i must remain unchanged for any translation $\mathbf{T}_j$, the eigenvalue λ_j must be a complex number of modulus unity. It can be written as

$$\lambda_j = \mathrm{e}^{\mathrm{i}\,\theta_j}\ , \tag{2.9}$$

θ_j being real.
Applying two translation operators successively to the Hamiltonian's eigenfunction ψ_i yields

$$\mathbf{T}_j\mathbf{T}_i\,\psi_i(\boldsymbol{r}) = \psi_i(\boldsymbol{r} + \boldsymbol{R}_i + \boldsymbol{R}_j) = \lambda_i\lambda_j\,\psi_i(\boldsymbol{r}) = \lambda_{i+j}\,\psi_i(\boldsymbol{r})\ , \tag{2.10}$$

with

$$\lambda_{i+j} = \mathrm{e}^{\mathrm{i}\,\theta_{i+j}} = \mathrm{e}^{\mathrm{i}\,(\theta_i+\theta_j)}\ . \tag{2.11}$$

The relation $\theta_{i+j} = \theta_i + \theta_j$ is satisfied if

$$\theta_i = \boldsymbol{k}\cdot\boldsymbol{R_i}\ , \tag{2.12}$$

where $\boldsymbol{k}$ is an arbitrary vector which is equivalent for each operation. This vector characterizes the particular wavefunction ψ_i and is thus part of its index i. Allowing for other quantum numbers, n, besides $\boldsymbol{k}$ the wavefunction $\psi_i(\boldsymbol{r})$ may be written as

$\psi_{n\boldsymbol{k}}(\boldsymbol{r})$ and the original single particle Schrödinger equation (2.1) reads

$$\left[-\frac{\hbar^2}{2m_e}\triangle + V(\boldsymbol{r})\right]\psi_{n\boldsymbol{k}}(\boldsymbol{r}) = \varepsilon_{n\boldsymbol{k}}\psi_{n\boldsymbol{k}}\left(\boldsymbol{r}\right) . \tag{2.13}$$

The wavefunction $\psi_{n\boldsymbol{k}}$ is called *Bloch function* because it satisfies

$$\psi_{n\boldsymbol{k}}(\boldsymbol{r}+\boldsymbol{R}_j) = \mathrm{e}^{\mathrm{i}\,\boldsymbol{k}\boldsymbol{R}_j}\psi_{n\boldsymbol{k}}(\boldsymbol{r}) , \tag{2.14}$$

which is known as *Bloch's theorem*. This theorem states that in a periodic potential the eigenstates ψ_i of the single particle Hamiltonian (2.2) can be written as a product of a plane wave and a function showing the potential's periodicity

$$\boxed{\psi_{n\boldsymbol{k}}(\boldsymbol{r}) = \mathrm{e}^{\mathrm{i}\,\boldsymbol{k}\boldsymbol{r}}u_{n\boldsymbol{k}}(\boldsymbol{r}) ,} \tag{2.15}$$

where

$$u_{n\boldsymbol{k}}(\boldsymbol{r}+\boldsymbol{R}_j) = u_{n\boldsymbol{k}}(\boldsymbol{r}) . \tag{2.16}$$

If equations (2.15) and (2.16) are combined Bloch's theorem in its version above, equation (2.14), can be found.
The vector $\boldsymbol{k}$ has the dimension of an inverse length and is of great importance in order to characterize the Bloch function. Due to its dimension $\boldsymbol{k}$ is a vector in *reciprocal space* and it is referred to a wave vector. In the periodic potential the Bloch function's wave vector $\boldsymbol{k}$ plays the role of the free electron's wave vector in the Sommerfeld model. But in contrast to Sommerfeld's description of solids the quantity $\hbar\boldsymbol{k}$ does not represent the Bloch wave's momentum. This is due to

$$\mathbf{p}\,\psi_{n\boldsymbol{k}}(\boldsymbol{r}) = \frac{\hbar}{\mathrm{i}}\nabla\psi_{n\boldsymbol{k}}(\boldsymbol{r}) = \frac{\hbar}{\mathrm{i}}\nabla\left[\mathrm{e}^{\mathrm{i}\,\boldsymbol{k}\boldsymbol{r}}u_{n\boldsymbol{k}}(\boldsymbol{r})\right] = \hbar\boldsymbol{k}\,\psi_{n\boldsymbol{k}}(\boldsymbol{r}) + \mathrm{e}^{\mathrm{i}\,\boldsymbol{k}\boldsymbol{r}}\,\nabla u_{n\boldsymbol{k}}(\boldsymbol{r}) , \tag{2.17}$$

showing that $\psi_{n\boldsymbol{k}}$ in general is not an eigenfuction of the momentum operator $\mathbf{p}$.
It can be proven that in a periodic potential the Bloch wave $\psi_{n\boldsymbol{k}}$ moves without any dissipation of energy with a well defined speed. As a result the electric resistivity of a crystal with perfect symmetry is zero [6].
Usually the solution of theoretical solid state physics problems is based on periodic boundary conditions, also known as Born-von Kàrmàn boundary conditions, for the Bloch function

$$\psi_{n\boldsymbol{k}}(\boldsymbol{r}+N_1\boldsymbol{a_1}) = \psi_{n\boldsymbol{k}}(\boldsymbol{r}) = \psi_{n\boldsymbol{k}}(\boldsymbol{r}+N_2\boldsymbol{a_2}) = \psi_{n\boldsymbol{k}}(\boldsymbol{r}+N_3\boldsymbol{a_3}). \tag{2.18}$$

2.2 The Reciprocal Lattice and Brillouin Zone

It has already been mentioned that the Bloch function's wave vector $\boldsymbol{k}$ is a vector in reciprocal space. This space is defined by

$$\boldsymbol{K}_s \cdot \boldsymbol{R}_j = 2\pi\, n_{sj} \ , \tag{2.19}$$

where n_{sj} is an integer. All vectors $\boldsymbol{K}_s$ build the *reciprocal lattice*. Any vector $\boldsymbol{K}_s$ of the reciprocal lattice can be written as a linear combination of the reciprocal lattice's basis vectors

$$\boldsymbol{K}_s = m_{s1}\boldsymbol{b_1} + m_{s2}\boldsymbol{b_2} + m_{s3}\boldsymbol{b_3} \ . \tag{2.20}$$

Due to the definition of the reciprocal space in equation (2.20) the basis vectors $\boldsymbol{b_1}$, $\boldsymbol{b_2}$ and $\boldsymbol{b_3}$ are given as

$$\boldsymbol{b_1} = 2\pi\frac{\boldsymbol{a_2}\times\boldsymbol{a_3}}{\boldsymbol{a_1}\cdot(\boldsymbol{a_2}\times\boldsymbol{a_3})},\ \boldsymbol{b_2} = 2\pi\frac{\boldsymbol{a_3}\times\boldsymbol{a_1}}{\boldsymbol{a_1}\cdot(\boldsymbol{a_2}\times\boldsymbol{a_3})},\ \boldsymbol{b_3} = 2\pi\frac{\boldsymbol{a_1}\times\boldsymbol{a_2}}{\boldsymbol{a_1}\cdot(\boldsymbol{a_2}\times\boldsymbol{a_3})} \ . \tag{2.21}$$

It is now shown how these definitions influence the Bloch function $\psi_{n\boldsymbol{k}}$. Therefore two wave vectors $\boldsymbol{k}$ and $\boldsymbol{k'}$, which differ by a reciprocal lattice vector $\boldsymbol{K}_s$

$$\boldsymbol{k'} = \boldsymbol{k} + \boldsymbol{K}_s \tag{2.22}$$

are considered. Applying Bloch's theorem (2.14) to a Bloch function $\psi_{n\boldsymbol{k'}}$ leads to

$$\psi_{n\boldsymbol{k'}}(\boldsymbol{r}+\boldsymbol{R}_j) = \mathrm{e}^{\mathrm{i}\,(\boldsymbol{k}+\boldsymbol{K}_s)\boldsymbol{R}_j}\psi_{n\boldsymbol{k'}}(\boldsymbol{r}) \ , \tag{2.23}$$

which due to equation (2.19) simplifies to

$$\psi_{n\boldsymbol{k'}}(\boldsymbol{r}+\boldsymbol{R}_j) = \mathrm{e}^{\mathrm{i}\boldsymbol{k}\boldsymbol{R}_j}\psi_{n\boldsymbol{k'}}(\boldsymbol{r}) \ . \tag{2.24}$$

Comparing equations (2.14) and (2.24), $\psi_{n\boldsymbol{k}}$ and $\psi_{n\boldsymbol{k'}}$ show the same eigenvalue λ_j under translations $\mathbf{T}_j$. Consequently the wave vectors $\boldsymbol{k}$ and $\boldsymbol{k'} = \boldsymbol{k} + \boldsymbol{K}_s$ are said to be equivalent which leads to the convention

$$\psi_{n\boldsymbol{k}}(\boldsymbol{r}) = \psi_{n\boldsymbol{k}+\boldsymbol{K}_s}(\boldsymbol{r}) \tag{2.25}$$

for any $\boldsymbol{K}_s$. For the Schrödinger equation (2.13) this equivalence implies that

$$\varepsilon_{n\boldsymbol{k}} = \varepsilon_{n\boldsymbol{k}+\boldsymbol{K}_s} \ . \tag{2.26}$$

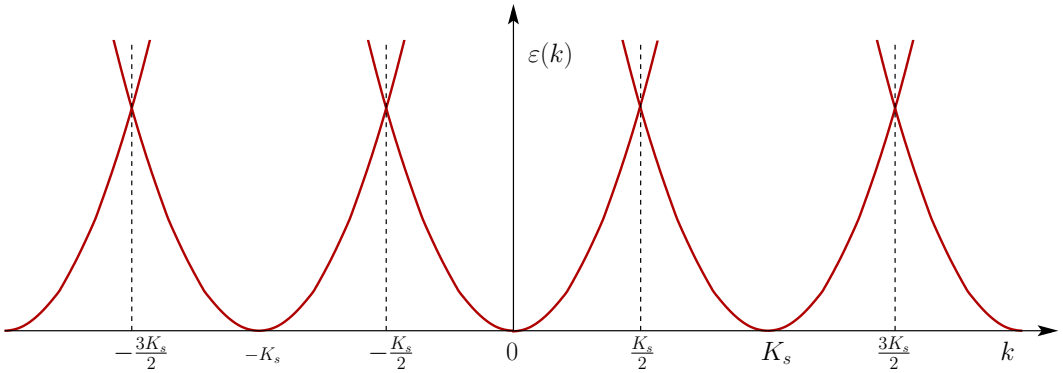

Figure 2.1: Periodic dispersion relations for a free electron in one dimension.

Consequently just by imposing the potential's periodicity the domain of the wave vector $\boldsymbol{k}$ is restricted to some unit cell in reciprocal space even if $V(\boldsymbol{r}) = 0$. As an example figure 2.1 shows the dispersion relations $\varepsilon(k)$ for a single electron in a vanishing periodic potential in one dimension.

A unit cell that exhibits the full symmetry of the reciprocal lattice is called *Brillouin zone*. The Brillouin zone is constructed as follows: An arbitrary lattice point is chosen as the origin and then the vectors connecting the origin with other lattice points are drawn. Next the planes that are perpendicular bisectors of these vectors are constructed. The Brillouin zone is the smallest volume containing the origin bounded by these planes.

In figure 2.1 the Brillouin zone is defined by the criterion $-\frac{K_s}{2} < k < \frac{K_s}{2}$. For a weak potential $V(\boldsymbol{r})$ the corrections to the energy-eigenvalues can be calculated in the context of perturbation theory. It can be shown that at the Brillouin zone boundary, where two energy parabolas cross, the energy differs from the free electron behaviour [6]. Due to effects of interference a so called *band gap* occurs and the energy's gradient vanishes at the Brilloin zone boundary, see figure 2.2. The entity of energies for all $\boldsymbol{k}$ vectors is called *band structure*. The regions between the band gaps are called *energy bands*. Bloch waves with energies in the gap region are surface states for instance. Another way to motivate the electronic band sturcture is the tight binding model which will be discussed in section 2.3.

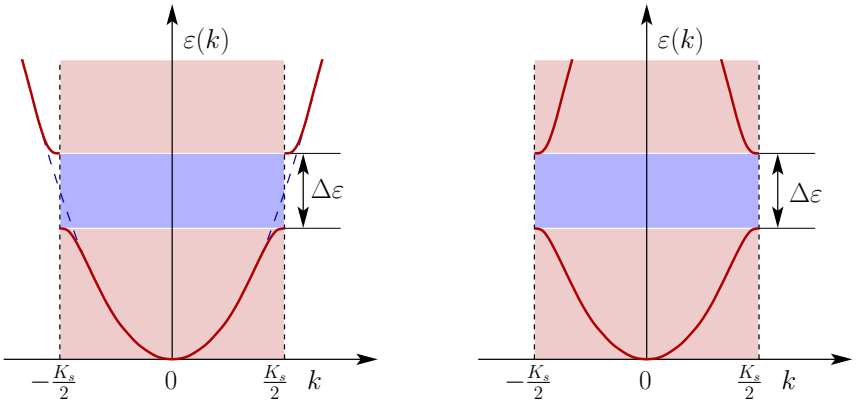

Figure 2.2: Extended and reduced zone scheme.

2.3 The Tight Binding Model

The models that have been discussed up to now are based on the assumption of free or quasi-free electrons. In contrast the so called *tight binding approximation* is introduced in this section. The following description can be found in [7]. The tight binding model is based on the assumption that a solid can be thought of as a periodic array of neutral atoms. The interaction of these atoms with one another should only be a small perturbation compared to the interaction between the various particles, electrons and protons, inside the respective atoms. As a basis for a perturbational description the electron wavefunctions are taken from the free atom. The only necessary additional change to the wavefunctions stems from the translational symmetry of the ideal crystal by assuming a translation invariance of the electron density leading to

$$\psi_{\boldsymbol{k}}(\boldsymbol{r}) = \sum_{l} \mathrm{e}^{\mathrm{i}\,\boldsymbol{k}\boldsymbol{R}_l}\, \phi\left(\boldsymbol{r} - \boldsymbol{R}_l\right) \ , \tag{2.27}$$

whereby the exponential function represents a plane wave, the so called Bloch factor, which is an eigenfunction of the translation operator $\mathbf{T}_l$ and $\phi\left(\boldsymbol{r} - \boldsymbol{R}_l\right)$ is the atomic wavefunction centered at $\boldsymbol{R}_l$. $\phi\left(\boldsymbol{r} - \boldsymbol{R}_l\right)$ is called Wannier-function. The geometry being assumed by this ansatz is shown in figure 2.3. For characterizing the crystal potential the model, which is sketched in figure 2.4, is applied. $U(\boldsymbol{r})$ is the unperturbed potential of the single free atom, while $V(\boldsymbol{r})$ is the actual crystal potential. This crystal potential is constructed by the superposition of the individual atomic potentials.
The Wannier functions ϕ are the solutions of the free atom Schrödinger equation

$$\mathbf{H}_0\, \phi(\boldsymbol{r}) = \left[-\frac{\hbar^2}{2m}\triangle + U(\boldsymbol{r})\right] \phi(\boldsymbol{r}) = \varepsilon_0\, \phi(\boldsymbol{r}) \ . \tag{2.28}$$

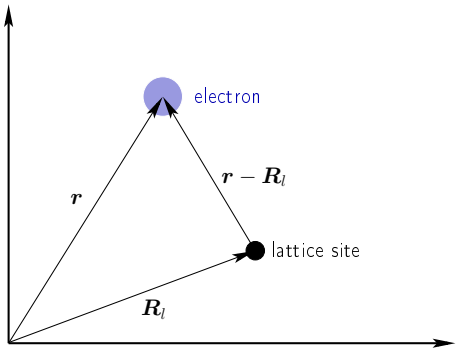

Figure 2.3: Geometry for the Tight Binding Model.

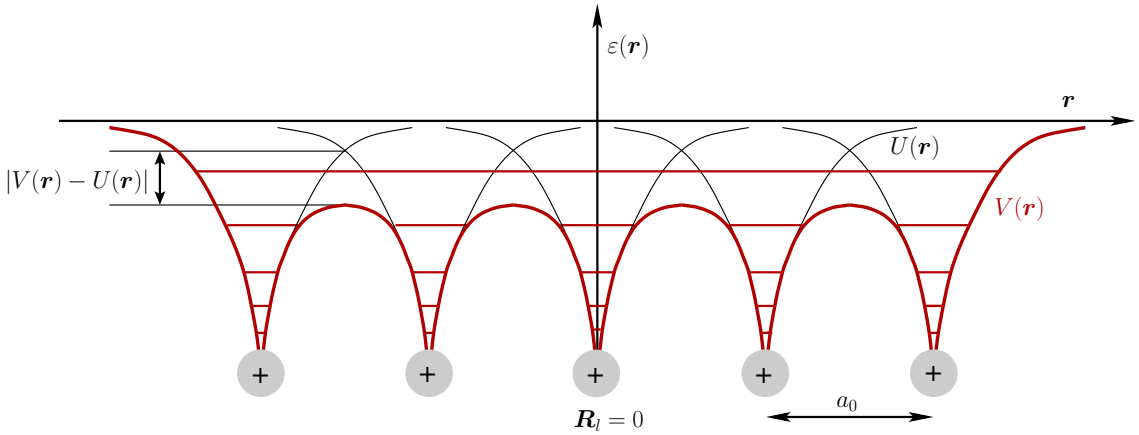

Figure 2.4: Assumed potentials in the tight binding model.

The crystal Hamiltonian is of the form

$$\mathbf{H} = -\frac{\hbar^2}{2m}\triangle + V(\boldsymbol{r}) \; . \tag{2.29}$$

Due to the lattice periodicity, equation (2.28) has to be fulfilled for an isolated atom at site $\boldsymbol{R}_l$ as well. The respective Hamiltonian $\mathbf{H}_l$ is given by

$$\mathbf{H}_l = -\frac{\hbar^2}{2m}\triangle + U(\boldsymbol{r} - \boldsymbol{R}_l) \; . \tag{2.30}$$

From now on the obvious spatial dependencies are omitted, $V(\boldsymbol{r}) = V$ etc. As the Wannier functions have been introduced in order to afford a treatment based on perturbation theory, the crystal Hamiltonian $\mathbf{H}$ is now expressed as follows

$$\mathbf{H} = \mathbf{H}_l + (\mathbf{H} - \mathbf{H}_l) = \mathbf{H} + (V - U) \; . \tag{2.31}$$

Calculating the expectation value of the crystal Hamilton operator $\langle H \rangle = \varepsilon$ for the assumed wavefunction (2.27) one obtains

$$\varepsilon = \frac{1}{N} \int \psi_{\boldsymbol{k}}^{*}\, \mathbf{H}\, \psi_{\boldsymbol{k}}\, \mathrm{d}^3 r = \frac{1}{N} \left[\int \psi_{\boldsymbol{k}}^{*}\, \mathbf{H}_l\, \psi_{\boldsymbol{k}}\, \mathrm{d}^3 r + \int \psi_{\boldsymbol{k}}^{*}\, (V - U)\, \psi_{\boldsymbol{k}}\, \mathrm{d}^3 r \right] , \tag{2.32}$$

at which

$$N = \langle \psi_{\boldsymbol{k}} | \psi_{\boldsymbol{k}} \rangle = \int \psi_{\boldsymbol{k}}^{*}\, \psi_{\boldsymbol{k}}\, \mathrm{d}^3 r \tag{2.33}$$

is the norm of the wavefunction. Knowing that $\psi_{\boldsymbol{k}}$ solves the eigenvalue problem

$$\mathbf{H}_l\, \psi_{\boldsymbol{k}} = \sum_l \mathrm{e}^{\mathrm{i}\boldsymbol{k}\boldsymbol{R}_l}\, \mathbf{H}_l\, \phi\,(\boldsymbol{r} - \boldsymbol{R}_l) = \varepsilon_0\, \psi_{\boldsymbol{k}} , \tag{2.34}$$

equation (2.32) can be simplified to

$$\begin{aligned} \varepsilon &= \varepsilon_0 + \int \psi_{\boldsymbol{k}}^{*}\, (V - U)\, \psi_{\boldsymbol{k}}\, \mathrm{d}^3 r \\ &= \varepsilon_0 + \frac{1}{N} \left[\sum_m \sum_l \mathrm{e}^{\mathrm{i}\boldsymbol{k}(\boldsymbol{R}_m - \boldsymbol{R}_l)} \int \phi^{*}\,(\boldsymbol{r} - \boldsymbol{R}_l)\; (V - U)\, \phi\,(\boldsymbol{r} - \boldsymbol{R}_l)\, \mathrm{d}^3 r \right] . \end{aligned} \tag{2.35}$$

The energy eigenvalue ε for the crystal Hamiltonian is thus expressed by a large component ε_0, which stems from the solution of the isolated atom and a small contribution which depends on the difference between the free atom potential U and the crystal potential V only. Now a transformation of the coordinates of the atomic positions $\boldsymbol{R} = \boldsymbol{R}_m - \boldsymbol{R}_l$ is carried out

$$(2.35) = \varepsilon_0 + \frac{1}{N} \sum_{\boldsymbol{R}=0,\, nn} \mathrm{e}^{-\mathrm{i}\boldsymbol{k}\boldsymbol{R}} \int \phi^{*}\,(\boldsymbol{r} - \boldsymbol{R})\, (V - U)\, \phi(\boldsymbol{r})\, \mathrm{d}^3 r\ . \tag{2.36}$$

This way the general summation over all lattice sites is transformed into a summation starting from the atom at the site with $\boldsymbol{R} = 0$ and is carried out further over its nearest-neighbors nn. In general this summation must be taken over the whole crystal. However, by assuming atomic wavefunctions whose amplitude rapidly decrease to zero for increasing values of $\boldsymbol{r}$, this summation can be reduced to next nearest-neighbor shells.

Now the summation in (2.36) is split up into two parts. The first part contains the information for $\boldsymbol{R} = 0$ (on-site contribution) and the other one covers the next nearest-neighbors (off-site contribution). The on- and off-site contribution involve two integrals which are abbreviated $-A$ and $-B$ describing the crystal field effects and the electron

hopping, which results from the atomic wavefunctions' overlap, respectively

$$-A = \frac{1}{N} \int \phi^*(\boldsymbol{r}) \, (V - U) \, \phi(\boldsymbol{r}) \, \mathrm{d}^3 r \, , \tag{2.37}$$

$$-B = \frac{1}{N} \int \phi^* \left(\boldsymbol{r} - \boldsymbol{R}\right) (V - U) \, \phi(\boldsymbol{r}) \, \mathrm{d}^3 r \, . \tag{2.38}$$

At this point one may assume that ϕ is an s-orbital and therefore spherically symmetric. Since $|\boldsymbol{r} - \boldsymbol{R}|$ is equivalent for all next nearest-neighbors, the hopping integral $-B$ always has the same value, so that the only remaining summation is that over the phase factors. If one restricts the summation to a single nearest-neighbor shell the energy ε reads

$$\varepsilon(\boldsymbol{k}) = \varepsilon_0 - A - B \sum_{nn} \mathrm{e}^{\mathrm{i}\boldsymbol{k}\boldsymbol{R}} \, . \tag{2.39}$$

For a simple cubic lattice with lattice constant a_0 one obtains for s-electrons

$$\varepsilon(\boldsymbol{k}) = \varepsilon_0 - A - 2B \left[\cos(a_0 k_x) + \cos(a_0 k_y) + \cos(a_0 k_z)\right] \, . \tag{2.40}$$

Consequently between the Brillouin zone's center, the Γ-point $\boldsymbol{k} = 0$, and the surface of the Brillouin zone the energy ε varies between $\varepsilon_0 - A \mp 6B$. It is obvious that the bandwidth is defined by the electron hopping. Figure 2.5 shows the s-band along the k_x direction between the Γ-point and the reciprocal lattice vector $k_x = \frac{\pi}{a_0}$. Due to

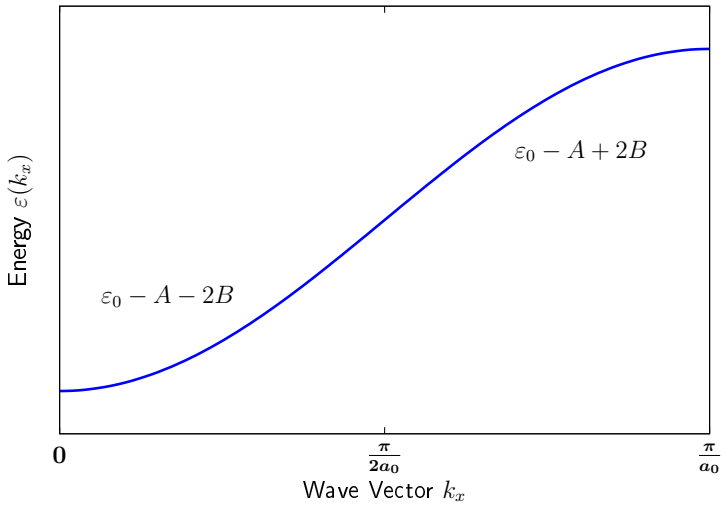

Figure 2.5: s-band along the k_x-direction for a simple cubic lattice.

equation (2.38) the hopping integral depends on the distance $|\boldsymbol{r} - \boldsymbol{R}|$ so that external pressure affects its value. As the overlap increases with increasing pressure the band-

width will also increase. As the density of states is defined as the number of states per energy interval, see figure 2.6, it decreases with increasing bandwidth. This is the

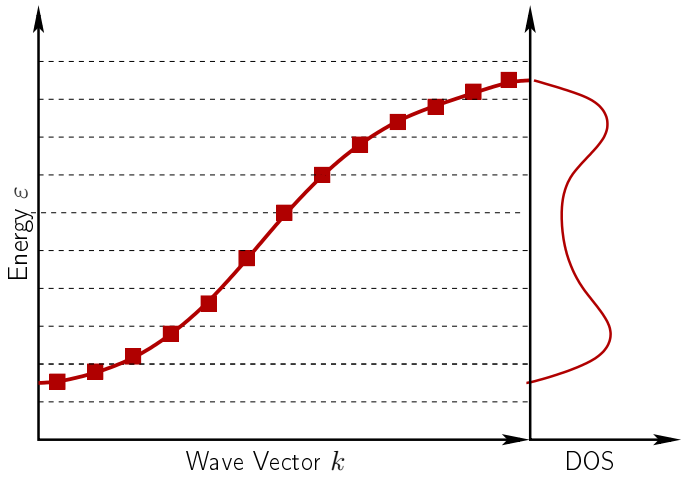

Figure 2.6: Sketch of how the density of states, DOS, is calculated.

reason why properties such as the specific heat C or the susceptibility χ which are proportional to the densitiy of states at the Fermi level are influenced by pressure.
In the case of a small wave vector $\boldsymbol{k}$, which is because of $|\boldsymbol{k}| = \frac{2\pi}{\lambda}$ linked up with a long wave length λ, equation (2.41) can be expanded into a Taylor series. This expansion yields

$$\varepsilon(\boldsymbol{k}) = \varepsilon_0 - A - 6B + B\, a_0^2 k^2 \,, \tag{2.41}$$

the well known parabolic dispersion of the free electron gas. In the long wave length limit the behaviour of electrons in a crystal can therefore be described by the Sommerfeld model. Due to their long wave length the electrons then only feel the mean value of the potential averaged over a large number of atomic sites.

Now that the origin of the electronic bandstructure has been motivated throughout this chapter the next chapter will concentrate on how the electronic structure can be calculated.

3 Methods of Treating Many Body Systems

3.1 Ritz's Variational Method

Most of the methods to treat many body sytems which will be discussed in the following are based on Ritz's variational method.

For a given Hamiltonian $\mathbf{H}$ with eigenbasis $|n\rangle$,

$$\mathbf{H}\,|n\rangle = E_n\,|n\rangle \tag{3.1}$$

and

$$\sum_n |n\rangle\langle n| = \mathbf{1}\ , \tag{3.2}$$

one obtains for an arbitrary state $|\psi\rangle$

$$\langle\psi|\mathbf{H}|\psi\rangle = \sum_n \langle\psi|n\rangle\langle n|\mathbf{H}|\psi\rangle\ . \tag{3.3}$$

Using equation (3.1) this can be simplified to

$$(3.3) = \sum_n E_n\,\langle\psi|n\rangle\langle n|\psi\rangle \tag{3.4}$$

Knowing that $E_n \geq E_0$ one can conclude

$$\langle\psi|\mathbf{H}|\psi\rangle \geq E_0\,\langle\psi|\psi\rangle \tag{3.5}$$

and finally

$$\frac{\langle\psi|\mathbf{H}|\psi\rangle}{\langle\psi|\psi\rangle} \geq E_0\ . \tag{3.6}$$

For the variational method by Ritz one has to choose the state $|\psi\rangle$ as a function of one or more parameters μ

$$|\psi\rangle = |\psi(\mu)\rangle\ , \tag{3.7}$$

and to search for a minimum of the resulting energy $E(\mu)$

$$E(\mu) = \frac{\langle\psi(\mu)|\mathbf{H}|\psi(\mu)\rangle}{\langle\psi(\mu)|\psi(\mu)\rangle} \tag{3.8}$$

achieving

$$\delta\left(E(\mu)\right) = 0\ . \tag{3.9}$$

The energy minimum calculated this way is according to equation (3.6) an upper boundary of the groundstate energy.
It can be shown that errors in the wavefunction lead to errors of quadratic order with respect to the energy. As a result the variational method is more accurate in identifying the energy than the wavefunction [8].

3.2 Thomas-Fermi Model

The Thomas-Fermi model is a simple model for treating an atom with N-electrons [9]. Moreover it is the first appoach which is based on the local electron density being discussed in this report. Later the local-density approximation and the generalized gradient approximation will be discussed in the context of density functional theory.

One starts using the well known relation

$$n = \frac{N}{V} = \frac{k_F^3}{3\pi^2} \tag{3.10}$$

between the electron density n and the Fermi wave vector $\boldsymbol{k}_F$ of the free Fermi gas. This relation will be derived in the following.
In reciprocal space the different $|\boldsymbol{k}\rangle$ states capture a volume of $\left(\frac{2\pi}{L}\right)^3$. For $T = 0$ all states within a sphere of radius $|\boldsymbol{k}_F|$ are fully occupied. According to Pauli's principle each $|\boldsymbol{k}\rangle$ state inside this so called Fermi sphere is occupied by a maximum of two electrons. These electrons occupying the same state have to differ with respect to their spin orientation. The Fermi sphere's volume can be calculated to

$$\int_0^{k_F} \mathrm{d}k\ k^2 \int \mathrm{d}\Omega = 4\pi \int_0^{k_F} \mathrm{d}k\ k^2 = \frac{4\pi}{3} k_F^3\ . \tag{3.11}$$

The number of possible states N is then given by

$$N = 2 \cdot \frac{\frac{4\pi}{3} k_F^3}{\frac{8\pi^3}{L^3}} = \frac{L^3 k_F^3}{3\pi^2} \ . \tag{3.12}$$

Considering that $L^3 = V$, V being the real space volume, one can show the relation between the electron density n and the Fermi wave vector k_F which was given in equation (3.10).

The Thomas-Fermi model is based on the assumption that the electronic interaction which is described by the potential $V(r)$ causes n and k_F to be spatial dependent. This way the density as well as the momentum become spatial dependent

$$\varepsilon_F = \frac{\hbar^2}{2m} k_F^2 (r) + V (r) \ , \tag{3.13}$$

m being the electron's mass. The spatial dependent Fermi wave vector $\boldsymbol{k}_F (r)$ is introduced by the "*local density approach*"

$$n (\boldsymbol{r}) = \frac{k_F^3 (\boldsymbol{r})}{3\pi^2} \ , \tag{3.14}$$

where relation (3.10) is used. Due to symmetry reasons the vector $\boldsymbol{r}$ in this equation is replaced by its modulus. Joining together (3.13) and (3.14) leads to

$$n (r) = \frac{1}{2\pi^2} \left\{ \frac{2m \left[\varepsilon_F - V (r) \right]}{\hbar^2} \right\}^{\frac{3}{2}} \ . \tag{3.15}$$

In order to be able to determine $n (r)$ and $V (r)$ a second equation which establishes a relation between these two functions is needed. For this purpose Poisson's equation in units of the Sommerfeld constant α_f is taken into account

$$\triangle V(r) = -4\pi \alpha_f \hbar c \, n (r) \ , \tag{3.16}$$

with

$$\alpha_f = \frac{e^2}{4\pi \varepsilon_0 \hbar c} \ , \tag{3.17}$$

and ε_0 not being an energy but the dielectric constant in this equation. Inserting (3.15) into (3.16) leads via some algebraic steps to the so called *Thomas-Fermi Equation*

$$\frac{d^2\chi}{dx^2} = \frac{\chi^{\frac{3}{2}}}{\sqrt{x}} \,. \tag{3.18}$$

In equation (3.18) the so called *Thomas-Fermi function*

$$\chi = \frac{r\left[\varepsilon_F - V\left(r\right)\right]}{Z\alpha_f \hbar c} \tag{3.19}$$

as well as a dimensionless factor

$$x = \frac{r}{b} \tag{3.20}$$

with

$$b = a\left(\frac{9\pi^2}{128Z}\right)^{\frac{1}{3}} \tag{3.21}$$

and a being Bohr's radius

$$a = \frac{\hbar}{mc}\frac{1}{\alpha_f} \tag{3.22}$$

have been introduced. By solving equation (3.18) an expression for the potential is found. The boundary conditions which are necessary for this solution are

$$\chi\left(0\right) = 1 \tag{3.23}$$

and

$$\chi\left(r_0\right) = 0 \,. \tag{3.24}$$

According to equation (3.15) r_0 can be seen as the classical reversal radius of a bound electron in the potential $V\left(r\right)$. From a classical point of view all electrons have to be located inside a shell of this radius

$$4\pi \int_0^{r_0} \mathrm{d}r \; r^2 \, n\left(r\right) = N \,. \tag{3.25}$$

Using the solution for the potential $V(r)$ the density $n(r)$ can be calculated using equation (3.15).
It can be shown that the Thomas-Fermi model can only describe atoms with $N \leq Z$. For neutral atoms with $N = Z$ one obtains the single particle potential

$$V\left(r\right) = -\frac{Z\alpha_f \hbar c}{r}\chi_0\left(\frac{r}{b}\right) \tag{3.26}$$

where χ_0 is equal for all neutral atoms. This equation describes in which way the attracting potential of the nucleus is modified for large distances by the electron-electron interaction.
According to [8] the Thomas-Fermi method fails for small values of r due to the strong variations of the potential in the vicinity of the core. For large distances r the method fails as well. In the region $\frac{a}{Z} < r < a$ where most of the electrons are localized the Thomas-Fermi model describes the potential in a suitable way.

3.3 The Hartree- and Hartree-Fock Approximation

As the Hartree- and the Hartree-Fock Approximation are commonly used they are referred to in various books such as [8]. These methods will be presented the same way as they are treated in [10].

3.3.1 The Hartree-Approximation

The Hartree-approximation is based on a product ansatz for the overall wavefunction Ψ_H which solves the Schrödinger equation of a many body system. The real approximation is a variation of the single particle wavefunctions of the overall system Ψ_H.

Considering the Hamiltonian of noninteracting particles

$$\mathbf{H}_0 = \sum_i -\frac{\hbar^2}{2m}\triangle_i + V(\boldsymbol{r}_i) \ , \tag{3.27}$$

shows that it can be solved by a product ansatz which is called *Hartree-ansatz*

$$\Psi_H(\boldsymbol{r}_1, ..., \boldsymbol{r}_N) = \prod_{i=1}^{N} \varphi_{\alpha_i}(\boldsymbol{r}_i) \ . \tag{3.28}$$

The single particle wavefunctions φ_{α_i} solve the single particle Schrödinger equation

$$\left[-\frac{\hbar^2}{2m}\triangle + V(\boldsymbol{r})\right] \varphi_{\alpha_i}(\boldsymbol{r}) = \varepsilon_{\alpha_i}\, \varphi_{\alpha_i}(\boldsymbol{r}) \ . \tag{3.29}$$

The Hartree-Ansatz (3.28) is an eigenstate of the noninteracting Hamiltonian $\mathbf{H}_0$

$$\mathbf{H}_0\,\Psi_H(\boldsymbol{r}_1,...,\boldsymbol{r}_N) = \sum_{i=1}^{N}\left[-\frac{\hbar^2}{2m}\triangle_i + V(\boldsymbol{r}_i)\right]\prod_{j=1}^{N}\varphi_{\alpha_j}(\boldsymbol{r}_j) \tag{3.30}$$

$$= (\varepsilon_{\alpha_1} + \varepsilon_{\alpha_2} + ... + \varepsilon_{\alpha_N})\prod_{j=1}^{N}\varphi_{\alpha_j}(\boldsymbol{r}_j) \tag{3.31}$$

$$= \sum_{i=1}^{N}\varepsilon_{\alpha_i}\,\Psi_H(\boldsymbol{r}_1,...\boldsymbol{r}_N) \tag{3.32}$$

$$= E\,\Psi_H(\boldsymbol{r}_1,...\boldsymbol{r}_N)\ . \tag{3.33}$$

The next step is to approximately determine the energy of an interacting system. The respective Hamiltonian reads

$$\mathbf{H} = \mathbf{H}_0 + \frac{1}{2}\sum_{i\neq j}U(|\boldsymbol{r}_i - \boldsymbol{r}_j|)\ . \tag{3.34}$$

The Hartree-approximation is based on Ritz's variational method. The constraint of the variation is that the norms of the single particle wavefunctions

$$\langle\varphi_{\alpha_i}|\varphi_{\alpha_i}\rangle = 1 \tag{3.35}$$

have to be conserved. The system's energy can be obtained by applying the Hartree-ansatz to the Hamiltonian $\mathbf{H}$ and calculating its expectation value

$$E = \langle\Psi_H|\mathbf{H}|\Psi_H\rangle\ . \tag{3.36}$$

Taking into account that the single particle states are orthogonal

$$\langle\varphi_{\alpha_i}|\varphi_{\alpha_j}\rangle = \delta_{ij}\ , \tag{3.37}$$

δ_{ij} being the Kronecker Symbol

$$\delta_{ij} = \begin{cases}1, & i = j\\ 0, & i \neq j\end{cases}\ , \tag{3.38}$$

one can calculate the expectation value (3.36)

$$E = \sum_i \int \mathrm{d}^3 r\, \varphi^*_{\alpha_i}(\boldsymbol{r}) \left(-\frac{\hbar^2}{2m} \triangle + V(\boldsymbol{r}) \right) \varphi_{\alpha_i}(\boldsymbol{r}) + \frac{1}{2} \sum_{i \neq j} \int \mathrm{d}^3 r \int \mathrm{d}^3 r'\, U(|\boldsymbol{r} - \boldsymbol{r}'|)\, |\varphi_{\alpha_i}(\boldsymbol{r})|^2\, |\varphi_{\alpha_j}(\boldsymbol{r}')|^2 \,.$$

Now the energy is minimized under the already mentioned constraint (3.35). This constraint is taken into account by Lagrange parameters E_{α_i}. In principle it would be necessary to perform the variation for the real as well as for the imaginary part of the single particle wavefunctions φ_{α_i}. Due to the fact that

$$\begin{pmatrix} \varphi_{\alpha_i} \\ \varphi^*_{\alpha_i} \end{pmatrix} = \begin{pmatrix} 1 & i \\ 1 & -i \end{pmatrix} \begin{pmatrix} \mathrm{Re}\, \varphi_{\alpha_i} \\ \mathrm{Im}\, \varphi_{\alpha_i} \end{pmatrix} \,, \tag{3.39}$$

the variation can be carried out either with respect to φ_{α_i} or $\varphi^*_{\alpha_i}$. One chooses to vary $\varphi^*_{\alpha_k}$ in order to obtain the N Hartree-equations for the single particle wavefunctions φ_{α_k}

$$\frac{\delta}{\delta\, \varphi^*_{\alpha_k}} \left[\langle \Psi_H | \mathbf{H} | \Psi_H \rangle - \sum_i E_{\alpha_i} \left(\langle \varphi_{\alpha_i} | \varphi_{\alpha_i} \rangle - 1 \right) \right] = 0 \,. \tag{3.40}$$

In order to be able to carry out the variation, equation (3.40) is projected onto real space

$$\frac{\delta}{\delta\, \varphi^*_{\alpha_k}(\boldsymbol{r})} \left[\sum_i \int \mathrm{d}^3 r'\, \varphi^*_{\alpha_i}(\boldsymbol{r}') \left(-\frac{\hbar^2}{2m} \triangle + V(\boldsymbol{r}') \right) \varphi_{\alpha_i}(\boldsymbol{r}') + \frac{1}{2} \sum_{i \neq j} \int \mathrm{d}^3 r' \int \mathrm{d}^3 r''\, U(|\boldsymbol{r}' - \boldsymbol{r}''|)\, |\varphi_{\alpha_i}(\boldsymbol{r}')|^2\, |\varphi_{\alpha_j}(\boldsymbol{r}'')|^2 - \sum_i E_{\alpha_i} \left(\int d^3 r' |\varphi_{\alpha_i}(\boldsymbol{r}')|^2 - 1 \right) \right] = 0 \,.$$

The variation results in

$$\left[-\frac{\hbar^2}{2m} \triangle + V(\boldsymbol{r}) + \sum_{i(\neq k)} \int \mathrm{d}^3 r'\, U(|\boldsymbol{r}' - \boldsymbol{r}|)\, |\varphi_{\alpha_i}(\boldsymbol{r}')|^2 \right] \varphi_{\alpha_k}(\boldsymbol{r}) = E_{\alpha_k} \varphi_{\alpha_k}(\boldsymbol{r}) \,. \tag{3.41}$$

Now the *effective potential* $V_k^{eff}(\boldsymbol{r})$ in which particle k moves is introduced as

$$V_k^{eff}(\boldsymbol{r}) = V(\boldsymbol{r}) + \sum_{i \neq k} \int \mathrm{d}^3 r' \, U(|\boldsymbol{r}' - \boldsymbol{r}|) \, |\varphi_{\alpha_i}(\boldsymbol{r}')|^2 \, . \tag{3.42}$$

The effective potential $V_k^{eff}(\boldsymbol{r})$ consists of the single particle potential $V(\boldsymbol{r})$ and a molecular field, which is created by all other particles of the system. One obtains the so called *Hartree-equations*

$$\left[-\frac{\hbar^2}{2m} \triangle + V_k^{eff}(\boldsymbol{r}) \right] \varphi_{\alpha_k}(\boldsymbol{r}) = E_{\alpha_k} \varphi_{\alpha_k}(\boldsymbol{r}) \, , \tag{3.43}$$

where the potentials $V_k^{eff}(\boldsymbol{r})$ depend on the orbitals $\varphi_{\alpha_k}(\boldsymbol{r})$.

3.3.2 The Hartree-Fock-Approximation

Due to the fact that the Hartree-ansatz is product-like it does not obey Pauli's principle because it is *not* totally antisymmetric with respect to the exchange of two particles

$$\Psi_H(\boldsymbol{r}_1, ..., \boldsymbol{r}_i, ..., \boldsymbol{r}_j, ..., \boldsymbol{r}_N) = (-1) \, \Psi_H(\boldsymbol{r}_1, ..., \boldsymbol{r}_j, ..., \boldsymbol{r}_i, ..., \boldsymbol{r}_N) \, , \tag{3.44}$$

with $\boldsymbol{r}_i = (\boldsymbol{x}_i, \sigma_i)$. Therefore the behaviour of electrons cannot be described correctly by the method discussed in the last section. To obtain a totally antisymmetric wavefunction which is a solution to the Schrödinger equation for noninteracting particles and thus an eigenstate of the Hamiltonian (3.27) one can apply the antisymmetrisation operator to the Hartree-ansatz (3.28)

$$|\Psi_{HF}\rangle = \sqrt{N!} \, \mathcal{A} \, |\Psi_H\rangle \, . \tag{3.45}$$

The state which is created this way is known as a *Slater determinant*

$$\Psi_{HF} = \frac{1}{\sqrt{N!}} \begin{vmatrix} \varphi_{\alpha_1}(\boldsymbol{r}_1) & \dots & \varphi_{\alpha_1}(\boldsymbol{r}_N) \\ \vdots & \ddots & \vdots \\ \varphi_{\alpha_N}(\boldsymbol{r}_1) & \dots & \varphi_{\alpha_N}(\boldsymbol{r}_N) \end{vmatrix} \, . \tag{3.46}$$

The wavefunction Ψ_{HF} of the total system is the *ansatz* of the *Hartree-Fock theory.*

The Hartree-Fock approximation is a variational method to the single particle states of the Slater determinant just as well as the Hartree-approximation. Consequently the

Hartree-Fock-approximation delivers an upper limit for the groundstate energy for a system of interacting fermions.

The first step of the approximation is to calculate the expactation value for the Hamiltonian of the interacting system (3.34)

$$\begin{aligned}\langle\Psi_{HF}|\mathbf{H}|\Psi_{HF}\rangle = \\ \sum_i \int \mathrm{d}^3r'\,\varphi^*_{\alpha_i}(\boldsymbol{r}')\left(-\frac{\hbar^2}{2m}\triangle + V(\boldsymbol{r}')\right)\varphi_{\alpha_i}(\boldsymbol{r}') \\ + \frac{1}{2}\sum_{i\neq j}\int \mathrm{d}^3r' \int \mathrm{d}^3r''\,\varphi^*_{\alpha_i}(\boldsymbol{r}')\varphi^*_{\alpha_j}(\boldsymbol{r}'')\,U(|\boldsymbol{r}'-\boldsymbol{r}''|)\,\varphi_{\alpha_j}(\boldsymbol{r}'')\varphi_{\alpha_i}(\boldsymbol{r}') \\ - \frac{1}{2}\sum_{i\neq j}\int \mathrm{d}^3r' \int \mathrm{d}^3r''\,\varphi^*_{\alpha_i}(\boldsymbol{r}')\varphi^*_{\alpha_j}(\boldsymbol{r}'')\,U(|\boldsymbol{r}'-\boldsymbol{r}''|)\,\varphi_{\alpha_j}(\boldsymbol{r}')\varphi_{\alpha_i}(\boldsymbol{r}'')\ .\end{aligned}$$

Then the energy is minimized analogously to the Hartree-approximation. Again the constraint of the variation is that the norm of the single particle states shall be conserved

$$\langle\varphi_{\alpha_i}|\varphi_{\alpha_i}\rangle = \int \mathrm{d}^3r'|\varphi_{\alpha_i}|^2 = 1\ . \tag{3.47}$$

The respective equation reads

$$\frac{\delta}{\delta\varphi^*_{\alpha_k}(\boldsymbol{r})}\left[\langle\Psi_{HF}|\mathbf{H}|\Psi_{HF}\rangle - \sum_i \varepsilon_{\alpha_i}\left(\int \mathrm{d}^3r'|\varphi_{\alpha_i}|^2 - 1\right)\right] = 0\ . \tag{3.48}$$

By means of the functional derivation one obtains the *Hartree-Fock equations*

$$\begin{aligned}\left[-\frac{\hbar^2}{2m}\triangle + V(\boldsymbol{r})\right]\varphi_{\alpha_k}(\boldsymbol{r}) + \sum_{i\neq k}\int \mathrm{d}^3r'\,U(|\boldsymbol{r}'-\boldsymbol{r}|)\,|\varphi_{\alpha_i}(\boldsymbol{r}')|^2\,\varphi_{\alpha_k}(\boldsymbol{r}) \\ - \sum_{i\neq k}\int \mathrm{d}^3r'\,\varphi_{\alpha_i}(\boldsymbol{r}')^*\,U(|\boldsymbol{r}'-\boldsymbol{r}|)\,\varphi_{\alpha_k}(\boldsymbol{r}')\varphi_{\alpha_i}(\boldsymbol{r}) \\ = \varepsilon_{\alpha_k}\varphi_{\alpha_k}(\boldsymbol{r})\ .\end{aligned} \tag{3.49}$$

A comparison of the Hartree-Fock Equations and the Hartree-Equations (3.43) reveals that they differ in a single term which is called the *exchange term*

$$-\sum_{i\neq k}\int \mathrm{d}^3r'\,\varphi_{\alpha_i}(\boldsymbol{r}')^*\,U(|\boldsymbol{r}'-\boldsymbol{r}|)\,\varphi_{\alpha_k}(\boldsymbol{r}')\varphi_{\alpha_i}(\boldsymbol{r})\ . \tag{3.50}$$

The exchange term is of pure quantum mechanical origin. It is a consequence of Pauli's principle and it has been shown by Heitler and London [11] for the H_2 molecule that this term is responsible for any kind of magnetic ordering.
The Hartree-Fock equations are complex integro differential equations for the single particle wavefunctions $\varphi_{\alpha_k}(\boldsymbol{r})$. Therefore simplifications of these equations are needed in order to solve them. As a consequence the solutions for the groundstate wavefunction Ψ_{HF} are only rough approximations.
Following Slater the exchange energy E_x of a free electron gas where the Fermi wave vector $\boldsymbol{k}_F$ is related to the electron density n via (3.10) within the Hartree-Fock approximation one finds that the exchange energy E_x is given by

$$E_x = -\left(\frac{3e^2}{2}\right)\left(\frac{3n}{8\pi}\right)^{\frac{1}{3}} . \tag{3.51}$$

It is therefore a power-law dependence of the electron density n [12]. This is the starting point for methods of approximation within the local-density approximation, LDA, which will be discussed in the next section.

3.4 Density Functional Theory

3.4.1 Hohenberg-Kohn Theorems

The First Hohenberg-Kohn Theorem

The usual way to solve a quantum mechanical problem is to solve the Schrödinger equation of the system, where the system's properties are characterized by the potential $\mathbf{V}$. The appoach of density functional theory [13, 14] is different. The first Hohenberg-Kohn theorem states that *the density $n(\boldsymbol{r})$ uniquely characterizes the potential, up to an arbitrary constant.* As a consequence the groundstate energy E_0 is a uniquely defined functional of the density $n(\boldsymbol{r})$

$$E_0 = E[n] . \tag{3.52}$$

This theorem can be proven as follows. It is assumed that there exist two potentials $\mathbf{V}$ and $\mathbf{V}'$ causing the same groundstate density $n_0(\boldsymbol{r})$. Shall ψ_0 be the respective groundstate wavefunction of the Hamiltonian

$$\mathbf{H} = \mathbf{T} + \mathbf{V}_{ee} + \mathbf{V} \tag{3.53}$$

and ψ_0' the groundstate wavefunction of

$$\mathbf{H}' = \mathbf{T} + \mathbf{V}_{ee} + \mathbf{V}' \; . \tag{3.54}$$

According to equation (3.6) ψ_0 and ψ_0' obey the inequality

$$\langle \psi_0 | \mathbf{H} | \psi_0 \rangle = E_0 < \langle \psi_0' | \mathbf{H} | \psi_0' \rangle \; . \tag{3.55}$$

Using equation (3.54) the Hamiltonian $\mathbf{H}$ can be written as

$$\mathbf{H} = \mathbf{H}' - (\mathbf{V}' - \mathbf{V}) \tag{3.56}$$

which simplifies inequality (3.55) to

$$E_0 < \langle \psi_0' | \left[\mathbf{H}' - (\mathbf{V}' - \mathbf{V}) \right] | \psi_0' \rangle = E_0' - \langle \psi_0' | \mathbf{V}' - \mathbf{V} | \psi_0' \rangle \; , \tag{3.57}$$

Now equation (3.57) is projected to real space using

$$\int \mathrm{d}^3 r \, |\boldsymbol{r}\rangle\langle\boldsymbol{r}| = \mathbf{1} \; . \tag{3.58}$$

This yields

$$E_0 < E_0' - \int \mathrm{d}^3 r \int \mathrm{d}^3 r' \, \langle \psi_0' | \boldsymbol{r} \rangle \langle \boldsymbol{r} | \mathbf{V}' - \mathbf{V} | \boldsymbol{r}' \rangle \langle \boldsymbol{r}' | \psi_0' \rangle \; . \tag{3.59}$$

and can be simplified to

$$E_0 < E_0' - \int \mathrm{d}^3 r \, n_0(\boldsymbol{r}) \left[V'(\boldsymbol{r}) - V(\boldsymbol{r}) \right] \; . \tag{3.60}$$

Analogously the variation principle yields

$$\langle \psi_0' | \mathbf{H}' | \psi_0' \rangle = E_0' < \langle \psi_0 | \mathbf{H}' | \psi_0 \rangle \; . \tag{3.61}$$

Proceeding as above leads via

$$\mathbf{H}' = \mathbf{H} + (\mathbf{V}' - \mathbf{V}) \tag{3.62}$$

and the assumption

$$n(\boldsymbol{r}) = \psi_0'^*(\boldsymbol{r}) \psi_0'(\boldsymbol{r}) = \psi_0^*(\boldsymbol{r}) \psi_0(\boldsymbol{r}) \tag{3.63}$$

to

$$E_0' < E_0 + \int \mathrm{d}^3 r \, n_0(\boldsymbol{r}) \left[V'(\boldsymbol{r}) - V(\boldsymbol{r}) \right] \ . \tag{3.64}$$

Summing up equations (3.60) and (3.64) yields the contradiction

$$E_0 + E_0' < E_0 + E_0' \ . \tag{3.65}$$

Hence the assumption in equation (3.63) has been wrong and the potential $V = V[n]$ is a uniquely defined functional of the density $n(\boldsymbol{r})$. Knowing the groundstate density $n(\boldsymbol{r})$ therefore the groundstate energy E_0, the groundstate wavefunction ψ_0 and thereby the expectation value of any operator can be calculated.

The Second Hohenberg-Kohn Theorem

If a functional $F[n]$ is defined as

$$F[n] = \langle \psi | \mathbf{T} + \mathbf{V}_{ee} | \psi \rangle \tag{3.66}$$

the energy functional $E[n]$ then reads

$$E[n] = F[n] + \int \mathrm{d}^3 r \, n(\boldsymbol{r}) \, V(\boldsymbol{r}) \ . \tag{3.67}$$

The second Hohenberg-Kohn theorem states that *for a many electron system the functional $E[n]$ for the total energy has a minimum equal to the groundstate energy E_0 at the groundstate density $n_0(\boldsymbol{r})$*

$$E_0 = E[n_0] = \min \left\{ E[n] \right\} \ . \tag{3.68}$$

3.4.2 Kohn-Sham Equations

Kohn and Sham used the variational principle, which is implied by the minimal properties of the energy functional in equation (3.68), to derive single-particle Schrödinger equations. For this purpose the functional $F[n]$ in equation (3.66) is split into three parts

$$F[n] = T[n] + \frac{e^2}{2} \int \mathrm{d}^3 r \int \mathrm{d}^3 r' \, \frac{n(\boldsymbol{r}) n(\boldsymbol{r}')}{|\boldsymbol{r} - \boldsymbol{r}'|} + E_{xc}[n] \tag{3.69}$$

which describe the kinetic, the direct electron-electron interaction energy (= Hartree energy) and the exchange-correlation energy. In contrast to the Hartree integral, an

explicit form of the functionals T and E_{xc} is unknown in general. Under the constraint of particle conservation

$$\int \mathrm{d}^3 r\, n(\boldsymbol{r}) = N \tag{3.70}$$

the variation of equation (3.67) is carried out

$$\frac{\delta E[n]}{\delta n(\boldsymbol{r})} + \mu \frac{\delta \left[N - \int \mathrm{d}^3 r\, n(\boldsymbol{r})\right]}{\delta n(\boldsymbol{r})} = 0 \,, \tag{3.71}$$

where μ is the respective Lagrange multiplier. Now the kinetic energy functional $T[n]$ is split up into a term T_0 implying the kinetic energy of noninteracting particles and T_{xc}, the kinetic exchange and correlation energy,

$$T[n] = T_0[n] + T_{xc}[n] \,. \tag{3.72}$$

By introducing orbitals ϕ_i

$$n(\boldsymbol{r}) = \sum_{i=1}^{N} |\phi_i(\boldsymbol{r})|^2 \tag{3.73}$$

the kinetic energy functional of noninteracting particles can be written as

$$T_0[n] = \sum_i \int \mathrm{d}^3 r\, \phi_i^*(\boldsymbol{r}) \left[-\frac{\hbar^2}{2m}\triangle\right] \phi_i(\boldsymbol{r}) \tag{3.74}$$

where the sum extends over the lowest N occupied states and hence its functional derivative can be determined. Due to equation (3.73) the variation can now be carried out with respect to the orbitals ϕ_i^* yielding the *Kohn-Sham equations*

$$\left[-\frac{\hbar^2}{2m}\triangle + V_k^{eff}(\boldsymbol{r})\right] \phi_i(\boldsymbol{r}) = \varepsilon_i \phi_i(\boldsymbol{r}) \tag{3.75}$$

with

$$V_k^{eff} = V_0(\boldsymbol{r}) + V_H(\boldsymbol{r}) + V_{xc}(\boldsymbol{r}) \tag{3.76}$$

where the Hartree-potential is given by

$$V_H(\boldsymbol{r}) = e^2 \int \mathrm{d}^3 r' \frac{n(\boldsymbol{r}')}{|\boldsymbol{r} - \boldsymbol{r}'|} \tag{3.77}$$

and the exchange-correlation term

$$V_{xc}(\boldsymbol{r}) = \frac{\delta\left(E_{xc}\right)}{\delta n(\boldsymbol{r})} \tag{3.78}$$

is still unknown and has to be approximated. The Kohn-Sham equations are single particle Schrödinger equations, where the external potential is replaced by an effective potential $V_k^{eff}(\boldsymbol{r})$ which depends on the density $n(\boldsymbol{r})$. The density itself depends via (3.73) on the single particle states ϕ_i. The Kohn-Sham equations thus constitute a self-consistent field problem. They build the basis of density functional theory. Although the Kohn-Sham equations have been derived to be single-particle Schrödinger equations, the eigenvalues ε_i have to be treated with care. These eigenvalues have on one hand successfully been used to interpret excitation spectra, on the other hand there are cases which are problematic [15].

3.5 Spin-Density Functional Theory

The effects of spin polarization have been taken into account in terms of density functional theory first by Barth and Hedin in 1972 [16]. The basic variables of this theory are the scalar electronic density $n(\boldsymbol{r})$ and the the vector of the magnetization density $\boldsymbol{m}(\boldsymbol{r})$. Instead of these four variables alternatively the 2×2 spin density matrix $\rho^{\alpha\beta}(\boldsymbol{r})$ can be used, where the indices α and β can have two values, either $+$ for spin up or $-$ for spin down. The relation between $\rho^{\alpha\beta}(\boldsymbol{r})$, $n(\boldsymbol{r})$ and $\boldsymbol{m}(\boldsymbol{r})$ is given by

$$n(\boldsymbol{r}) = \sum_{\alpha} \rho^{\alpha\alpha}(\boldsymbol{r}), \quad \boldsymbol{m}(\boldsymbol{r}) = \sum_{\alpha\beta} \boldsymbol{\sigma}^{\alpha\beta}\rho^{\alpha\beta}(\boldsymbol{r}) \tag{3.79}$$

as well as

$$\rho^{\alpha\beta}(\boldsymbol{r}) = \frac{1}{2}\left[n(\boldsymbol{r})\delta^{\alpha\beta} + \boldsymbol{m}(\boldsymbol{r})\boldsymbol{\sigma}^{\alpha\beta}\right] \tag{3.80}$$

where $\boldsymbol{\sigma}$ is a vector consisting of the Pauli spin matrices

$$\boldsymbol{\sigma} = \begin{pmatrix} \sigma_x \\ \sigma_y \\ \sigma_z \end{pmatrix} \tag{3.81}$$

with

$$\sigma_x = \begin{pmatrix} 0 & 1 \\ 1 & 0 \end{pmatrix}, \ \sigma_y = \begin{pmatrix} 0 & -\mathrm{i} \\ \mathrm{i} & 0 \end{pmatrix}, \ \sigma_z = \begin{pmatrix} 1 & 0 \\ 0 & -1 \end{pmatrix} . \tag{3.82}$$

According to [16] the Hohenberg-Kohn-Sham spin-density functional is given by

$$E\left[\rho^{\alpha\beta}\right] = T\left[\rho^{\alpha\beta}\right] + \frac{e^2}{2}\int \mathrm{d}^3r \int \mathrm{d}^3r' \, \frac{n(\boldsymbol{r})n(\boldsymbol{r}')}{|\boldsymbol{r}-\boldsymbol{r}'|} + \sum_{\alpha\beta}\int \mathrm{d}^3r \, V_{ext}^{\alpha\beta}(\boldsymbol{r})\rho^{\alpha\beta}(\boldsymbol{r}) + E_{xc}\left[\rho^{\alpha\beta}\right] \ . \tag{3.83}$$

Therefore it is a sum of the kinetic energy T of non-interacting electrons, the Hartree energy, describing the direct electron-electron interaction, the interaction energy with the external potential $V_{ext}^{\alpha\beta}$ and the exchange correlation energy. Moreover it is assumed that the exchange correlation energy functional $E_{xc}\left[n^{\alpha\beta}(\boldsymbol{r})\right]$ contains the kinetic energy exchange correlation funcitonal $T_{xc}\left[n^{\alpha\beta}(\boldsymbol{r})\right]$. The external potential accounts for the Coloumb interaction of the electrons and the nuclei as well as the interaction with an external magnetic field. Once again the functional for the kinetic energy is unknown. Consequently an ansatz for the density matrix is made

$$\rho^{\alpha\beta}(\boldsymbol{r}) = \sum_i \phi_i^{*\,\alpha}(\boldsymbol{r})\,\phi_i^{\beta}(\boldsymbol{r}) \ . \tag{3.84}$$

The ϕ_i^{α} are single particle wavefunctions with spin α. The sum extends over all occupied orbitals. Now the kinetic energy functional can be written as

$$T\left[\rho^{\alpha\beta}\right] = \sum_{\alpha i}\int \mathrm{d}^3r \, \phi^{*\,\alpha}(\boldsymbol{r})\left[-\frac{\hbar}{2m}\triangle\phi_i^{\alpha}\right] \tag{3.85}$$

and the variation of the energy functional (3.83) is carried out with respect to the single particle wavefunctions. This leads to the Kohn-Sham equations

$$\sum_{\beta}\left[-\frac{\hbar^2}{2m}\triangle\,\delta^{\alpha\beta} + V_k^{eff,\alpha\beta}(\boldsymbol{r}) - \varepsilon_i\delta^{\alpha\beta}\right]\phi_i^{\beta} = 0 \ . \tag{3.86}$$

Again the ε_i are Lagrange parameters of the variation which are a consequence of the constraint that the norm of the single particle wavefunctions has to be conserved throughout the variation. The effective single particle potential is given as

$$V_k^{eff,\alpha\beta}(\boldsymbol{r}) = e^2\int \mathrm{d}^3r' \frac{n(\boldsymbol{r}')}{|\boldsymbol{r}-\boldsymbol{r}'|}\,\delta^{\alpha\beta} + V_{ext}^{\alpha\beta}(\boldsymbol{r}) + V_{xc}^{\alpha\beta}(\boldsymbol{r}) \tag{3.87}$$

with

$$V_{xc}^{\alpha\beta}(\boldsymbol{r}) = \frac{\delta E_{xc}\left[\rho\right]}{\delta\rho^{\alpha\beta}} \ . \tag{3.88}$$

The density matrix $\rho(\boldsymbol{r})$ which has been introduced in equation (3.84) is a hermitian 2×2 matrix. It can be diagonalized by the unitary transformation

$$\sum_{\alpha\beta} U^{i\alpha}(\boldsymbol{r})\, \rho^{\alpha\beta}(\boldsymbol{r})\, U^{\beta j\,\dagger}(\boldsymbol{r}) = \delta^{ij}\rho^{i}(\boldsymbol{r}) \tag{3.89}$$

which implies

$$\frac{\delta\rho^{i}}{\delta\rho^{\alpha\beta}} = U^{i\alpha}U^{\beta j\,\dagger}\,. \tag{3.90}$$

The matrix $\mathbf{U}(\boldsymbol{r}) = \mathbf{U}\left(\theta(\boldsymbol{r}), \varphi(\boldsymbol{r})\right)$ turns out to be the common spin-$\frac{1}{2}$ rotation matrix

$$\mathbf{U}\left(\theta, \varphi\right) = \begin{pmatrix} \cos\frac{\theta}{2} & \sin\frac{\theta}{2} \\ -\sin\frac{\theta}{2} & \cos\frac{\theta}{2} \end{pmatrix} \begin{pmatrix} \exp\left(\frac{\mathrm{i}\varphi}{2}\right) & 0 \\ 0 & \exp\left(-\frac{\mathrm{i}\varphi}{2}\right) \end{pmatrix} \tag{3.91}$$

and θ and φ are polar angles that depend on the position $\boldsymbol{r}$. In many applications, for instance in ferromagnetic and antiferromagnetic solids, a common magnetization axis exists for all atoms. The unitary operator $\mathbf{U}(\boldsymbol{r})$ becomes independent of $\boldsymbol{r}$ in this case. This has the simplifying consequence that the energy and all other physical obervables are functionals of the electron density $n(\boldsymbol{r})$ and of the magnitude of the magnetization density $m(\boldsymbol{r}) = |\boldsymbol{m}(\boldsymbol{r})|$ rather than of the vector $\boldsymbol{m}(\boldsymbol{r})$ [17].

3.6 Density-Functional-Theory for Noncollinear Systems

The present section will introduce the concept of noncollinearity in density functional theory. For this reason equation (3.90) is used to derive an expression for the energy exchange correlation potential (3.88) using the eigenvalues ρ^{i} of the density matrix

$$V_{xc}^{\alpha\beta} = \frac{\delta E_{xc}}{\delta\rho^{\alpha\beta}} = \sum_{i=1}^{2} \frac{\delta E_{xc}}{\delta\rho^{i}} \frac{\delta\rho^{i}}{\delta\rho^{\alpha\beta}} = \sum_{i=1}^{2} \frac{\delta E_{xc}}{\delta\rho^{i}}\, U^{i\alpha}U^{\beta j\,\dagger}\,. \tag{3.92}$$

As it is shown in [15] the exchange-correlation potential can be expressed in terms of the rotated Pauli spin matrix

$$\tilde{\sigma}_z = \mathbf{U}^{\dagger}\sigma_z\mathbf{U} = \begin{pmatrix} \cos\theta & \mathrm{e}^{-\mathrm{i}\varphi}\sin\theta \\ \mathrm{e}^{\mathrm{i}\varphi}\sin\theta & -\cos\theta \end{pmatrix}\,. \tag{3.93}$$

Under the assumption that the external potential $\mathbf{V}_{ext}$ is diagonal the matrix of the effective potential can be written as

$$\mathbf{V}_k^{eff} = V_0\mathbf{1} + \Delta V\tilde{\sigma}_z \tag{3.94}$$

where V_0 is given as

$$V_0 = V_{ext} + e^2\int \mathrm{d}^3r' \, \frac{n(\boldsymbol{r}')}{|\boldsymbol{r}-\boldsymbol{r}'|} + \frac{1}{2}\sum_{i=1}^{2}\frac{\delta E_{xc}}{\delta\rho^i} \tag{3.95}$$

and ΔV accounts to

$$\Delta V = \frac{1}{2}\left(\frac{\delta E_{xc}}{\delta\rho^1} - \frac{\delta E_{xc}}{\delta\rho^2}\right) . \tag{3.96}$$

Consequently a solution of

$$\left[-\mathbf{1}\frac{\hbar^2}{2m}\triangle + \mathbf{V}_k^{eff}(\boldsymbol{r})\right]\boldsymbol{\phi}(\boldsymbol{r}) = \boldsymbol{\varepsilon}\boldsymbol{\phi}(\boldsymbol{r}) , \tag{3.97}$$

where $\boldsymbol{\phi}$ is a two component spinor, and the effective potential is given by

$$\mathbf{V}_k^{eff} = \mathbf{1}V_0(\boldsymbol{r}) + \Delta V(\boldsymbol{r})\mathbf{U}^\dagger(\boldsymbol{r})\sigma_z\mathbf{U}(\boldsymbol{r}) , \tag{3.98}$$

has to be found.

According to [15] the spin density is small between the atoms so that the portions of the nonvanishing spin density can be enclosed by atomic spheres whose size may be chosen such that they cover all of space. Inside those spheres the spin quantization axis is assumed to be equal for all points $\boldsymbol{r}$. In the case of noncollinearity the direction of the vector of magnetization may differ from sphere to sphere. Consequently a local coordinate system is introduced for each sphere and the $\boldsymbol{r}$ dependence of the matrix $\mathbf{U}$ is replaced by a discrete index ν accounting for the different atomic spheres. Equation (3.97) then reads

$$\left[-\mathbf{1}\frac{\hbar^2}{2m}\triangle + \mathbf{U}_\nu^\dagger\,\mathbf{V}_\nu(\boldsymbol{r})\,\mathbf{U}_\nu\right]\boldsymbol{\phi}_\nu(\boldsymbol{r}) = \boldsymbol{\varepsilon}_\nu\boldsymbol{\phi}_\nu(\boldsymbol{r}) , \tag{3.99}$$

where the effective potential of atom ν is defined as

$$\mathbf{V}_\nu = \mathbf{1}V_{0\,\nu}(\boldsymbol{r}) + \Delta V_\nu(\boldsymbol{r})\sigma_z . \tag{3.100}$$

In the local coordinate system the density matrix is diagonal. The angles θ_ν and φ_ν give the orientation of the local coordinate system with respect to the global coordinate system which is attached to the crystal lattice.

3.7 Local-Density Approximation

The Kohn-Sham equations as they have been presented in section (3.4.2) contain the exchange-correlation functional V_{xc}. It has already been mentioned that the exchange energy of the electron gas is the basis of the local density approximation, LDA. The ansatz of the local-density approximation is to write the exchange-correlation functional as

$$E_{xc}[n] = \int \mathrm{d}^3 r \, n(\boldsymbol{r}) \, \epsilon_{xc} \left(n(\boldsymbol{r}) \right) \tag{3.101}$$

where it is assumed that the kinetic exchange-correlation energy is included in E_{xc}. ϵ_{xc} is a function of the density instead of a functional. Equation (3.101) may be viewed as dividing the inhomogenous electron system into small boxes where each box contains a homogenous interacting electron gas with a density $n(\boldsymbol{r})$ appropriate for the box at $\boldsymbol{r}$.

Using the Hartree-Fock exchange energy, equation (3.51) it is possible to find an expression for ϵ_{xc}, where the correlation energy for instance stems from quantum Monte Carlo simulations. The local-density approximation can be carried out for spin polarized problems as well. As it is based on the homogenous electron gas it is valid when the spin densities are slowly varying over space. As a result the local-density approximation often fails in the descriptions of atoms and molecules where density is not slowly varying [15].

3.8 Generalized Gradient Approximation

The generalized gradient approximation, GGA, is an improvement of the local-density approximation. This method relies on the fact that one is rather free in determining the exchange-correlation energy E_{xc}. The improvement consists in the inclusion of derivative terms. Consequently the exchange-correlation energy within a generalized gradient approximation delivers some semi-local information

$$E_{xc}^{GGA}[n] = \int \mathrm{d}^3 r \, \epsilon_{xc}^{GGA} \left(n\left(\boldsymbol{r}\right), \left|\nabla n\left(\boldsymbol{r}\right)\right| \right) \ . \tag{3.102}$$

There is neither a standard functional for the local density approximation nor for the generalized gradient approximation. The present work uses the PBE functional by Perdew, Burke and Ernzerhof [19].

3.9 The L(S)DA + U Approach

In the case of systems with strongly correlated d and f electrons the methods that have been discussed up to now often fail. The strong correlations are caused by the extensive overlap of the electrons' localized orbitals, which leads to strong Coulomb interactions. In order to take into account the local Coloumb interactions one supplements the LDA Hamiltonian $\mathbf{H}_{\mathrm{LDA}}$ with a term representing the on site Coulomb repulsion by a Hubbard U and an exchange energy term J. In the formalism of second quantization the respective Hamiltonian reads

$$\begin{aligned}\mathbf{H} = \mathbf{H}_{\mathrm{LDA}} - \mathbf{H}^{U}_{\mathrm{LDA}} + \frac{1}{2}\sum_{il}{\sum_{m\sigma,m'\sigma'}}' U^{\sigma\sigma'}_{mm'}\mathbf{n}_{ilm\sigma}\mathbf{n}_{ilm'\sigma'} \\ - \frac{1}{2}\sum_{il}{\sum_{m\sigma,m'}}' J_{mm'}\mathbf{c}^{\dagger}_{ilm\sigma}\mathbf{c}^{\dagger}_{ilm'\overline{\sigma}}\mathbf{c}_{ilm'\sigma}\mathbf{c}_{ilm\overline{\sigma}}\ ,\end{aligned} \tag{3.103}$$

where $\mathbf{n}_{ilm\sigma} = \mathbf{c}^{\dagger}_{ilm\sigma}\mathbf{c}_{ilm\sigma}$ and $\mathbf{c}^{\dagger}_{ilm\sigma}$ is a fermionic creation operator. The prime over the sum in equation (3.103) indicates that at least two of the indices of an operator have two be different. Moreover $\overline{\sigma} = \downarrow$ ($\uparrow$) for $\sigma = \uparrow$ ($\downarrow$). A term $\mathbf{H}^{U}_{\mathrm{LDA}}$ is subtracted to avoid double-counting of those contributions of the local Coulomb interaction which are already contained in $\mathbf{H}_{\mathrm{LDA}}$. Nevertheless double-counting cannot be avoided totally. Therefore the LDA energy of the d electrons is corrected by the approximation

$$E^{U}_{\mathrm{LDA}} = \frac{1}{2}\overline{U}n_d(n_d - 1) - \frac{1}{2}\overline{J}\sum_{\sigma} n_{d\sigma}(n_{d\overline{\sigma}} - 1)\,, \tag{3.104}$$

where $n_{d\sigma} = \sum_m \langle \mathbf{n}_{ilm\sigma}\rangle$ is the total number of interacting electrons per spin and $n_d = \sum_\sigma n_{d\sigma}$. $\overline{U}$ is the average Coloumb repulsion and $\overline{J}$ the average exchange energy [20].

In this thesis the rotationally invariant L(S)DA + U approach of Dudarev et al. [21]

$$E_{\mathrm{LSDA}+U} = E_{\mathrm{LSDA}} + \frac{\overline{U} - \overline{J}}{2}\sum_{\sigma}\left[\left(\sum_{m} n^{\sigma}_{m,m}\right) - \left(\sum_{m,m'} \mathbf{n}^{\sigma}_{m,m'}\mathbf{n}^{\sigma}_{m',m}\right)\right] \tag{3.105}$$

is used. This approach has first been used to describe the localized $3d$ electrons on Nickel sites in NiO. In contrast to the common approach which has been discussed above, $\overline{U}$ and $\overline{J}$ do not enter the energy correction to the usual LDA energy seperatly in this approach. Only their difference $\overline{U} - \overline{J}$ is important. Due to the fact that the PAW potentials, which are used for all calculations of this work, are built for the PBE functional it should strictly be spoken about PBE + U calculations.

3.10 Hartree-Fock Hybrid Functionals

In section (3.3.2) the Hartree-Fock approximation for many body systems has been discussed. The result of this discussion were the so called Hartree-Fock equations (3.49). The remarkable term of these equations is the exchange term, which is caused by the antisymmetry of the Slater determinant. This exchange term lowers the energy of the system due to the fact that it takes into acount that particles with like spin are not allowed to stay at the same place.
As the name suggests the Hartree-Fock hybrid functional method is based on the construction of hybrid functionals which are a mixture of the Hartree-Fock exchange and the usual GGA term. On the contrary the correlation energy is only treated by GGA. The exchange correlation energy for the hybrid functional method is therefore defined as

$$E_{xc}^{hybrid} = aE_x^{HF} + (1-a)E_x^{GGA} + E_c^{GGA} \ . \tag{3.106}$$

In equation (3.106) a mixing coefficient a has been introduced. This coefficient is determined by using a comparison of other advanced methods of treating many body systems. Although the hybrid functional method was an improvement in comparsion to the GGA, calculations in solids using this method were nearly impossible until 2003. This was caused by the problem that the Coulomb potential, which occurs in the Hartree-Fock term, decays slowly. Therefore a lot of computing power was needed for these calculations.
In 2003 Heyd, Scuseria and Ernzerhof came up with a new hybrid functional which is based on the assumption of a screened Coulomb potential for the exchange term [22]. By establishing this assumption and by distinguishing long- and short ranged parts of the Coulomb interaction they solved the problem caused by the $\frac{1}{r}$ potential's decay.
After modifications of the respective HSE03 functional the so called HSE06 functional has been introduced in 2006. This functional has been used for the HSE calculations of this work.

4 Spin Spiral Structures

4.1 Motivation

In general non-collinear systems have to be treated with the methods that have been introduced in chapter 3. The treatment of the special case of periodical spin spiral structures will be discussed now. The crystal lattice is defined by three Bravais vectors $\boldsymbol{a_1}$, $\boldsymbol{a_2}$ and $\boldsymbol{a_3}$ and a respective basis

$$\boldsymbol{R}_j = n_{1j}\boldsymbol{a_1} + n_{2j}\boldsymbol{a_2} + n_{3j}\boldsymbol{a_3} \; . \tag{4.1}$$

In chapter 3.6, where the treatment of non-collinear systems from first principles has been discussed, an index ν for the different atomic spheres within the unit cell has been introduced. Each atom inside the unit cell is characterized by its position $\boldsymbol{\tau}_\nu$ and its spin quantization axis which is defined by the angles θ_ν and φ_ν. The atomic information is defined by the potential $\mathbf{V}_\nu(r_{j\nu})$ where $r_{j\nu} = |\boldsymbol{r} - \boldsymbol{R}_j - \boldsymbol{\tau}_\nu|$. The potential is spherical and centered at the lattice point $\boldsymbol{r}_{j\nu} = \boldsymbol{R}_j + \boldsymbol{\tau}_\nu$. Moreover the potential vanishes outside a shell $r_{j\nu} > s_{j\nu}$.
For mapping the spinor $\boldsymbol{\phi}_\nu = (\phi_{\uparrow\nu}, \phi_{\downarrow\nu})$ onto the global quantization axis the already mentioned spin-$\frac{1}{2}$ rotation matrix $\mathbf{U}_\nu(\theta_\nu, \varphi_\nu)$ is used

$$\phi_\sigma = \mathbf{U}_\nu(\theta_\nu, \varphi_\nu)\, \phi_{\nu\sigma} \; . \tag{4.2}$$

The Hamiltonian of such a system is given by the kinetic energy plus the sum over all effective potentials in the global representation

$$\mathbf{H} = -\mathbf{1}\frac{\hbar^2}{2m}\triangle + \sum_{j\nu} \mathbf{U}_\nu^\dagger \, \mathbf{V}_\nu(r_{j\nu}) \, \mathbf{U}_\nu \; , \tag{4.3}$$

equation (3.99).

In chapter 2 it has been shown that for a periodic crystal struture the translation operator $\mathbf{T}_j$ commutes with the Hamiltonian leading to Bloch's theorem.

In a material which exhibits spin spiral behaviour the magnetic moments are trav-

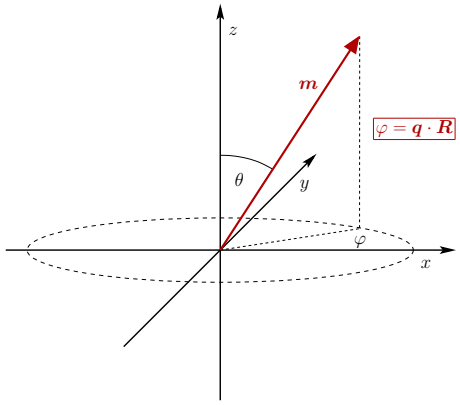

Figure 4.1: Vector of magnetization $\boldsymbol{m}$ for a distinct lattice position.

elled periodically through the lattice. As a consequence the direction of the vector of magnetization $\boldsymbol{m}_{j\nu}$ of atom ν varies for different lattice positions $\boldsymbol{R}_j$

$$\boldsymbol{m}_{j\nu} = m_\nu \begin{pmatrix} \cos\left(\boldsymbol{q} \cdot \boldsymbol{R}_j + \varphi_\nu\right) \sin\theta_\nu \\ \sin\left(\boldsymbol{q} \cdot \boldsymbol{R}_j + \varphi_\nu\right) \sin\theta_\nu \\ \cos\theta_\nu \end{pmatrix} . \tag{4.4}$$

Here m_ν is the magnitude of the magnetic moment at site $\boldsymbol{\tau}_\nu$. Figure 4.1 shows the underlying geometry. The moments for distinct lattice sites are consequently no longer parallel as it is the case for the situation described above. Figure 4.2 shows a sketch of a conical and a flat spin spiral structure. In such a structure the angle φ depends on the lattice index j leading to

$$\varphi_{j\nu} = \varphi_\nu + \boldsymbol{q} \cdot \boldsymbol{R}_j \, . \tag{4.5}$$

4.2 Generalized Bloch Theorem

It has been shown that for materials with spin spiral structures the first Brillouin zone still governs all of the information, which leads to the generalized Bloch theorem. This theorem can only be proven in absence of spin orbit coupling.
The symmetry operators $\{\mathbf{U}_{j\nu}|\mathbf{T}_j\}$ which describe a spin spiral structure combine a translation $\mathbf{T}_j$, see equation (2.5), and a spin rotation by the angle $\boldsymbol{q} \cdot \boldsymbol{R}_j$, which is described by the rotation matrix $\mathbf{U}_{j\nu}(\theta_\nu, \varphi_\nu + \boldsymbol{q} \cdot \boldsymbol{R}_j)$. These symmetry operators act

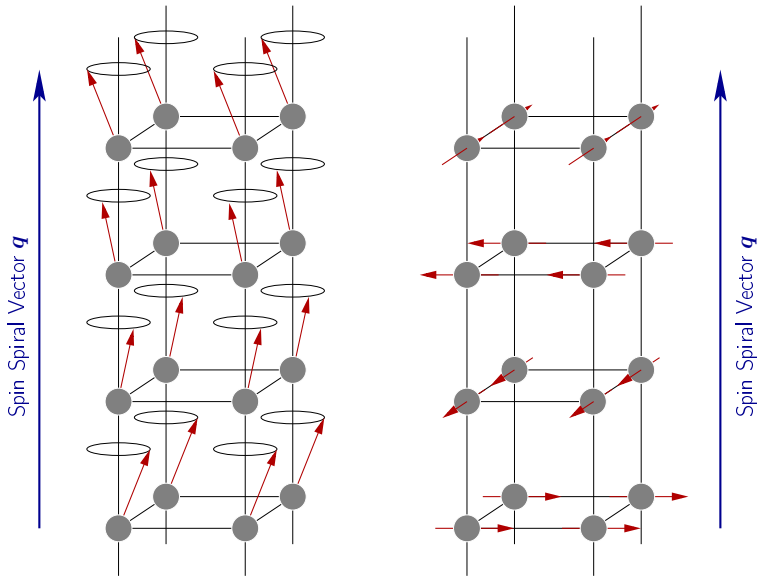

Figure 4.2: Conical and flat spin spiral structures.

on a spinor function $\boldsymbol{\phi}_\nu(\boldsymbol{r})$ as

$$\{\mathbf{U}_{j\nu}|\mathbf{T}_j\}\boldsymbol{\phi}_\nu(\boldsymbol{r}) = \begin{pmatrix} \cos\frac{\theta_\nu}{2} & \sin\frac{\theta_\nu}{2} \\ -\sin\frac{\theta_\nu}{2} & \cos\frac{\theta_\nu}{2} \end{pmatrix} \begin{pmatrix} \mathrm{e}^{\frac{\mathrm{i}(\varphi_\nu+\boldsymbol{q}\cdot\boldsymbol{R}_j)}{2}} & 0 \\ 0 & \mathrm{e}^{-\frac{\mathrm{i}(\varphi_\nu+\boldsymbol{q}\cdot\boldsymbol{R}_j)}{2}} \end{pmatrix} \boldsymbol{\phi}_\nu(\boldsymbol{r}+\boldsymbol{R}_j)\ . \quad (4.6)$$

The rotation matrix $\mathbf{U}_{j\nu}$ can be split into a lattice periodic part $\mathbf{\Pi}_j(\boldsymbol{q}\cdot\boldsymbol{R}_j)$ and a lattice independent part $\mathbf{U}_\nu(\theta_\nu,\varphi_\nu)$

$$\mathbf{U}_{j\nu}(\theta_\nu,\varphi_\nu+\boldsymbol{q}\cdot\boldsymbol{R}_j) = \mathbf{U}_\nu(\theta_\nu,\varphi_\nu)\mathbf{\Pi}_j(\boldsymbol{q}\cdot\boldsymbol{R}_j) \quad (4.7)$$

where $\mathbf{U}_\nu$ is again the spin-$\frac{1}{2}$ rotation matrix, see equation (3.91), and $\mathbf{\Pi}_j$ is given by

$$\mathbf{\Pi}_j(\boldsymbol{q}\cdot\boldsymbol{R}_j) = \begin{pmatrix} \mathrm{e}^{\frac{\mathrm{i}\boldsymbol{q}\boldsymbol{R}_j}{2}} & 0 \\ 0 & \mathrm{e}^{-\frac{\mathrm{i}\boldsymbol{q}\boldsymbol{R}_j}{2}} \end{pmatrix}\ . \quad (4.8)$$

The Hamiltonian of a spin spiral $\mathbf{H}_{\boldsymbol{q}}$ now reads

$$\mathbf{H}_{\boldsymbol{q}} = -\frac{\hbar^2}{2m}\triangle\mathbf{1} + \sum_{j\nu}\mathbf{\Pi}_j^\dagger(\boldsymbol{q}\cdot\boldsymbol{R}_j)\mathbf{U}_\nu^\dagger(\theta_\nu,\varphi_\nu)\mathbf{V}_\nu(r_{j\nu})\mathbf{U}_\nu(\theta_\nu,\varphi_\nu)\mathbf{\Pi}_j(\boldsymbol{q}\cdot\boldsymbol{R}_j)\ , \quad (4.9)$$

and it commutes with the helix-operators $\{\mathbf{\Pi}_j(\boldsymbol{q}\cdot\boldsymbol{R}_j)|\mathbf{T}_j\}$

$$[\{\mathbf{\Pi}_j(\boldsymbol{q}\cdot\boldsymbol{R}_j)|\mathbf{T}_j\},\mathbf{H}_{\boldsymbol{q}}] = 0\ . \quad (4.10)$$

These operators obey the law of multiplication

$$\{\mathbf{\Pi}_j(\boldsymbol{q}\cdot\boldsymbol{R}_j)|\mathbf{T}_j(\boldsymbol{R}_j)\}\{\mathbf{\Pi}_j(\boldsymbol{q}\cdot\boldsymbol{R}'_j)|\mathbf{T}_j(\boldsymbol{R}'_j\} = \{\mathbf{\Pi}_j\left[\boldsymbol{q}\cdot\left(\boldsymbol{R}_j+\boldsymbol{R}'_j\right)\right]|\mathbf{T}_j(\mathbf{R}_j+\mathbf{R}'_j)\} \quad (4.11)$$

and therefore form a cyclic abelian group [23]. As a consequence the helix-operators are isomorphic with the lattice translation operator $\mathbf{T}_j$. If two groups are isomorphic they have the same irreducible representation. Due to the fact that the irreducible representation of ordinary space translations constitutes Bloch's theorem, see equation (2.14), the already mentioned *generalized Bloch theorem* for a spin spiral structure

$$\{\mathbf{\Pi}_j(\boldsymbol{q}\cdot\boldsymbol{R}_j)|\mathbf{T}_j(\boldsymbol{R}_j)\}\,\boldsymbol{\psi}_{\boldsymbol{k}}(\boldsymbol{r}) = \mathrm{e}^{\mathrm{i}\boldsymbol{k}\boldsymbol{R}_j}\boldsymbol{\psi}_{\boldsymbol{k}}(\boldsymbol{r}) \quad (4.12)$$

is obtained.

In equation (4.12) the spinors $\boldsymbol{\psi}_{\boldsymbol{k}}$ are eigenspinors of the Hamiltonian $\mathbf{H}_{\boldsymbol{q}}$ due to equation (4.10). It is possible to derive the generalized Bloch theorem because a spin spiral $\boldsymbol{m}_{j\nu}$ as it has been defined in equation (4.5) does not break the translational symmetry of the lattice. The generalized Bloch theorem is independent of the choice of $\boldsymbol{q}$. A practical consequence of this fact is that no supercells are needed to solve the Kohn-Sham-Schrödinger equation in the presence of spin spirals. It therefore suffices to pick any $\boldsymbol{q}$ inside the first Brillouin zone of the crystal. $\boldsymbol{q}$-vectors outside the first Brillouin zone yield no new information. [15]

5 Heisenberg Model

5.1 Magnons

The quantum mechanical Heisenberg Model is a model to describe the pairwise interaction of localized spins, which leads to a long range magnetic order. In contrast to the Weiss model the Heisenberg model treats the spins as quantum mechanical observables. Another difference between these two models is that the Heisenberg model is not a mean field model. The Heisenberg Hamiltonian [7] reads

$$\mathbf{H} = -I_h \sum_{l\,\delta} \boldsymbol{S}_l \boldsymbol{S}_{l+\delta} - g_j \mu_B H_{ext} \sum_l S_{zl} \; . \tag{5.1}$$

It is assumed that the spins sit on lattice sites l. The index δ is used to replace the vector pointing to the nearest-neighbor sites. I_h is the so called exchange integral which is defined positive for the ferromagnetic and negative for the antiferromagnetic case. H_{ext} is an external magnetic field which is applied along the z axis. This field is greater than zero so that for $T = 0\,\mathrm{K}$ all spins are aligned parallel to this field. A ground state is formed, which is described by a state vector $|0\rangle$.
As it is shown in detail in [7] the Heisenberg Hamiltonian can be rewritten in magnon variables. It should be noted that the magnon operators which occur throughout this calculation are of bosonic character. This can be explained by figure 5.1, which shows a single particle excitation moving through a chain of ferromagnetically ordered spins. If a spin travels through the chain always two neighboring spins are involved and therefore the excitation is of bosonic character. In reality such single particle excitations are unlikely because they cost to much energy. Instead of single particle excitations, collective excitations, so called spin waves can be verfied. Quantized spin waves are called magnons. These magnons can be obtained by solving the Heisenberg

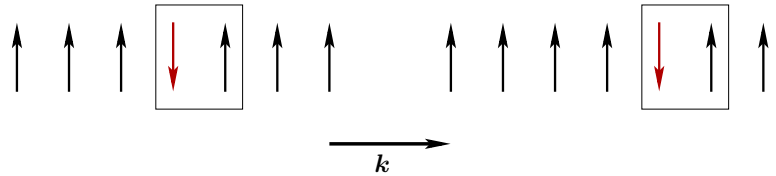

Figure 5.1: Single particle excitation moves through chain of spins.

model using magnon variables. The respective dispersion relation reads

$$\omega_{\boldsymbol{k}} = 2I_h Sz \left[1 - \frac{1}{z}\sum_{\delta} \cos\left(\boldsymbol{k}\boldsymbol{\delta}\right)\right] + g_j \mu_B H_{ext} \ , \tag{5.2}$$

where z is the number of nearest neighbors. In (5.2) the cosine can be expanded as

$$\cos x = 1 - \frac{x^2}{2} + \ldots \tag{5.3}$$

so that $\omega_{\boldsymbol{k}}$ becomes

$$\omega_{\boldsymbol{k}} \simeq I_h S \sum_{\delta} \left(\boldsymbol{k}\boldsymbol{\delta}\right)^2 + g_j \mu_B H_{ext} \ . \tag{5.4}$$

For a cubic lattice with lattice constant a_0 this expression can be simplified to

$$\omega_{\boldsymbol{k}} = g_j \mu_B H_{ext} + 2I_h S \left(\boldsymbol{k} a_0\right)^2 \tag{5.5}$$

$$= g_j \mu_B H_{ext} + Dk^2 \ . \tag{5.6}$$

In equation (5.6) the spin wave stiffness constant D has been introduced. It can be measured by inelastic neutron scattering. Figure 5.2 shows a classical representation of an excitation described by the Heisenberg model. Figure 5.3 shows a typical magnon dispersion as well as the quadratic approximation for low excitation energies.

5.2 Mean Field Solutions of the Heisenberg Model

In a general way the Heisenberg model not only takes into account the interaction between the nearest-neighbor shell but in fact sums over a larger number of neighboring shells

$$\mathbf{H} = -\sum_{i \neq j} I_{ij} \boldsymbol{S}_i \boldsymbol{S}_j \tag{5.7}$$

where I_{ij} are the exchange integrals between spins located on sites i and j. In order to simplify this model different approaches have been suggested such as the Ising model and the XY-model. In this section we will discuss a mean field ansatz.

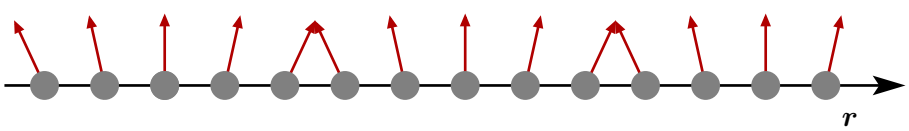

Figure 5.2: Example for an excitation described by the Heisenberg model.

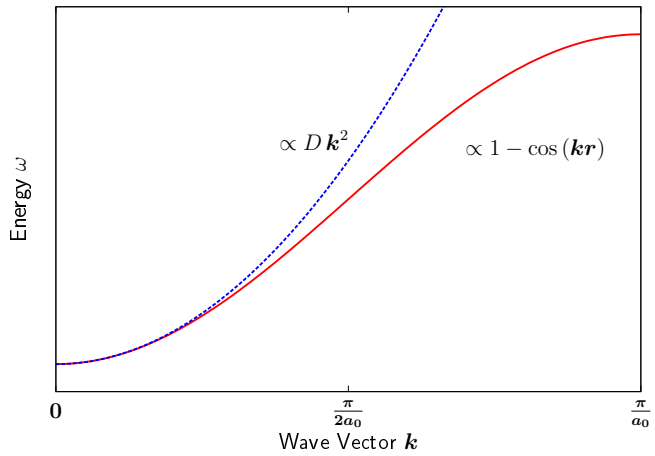

Figure 5.3: Magnon dispersion and quadratic approximation.

In the mean field ansatz the pairwise interaction in equation (5.7) is replaced by the interaction of a single spin with a field, which is generated by all the other neighboring ones. This is achieved by replacing the spin operator by its mean value plus deviations from it, which are commonly referred to as fluctuations

$$\boldsymbol{S}_k = \langle \boldsymbol{S}_k \rangle + (\boldsymbol{S}_k - \langle \boldsymbol{S}_k \rangle) \ . \tag{5.8}$$

This expression now enters equation (5.7)

$$(5.7) = -\sum_{i \neq j} I_{ij} \left\{ \left[\langle \boldsymbol{S}_i \rangle + (\boldsymbol{S}_i - \langle \boldsymbol{S}_i \rangle) \right] \left[\langle \boldsymbol{S}_j \rangle + (\boldsymbol{S}_j - \langle \boldsymbol{S}_j \rangle) \right] \right\} \ . \tag{5.9}$$

Now the terms are multiplied out and terms which are of second order in the fluctuations are neglected. This yields the molecular field Hamiltonian

$$\begin{aligned} \mathbf{H}_{MF} &= \sum_{i \neq j} I_{ij} \langle \boldsymbol{S}_i \rangle \langle \boldsymbol{S}_j \rangle - \sum_{i \neq j} I_{ij} \left(\boldsymbol{S}_j \langle \boldsymbol{S}_i \rangle + \boldsymbol{S}_i \langle \boldsymbol{S}_j \rangle \right) \\ &= \sum_{i \neq j} I_{ij} \langle \boldsymbol{S}_i \rangle \langle \boldsymbol{S}_j \rangle - \sum_i \boldsymbol{S}_i \left[2 \sum_j I_{ij} \langle \boldsymbol{S}_j \rangle \right] \ . \end{aligned} \tag{5.10}$$

While the first term in equation (5.10) is a constant, the second term can be interpreted as as a spin on lattice site i interacting with a field, which is produced by all neighboring spins at lattice sites j. Since this form of interaction is equal to the interaction which

is described by the Weiss model, the solution to the problem is the Brillouin function

$$\mathcal{B}(a, J) = \frac{2J+1}{2J} \coth\left(a\frac{2J+1}{2J}\right) - \frac{1}{2J}\coth\left(\frac{a}{2J}\right) \ , \tag{5.11}$$

where

$$a = \frac{Jg_j\mu_B H}{k_B T} \ . \tag{5.12}$$

The Curie temperature is thus given by

$$T_C = \frac{2S(S+1)}{3k_B}\frac{1}{N}\sum_{i\neq j} I_{ij} \tag{5.13}$$

For an fcc lattice this results in

$$T_C = \frac{2S(S+1)}{3k_B}\frac{1}{78}\left(12J_1 + 6J_2 + 24J_3 + 12J_4 + 24J_5\right) \tag{5.14}$$

where the summation is taken up to the 5^{th} neighbor shell. For a bcc lattice (5.13) yields

$$T_C = \frac{2S(S+1)}{3k_B}\frac{1}{58}\left(8J_1 + 6J_2 + 12J_3 + 24J_4 + 8J_5\right) \tag{5.15}$$

The results for T_C are usually in fair agreement with experiment, although they are systematically too high, which is typically of the mean field approximation, which suppresses additional quantum fluctuations [7].

6 Spin Spiral Calculations using VASP

6.1 Vienna Ab-initio Simulation Package, VASP

The *Vienna Ab-initio Simulation Package*, VASP, is a computer program for atomic scale materials modelling, e.g. electronic structure calculations and quantum mechanical molecular dynamics, from first principles.
VASP computes an approximate solution to the many-body Schrödinger equation, either within density functional theory (DFT), solving the Kohn-Sham equations, or within the Hartree-Fock (HF) approximation, solving the Roothaan equations. Hybrid functionals that mix the Hartree-Fock approach with density functional theory are implemented as well. Furthermore, Green's functions methods and many-body perturbation theory are available in VASP.
In VASP, central quantities, like the one-electron orbitals, the electronic charge density, and the local potential are expressed in plane wave basis sets. The interactions between the electrons and ions are described using norm-conserving or ultrasoft pseudopotentials, or the projector-augmented-wave method [24].

6.2 Controlling Spin Spiral Calculations

This section will give an introduction to the additional tags which have to be defined in the INCAR file in order to make VASP calculate spin spirals. Before going into details is has to be mentioned that the Hartree-Fock hybrid functional by Heyd, Scuseria and Ernzerhof [22] can not be used in the context of spin spiral calculations because of the way spin spirals are implemented in the program. In order to give an appropriate description of semiconductors and insulators one therefore has to switch to the L(S)DA+U approach which has been discussed in section 3.9. Due to the fact that spin spiral excitations are a Fermi surface effect the k-mesh should be chosen as dense as possible.

A non-collinear version of VASP has to be used for these kind of calculations. Non-

collinearity is switched on by setting

$$\text{LNONCOLLINEAR} = \text{TRUE}$$

in the INCAR file. For non-collinear calculations the partial DOS and the PROCAR file are written only if one abstains from parallelization. This is done by setting

$$\text{NPAR} = 1 \ .$$

Usually VASP performs a symmetry analysis and only calculates the energies of the irreducible part of the Brillouin zone. It is recommended to switch off the symmetry analysis for spin spiral calculations

$$\text{ISYM} = 0 \ .$$

The routines for spin spiral calculations are switched on via

$$\text{LSPIRAL} = \text{TRUE} \ .$$

The spin spiral wave vector $\boldsymbol{q}$ is defined by

$$\text{QSPIRAL} = q_x \ q_y \ q_z \ ,$$

where q_x, q_y and q_z have to be defined in reciprocal coordinates.

Although it is in prinicple possible to calculate conical spin spirals with VASP, it is recommended to set

$$\text{LZEROZ} = \text{TRUE} \ .$$

This restrains the magnetic moments to the x-y-plane and therefore realizes a flat spin spiral as it has been shown in figure 4.2. A possibility to realize conical spin spirals is to use the constrained moment routines, which force the system to a distinct magnetic state.

Due to how spin spirals are implemented in the VASP program the information about the local moments, which is usually provided if one sets LORBIT = 11, is lost in the case of spin polarized calculations. Nevertheless there is a way to gain this information.

Therefore following tags have to be specified:

$$\begin{aligned} \text{RWIGS} &= r_1 \ \ldots \ r_n \qquad n \ldots \text{number of ion species} \\ \text{I\_CONSTRAINED\_M} &= 1 \\ \text{LAMBDA} &= 0 \\ \text{M\_CONSTR} &= x_1 \ y_1 \ z_1 \ \ldots \ x_n \ y_n \ z_n \qquad n \ldots \text{number of ions.} \end{aligned}$$

This way the constrained moment routines are switched on. Due to the fact that LAMBDA is set to zero, the constraints do not influence the calculation but additional output in the OSZICAR file for each electronic step is produced. This additional output is the local magnetic moment on each atom. These local magnetic moments are gained by integrating the magnetization density inside spheres of radius RWIGS, the Wigner-Seitz radius, about the atomic positions. Consequently the Wigner-Seitz radius must be specified for each of the n atoms in the cell.

It should be noted that only the magnetic moments which are written to the OSZICAR file are reliable. The values that can be found in the OUTCAR file are wrong due to the use of wrong projection operators.

In contrast to usual calculations two cutoff energies have to be defined for spin spiral calculations. This is because the basis sets at the points k, $k + \frac{q}{2}$ and $k - \frac{q}{2}$ differ. Consequently the cutoff energy, which is specified by the ENCUT-tag must be high enough such that all reciprocal lattice vectors $\boldsymbol{K}$ belonging to the basis sets of $k + \frac{q}{2}$ and $k - \frac{q}{2}$ for an initial energy cutoff, which is defined by the ENINI-tag, are contained. A definition that should usually hold is

$$\begin{aligned} \text{ENINI} &= \text{ENMAX} \\ \text{ENCUT} &= \text{ENINI} + 100 \end{aligned}$$

where ENMAX is the maximum value for the energy cutoff of the system's potentials in eV.

In the course of this work it turned out that the conjugate gradient algorithm is most stable in the context of spin spiral calculations. It is used if

$$\text{ALGO} = \text{Conjugate}$$

is set in the INCAR file.

Usually VASP calculations converge within 60 electronic steps. However spin spiral calculations often converge really slow. Therefore never mind if a spin spiral calculation needs about 150 steps until convergence is reached, since the energies involved are at least of one order of magnitude below the energy for magnetic ordering.

One of the most important points in the context of spin spiral calculations using the VASP program is that the magnetic moments have to be initalized with well suited starting values. This is most important for systems with more than one atom in the unit cell. This is because additional atoms in the unit cell cause additional degrees of freedom and the system may converge to states the user might not expect. The magnetic moments can be initialized using the MAGMOM-tag. An example for how a proper initialization looks like is given in section 6.4.

In order to give an idea of what might happen if one does not initialize the magnetic moments properly a spin spiral calculation for bcc Fe is discussed. In this example the unit cell of bcc Fe has once been built using the standard bcc lattice vectors

$$\boldsymbol{a}_1 = \frac{a}{2}\begin{pmatrix}-1\\1\\1\end{pmatrix},\ \boldsymbol{a}_2 = \frac{a}{2}\begin{pmatrix}1\\-1\\1\end{pmatrix},\ \boldsymbol{a}_3 = \frac{a}{2}\begin{pmatrix}1\\1\\-1\end{pmatrix} \tag{6.1}$$

with one atom in the basis and the other time it has been built using the lattice vectors of a simple cubic cell

$$\boldsymbol{a}_1 = a\begin{pmatrix}1\\0\\0\end{pmatrix},\ \boldsymbol{a}_2 = a\begin{pmatrix}0\\1\\0\end{pmatrix},\ \boldsymbol{a}_3 = a\begin{pmatrix}0\\0\\1\end{pmatrix} \tag{6.2}$$

and two atoms in the basis introducing new degrees of freedom. Figure 6.1 shows a sketch of the crystal structure. The spin spiral wave vector is defined to be parallel to the z-axis. Although the cell is defined in different ways, the dispersion relation is expected to be equivalent for both cases. Figures 6.2a and 6.2b show the results of the calculations for either the magnetic moments being initialized or not at a lattice constant of $a = 5.8$ Å. Due to the additional degrees of freedom the system converged back to the ferromagnetic state for values of $\frac{q}{q_{max}} \geq \frac{1}{2}$ in the not initalized case.

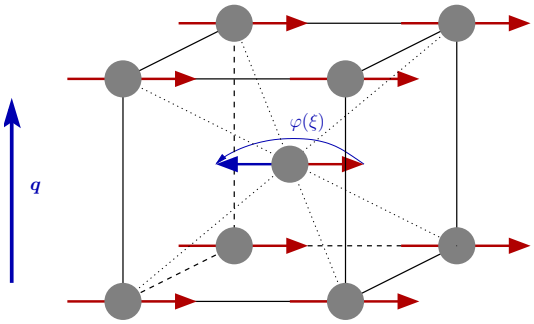

Figure 6.1: Magnetic structure of bcc Fe for $\boldsymbol{q} = \left(0, 0, \frac{2\pi\xi}{a}\right)$, $0 \leq \xi \leq 1$.

6.3 The QSPIRAL-tag

The QSPIRAL-tag defines the spin spiral wave vector $\boldsymbol{q}$, which has to be given in reciprocal coordinates. This section shows how these coordinates are calculated. In order to save some time in future a program that calculates these reciprocal coordinates has been written. This program and how it is used will also be part of this section.

6.3.1 Calculation of q in reciprocal coordinates

Motivation: fcc Lattice, Direction [001]

To generate a magnetic configuration which is equal to figure 6.3b throughout a spin spiral calculation the ansatz

$$\begin{pmatrix} 0 \\ 0 \\ q_z \end{pmatrix} \cdot \begin{pmatrix} r_x \\ r_y \\ \frac{a}{2} \end{pmatrix} = \pi \tag{6.3}$$

is made, where a is the lattice constant. This ansatz leads to

$$q_z \cdot \frac{a}{2} = \pi \ , \tag{6.4}$$

and results in

$$\boldsymbol{q} = \begin{pmatrix} 0 \\ 0 \\ \frac{2\pi}{a} \end{pmatrix} \ . \tag{6.5}$$

Now $\boldsymbol{q}$ has to be transformed to its representation in reciprocal space. As known from basic algebra any vector $\boldsymbol{v}$ can be written in terms of the reciprocal basis

$$\boldsymbol{v} = \sum_{i=1}^{3} x_i \, \boldsymbol{g_i} \ , \tag{6.6}$$

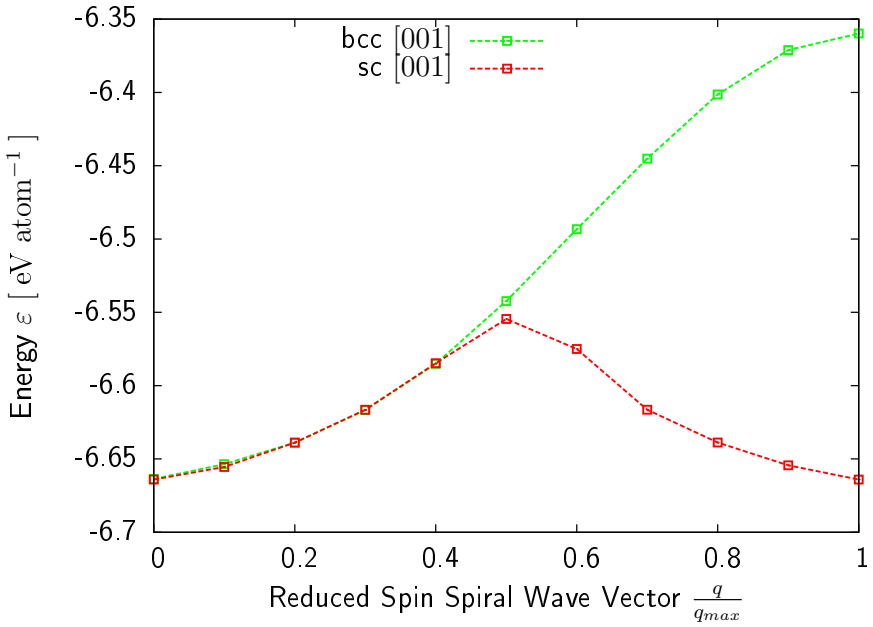

(a) Magnetic moments not initialized.

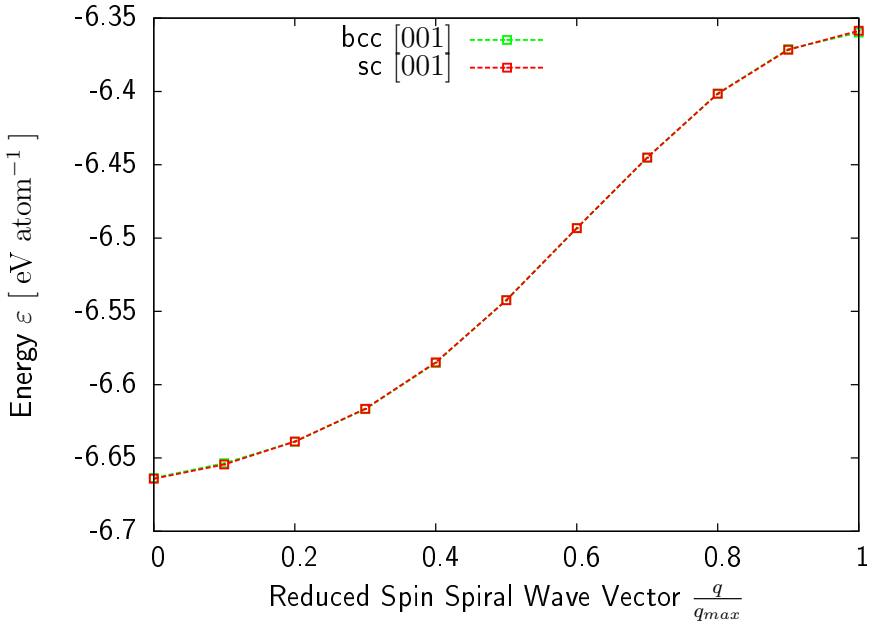

(b) Magnetic moments initialized properly.

Figure 6.2: Comparsion of spin spiral calculations in the crystallographic [001] direction of bcc Fe using different representations of the cell. bcc stands for the calculation where the usual bcc lattice vectors have been used, while sc stands for simple cubic. In cartesian coordinates $\boldsymbol{q}_{max} = \left(0, 0, \frac{2\pi}{a}\right)$.

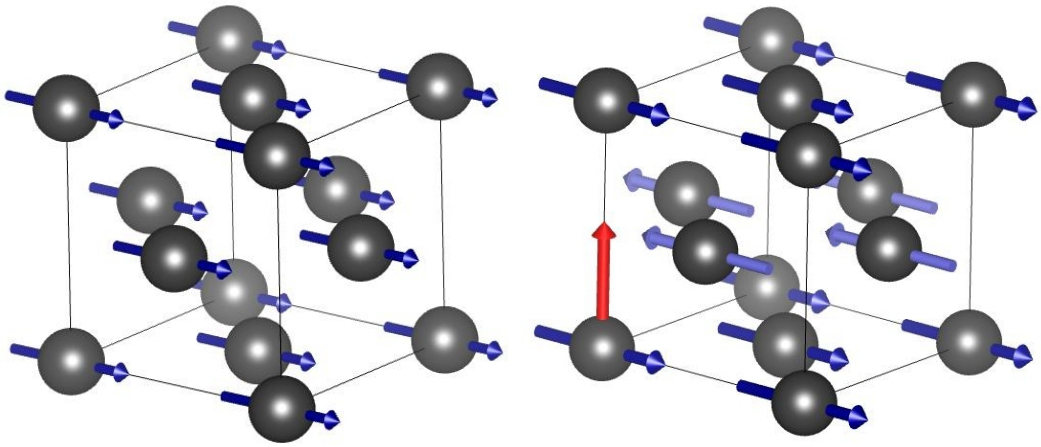

(a) $\boldsymbol{q} = (0, 0, 0)$ (b) $\boldsymbol{q} = \boldsymbol{q}_{max} = \left(0, 0, \frac{2\pi}{a}\right)$

Figure 6.3: Magnetic structure of fcc Fe for different spin spiral vectors.

where the $\boldsymbol{g}_i$ are the reciprocal basis vectors and the x_i are the respective reciprocal coordinates of $\boldsymbol{v}$. The transformation can be done using a matrix which can be calculated using the Gauß-Jordan algorithm. Due to the fact that one of the two basis sets is the cartesian basis this task simplifies to solving following system of equations

$$x_1 \boldsymbol{g}_1 + x_2 \boldsymbol{g}_2 + x_3 \boldsymbol{g}_3 = \begin{pmatrix} 0 \\ 0 \\ \frac{2\pi}{a} \end{pmatrix} . \tag{6.7}$$

Knowing that the reciprocal lattice vectors of an fcc lattice are

$$\boldsymbol{g}_1 = \frac{2\pi}{a} \begin{pmatrix} -1 \\ 1 \\ 1 \end{pmatrix}, \; \boldsymbol{g}_2 = \frac{2\pi}{a} \begin{pmatrix} 1 \\ -1 \\ 1 \end{pmatrix}, \; \boldsymbol{g}_3 = \frac{2\pi}{a} \begin{pmatrix} 1 \\ 1 \\ -1 \end{pmatrix} , \tag{6.8}$$

the reciprocal coordinates x_i can be calculated to be $x_1 = x_2 = \frac{1}{2}$ and $x_3 = 0$. Figure 6.4 shows a comparison of spin spiral calculations along the crystallographic [001] direction for fcc Fe at a lattice constant $a = 3.58$ Å for different representations of the unit cell (simple cubic bravais lattice + 4 atoms in the basis vs. standard fcc bravais lattice + 1 atom in the basis). A spin spiral groundstate is predicted for $\frac{q}{q_{max}} = 0.6$ by this calculation. Further examinations of fcc Fe can be found in [4].
Figure 6.4 may be seen as a proof that the calculated energy does not depend on the Bravais lattice, which is used to represent the material as long as the spin spiral wave

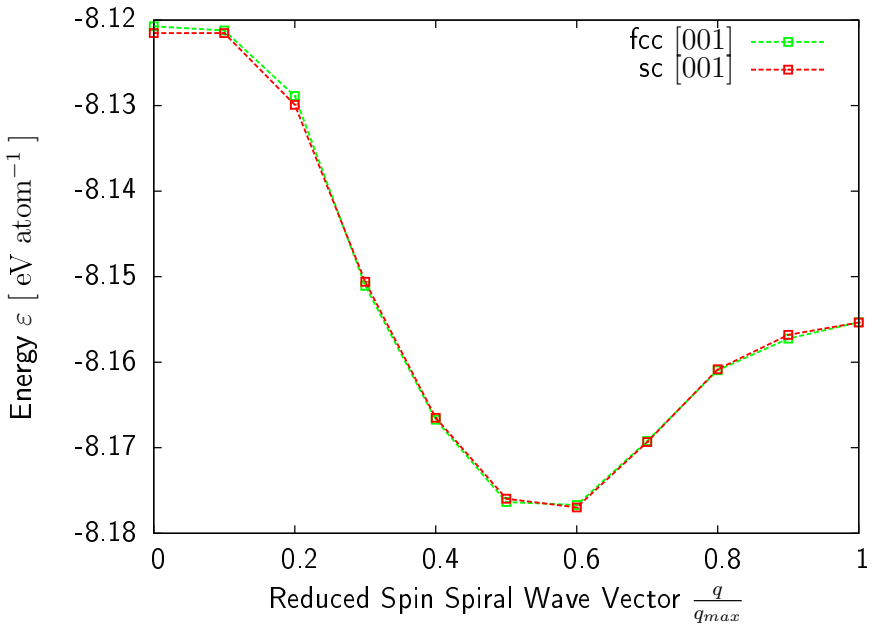

Figure 6.4: Comparison of spin spiral calculations for fcc Fe based on different representations of the cell.

vector's reciprocal coordinates are defined consistently via the QSPIRAL-tag in the INCAR file.

Ansatz for arbitrary directions of q

In order to derive equations which can be used as a starting point for an automated calculation of the spin spiral vector's reciprocal coordinates, one starts as follows. Shall

$$\boldsymbol{r}' = \begin{pmatrix} r'_x \\ r'_y \\ r'_z \end{pmatrix} \tag{6.9}$$

be a lattice position within a plane orthogonal to $\boldsymbol{q}$, which is characterized by

$$\boldsymbol{q} \cdot \boldsymbol{\Delta r} = \boldsymbol{q} \cdot \boldsymbol{r}' = \pi \ . \tag{6.10}$$

where $\boldsymbol{\Delta r} = \boldsymbol{r}' - \boldsymbol{r}''$, with $\boldsymbol{r}'' = (0, 0, 0)$. If equation (6.10) is fulfilled for an ion at lattice site $\boldsymbol{r}$, its magnetic moment is directed oppositely to the magnetic moment of

the atom being placed at the origin of the lattice. Now the ansatz

$$\begin{pmatrix} q_x \\ q_y \\ q_z \end{pmatrix} = \alpha \begin{pmatrix} r'_x \\ r'_y \\ r'_z \end{pmatrix} \tag{6.11}$$

is made. This ansatz does not only constrain the spin spiral wave vector's direction but also defines the spin spiral's phase planes to be orthogonal to $\boldsymbol{r}'$. By using (6.11) equation (6.10) can be simplified to

$$\alpha \left(r_x'^2 + r_y'^2 + r_z'^2 \right) = \pi \; . \tag{6.12}$$

Consequently the coefficient α reads

$$\alpha = \frac{\pi}{r_x'^2 + r_y'^2 + r_z'^2} \; , \tag{6.13}$$

and the components of $\boldsymbol{q}$ result in

$$q_x = \frac{r'_x \, \pi}{r_x'^2 + r_y'^2 + r_z'^2} \; , q_y = \frac{r'_y \, \pi}{r_x'^2 + r_y'^2 + r_z'^2} \; , q_z = \frac{r'_z \, \pi}{r_x'^2 + r_y'^2 + r_z'^2} \; . \tag{6.14}$$

Example: fcc Lattice, Direction [111]

As an example the reciprocal coordinates of $\boldsymbol{q}$ are calculated for the crystallographic [111] direction in an fcc lattice. A possible ansatz is to choose $\boldsymbol{\Delta r}$ as

$$\boldsymbol{\Delta r} = \boldsymbol{r}' = \begin{pmatrix} a \\ a \\ a \end{pmatrix} \; . \tag{6.15}$$

Using equations (6.14) $\boldsymbol{q}$ can be written as

$$\boldsymbol{q} = \frac{\pi}{3a} \begin{pmatrix} 1 \\ 1 \\ 1 \end{pmatrix} \; . \tag{6.16}$$

To obtain the reciprocal coordinates of $\boldsymbol{q}$ one has to transform $\boldsymbol{q}$ to reciprocal space as it has been shown above. Of course the reciprocal lattice vectors are again given

by (6.8). The respective system of equations reads

$$\frac{2\pi}{a}\left[-x_1 + x_2 + x_3\right] = \frac{\pi}{3a} \tag{6.17}$$

$$\frac{2\pi}{a}\left[x_1 - x_2 + x_3\right] = \frac{\pi}{3a} \tag{6.18}$$

$$\frac{2\pi}{a}\left[x_1 + x_2 - x_3\right] = \frac{\pi}{3a} \tag{6.19}$$

and leads to $x_1 = x_2 = x_3 = \frac{1}{6}$.

6.3.2 The program QSPIRAL

Using QSPIRAL

In the course of this work on spin spiral calculations a C program that calculates the spin spiral wave vector $\boldsymbol{q}$ in reciprocal coordinates has been written. The executable version of this program has been called QSPIRAL. It is executed by the command

```
> ./QSPIRAL [path of POSCAR file] [ x1 x2 x3 ]
```

The first parameter is the path of the POSCAR file. From the POSCAR file the lattice constant and the Bravais vectors are read. The second parameter are three numbers. These numbers are the coefficients that are needed to depict $\boldsymbol{\Delta r}$ in the Bravais system. In an fcc lattice the Bravais vectors are

$$\boldsymbol{a}_1 = \frac{a}{2}\begin{pmatrix}0\\1\\1\end{pmatrix},\ \boldsymbol{a}_2 = \frac{a}{2}\begin{pmatrix}1\\0\\1\end{pmatrix},\ \boldsymbol{a}_3 = \frac{a}{2}\begin{pmatrix}1\\1\\0\end{pmatrix}\ . \tag{6.20}$$

The coordinates with respect to these Bravais vectors of the vector

$$\boldsymbol{\Delta r} = \boldsymbol{r}' = x_1\boldsymbol{a}_1 + x_2\boldsymbol{a}_2 + x_3\boldsymbol{a}_3 = \frac{a}{2}\begin{pmatrix}0\\0\\1\end{pmatrix} \tag{6.21}$$

are $x_1 = x_2 = 0.5$ and $x_3 = -0.5$. In this case and if the POSCAR file is located in the same directory as the program, QSPIRAL it is executed by[1]:

[1] It should be noted that in systems where $\boldsymbol{r}'' \neq (0,0,0)$ the resulting shift must be taken into account by the user.

```
> ./QSPIRAL POSCAR 0.5 0.5 -0.5
```

As in the example above the reciprocal coordinates for the spin spiral wave vector turn out to be 0.5, 0.5, 0.0, see listing 6.1. The program's output moreover contains the Bravais vectors in cartesian coordinates, the vector $\boldsymbol{\Delta r}$, which defines the crystal direction of the spin spiral, the spin spiral wave vector $\boldsymbol{q}$ in cartesian coordinates, the lattice constant as well as the cell volume, and the reciprocal lattice vectors in cartesian coordinates.

```
1  ###############################################
   #                Bravais Lattice              #
3  ###############################################

5     [    0.000000,    1.788400,    1.788400 ]
      [    1.788400,    0.000000,    1.788400 ]
7     [    1.788400,    1.788400,    0.000000 ]

9  ###############################################
   #          Chosen Crystal Direction           #
11 ###############################################

13    [    0.000000,    0.000000,    1.788400 ]

15 ###############################################
   #         q in Cartesian Coordinates          #
17 ###############################################

19    [    0.000000,    0.000000,    1.756650 ]

21 ###############################################
   #       Lattice Constant & Cell Volume        #
23 ###############################################

25       a = 3.57680000, V = 11.43994613

27 ###############################################
   #         Reciprocal Lattice Vectors          #
29 ###############################################

31    [   -1.756650,    1.756650,    1.756650 ]
      [    1.756650,   -1.756650,    1.756650 ]
33    [    1.756650,    1.756650,   -1.756650 ]

35 ###############################################
   #                                             #
37 #                Q S P I R A L                #
   #                                             #
39 #     0.50000000    0.50000000    0.00000000  #
   #                                             #
41 ###############################################
```

Listing 6.1: Output of QSPIRAL for a spin spiral along the z-axis in fcc Fe.

Source Code of QSPIRAL

The program QSPIRAL is based on a Gauß-Jordan algorithm to solve the system of equations which has been solved by hand in the sections above. Listing 6.2 shows the source code of the program.

```
// LIBRARIES

#include <stdio.h>
#include <stdlib.h>
#include <string.h>
#include <math.h>

// TYPE DEFINITIONS

struct vector
{
  double x, y, z;
};

// DEFINITION OF FUNCTIONS

struct vector xprod(struct vector a, struct vector b)
{
  struct vector temp;

  temp.x = a.y*b.z - a.z*b.y;
  temp.y = a.z*b.x - b.z*a.x;
  temp.z = a.x*b.y - a.y*b.x;

  return temp;
}

double inprod(struct vector a, struct vector b)
{
  return a.x*b.x + a.y*b.y + a.z*b.z;
}

struct vector mult(double number, struct vector a)
{
  struct vector temp;

  temp.x = number*a.x;
  temp.y = number*a.y;
  temp.z = number*a.z;

  return temp;
}

struct vector add(struct vector a, struct vector b)
{
  struct vector temp;

  temp.x = a.x + b.x;
```

```
49    temp.y = a.y + b.y;
      temp.z = a.z + b.z;
51
      return temp;
53  }

55  void printMATRIX(double matrix[3][5])
    {
57    int i, j;

59    for (i=0; i<3; i++)
      {
61      for (j=0; j<5; j++)
        {
63        printf("%10lf ", matrix[i][j]);
        }
65      printf("\n");
      }
67  }

69  void printVECTOR(struct vector a)
    {
71    printf("    [ %10lf, %10lf, %10lf ]\n", a.x, a.y, a.z);
    }
73
    // MAIN FUNCTION
75
    int main(int argc, char** argv)
77  {
      struct vector r, q_real, q_rec, temp, temp1, bravais[3], reciprocal[3];
79    char *filename=argv[1], dummystring[1000];
      double matrix[3][5], value, change, lattconst, volume;
81    int i, j, k, l, count;
      FILE *file;
83
      // OPEN POSCAR FILE TO READ LATTICE CONSTANT AND BRAVAIS VECTORS
85
      file = fopen(filename, "r");
87    fgets(dummystring, 1000, file);
      fscanf(file, "%lf", &lattconst);
89
      printf("#################################################\n");
91    printf("#                Bravais Lattice                #\n");
      printf("#################################################\n");
93    printf("\n");

95    for (i=0; i<3; i++)
      {
97      fscanf(file, "%lf %lf %lf", &(temp.x), &(temp.y), &(temp.z));
        bravais[i] = mult(lattconst, temp);
99      printVECTOR(bravais[i]);
      }
101   fclose(file);

103   printf("\n");
```

```
    printf("#####################################################\n");
105 printf("#          Chosen Crystal Direction                 #\n");
    printf("#####################################################\n");
107 printf("\n");

109 // r = x*a1 + y*a2 + z*a3 (x,y,z = user input)

111 temp1 = add(mult(atof(argv[2]), bravais[0]),mult(atof(argv[3]), bravais[1]));
    r = add(temp1, mult(atof(argv[4]), bravais[2]));
113
    printVECTOR(r);
115
    printf("\n");
117 printf("#####################################################\n");
    printf("#         q in Cartesian Coordinates                #\n");
119 printf("#####################################################\n");
    printf("\n");
121
    // q_real * r = pi
123
    q_real.x = (M_PI*r.x)/inprod(r,r);
125 q_real.y = (M_PI*r.y)/inprod(r,r);
    q_real.z = (M_PI*r.z)/inprod(r,r);
127
    printVECTOR(q_real);
129
    printf("\n");
131 printf("#####################################################\n");
    printf("#       Lattice Constant & Cell Volume              #\n");
133 printf("#####################################################\n");
    printf("\n");
135
    // volume = a1 * ( a2 x a3 )
137
    volume = inprod(bravais[0], xprod(bravais[1], bravais[2]));
139
    printf("      a = %10.8lf , V = %10.8lf\n", lattconst , volume);
141
    printf("\n");
143 printf("#####################################################\n");
    printf("#         Reciprocal Lattice Vectors                #\n");
145 printf("#####################################################\n");
    printf("\n");
147
    // b1 = 2*pi * ( a2 x a3 ) / volume
149 // b2 = 2*pi * ( a3 x a1 ) / volume
    // b3 = 2*pi * ( a1 x a2 ) / volume
151
    reciprocal[0]=mult(2.0*M_PI/volume, xprod(bravais[1],bravais[2]));
153 reciprocal[1]=mult(2.0*M_PI/volume, xprod(bravais[2],bravais[0]));
    reciprocal[2]=mult(2.0*M_PI/volume, xprod(bravais[0],bravais[1]));
155
    for (i=0; i<3; i++) printVECTOR(reciprocal[i]);
157
    // INITIALIZE THE MATRIX FOR SOLVING THE SYSTEM OF EQUATIONS
```

```
159
    // x1*b1 + x2*b2 + x3*b3 = q_real  =>  matrix*x_i = q_real
161
    for (i=0; i<3; i++) matrix[i][0] = i+1;
163
    for (i=1; i<4; i++)
165 {
      matrix[0][i]=reciprocal[i-1].x;
167   matrix[1][i]=reciprocal[i-1].y;
      matrix[2][i]=reciprocal[i-1].z;
169 }

171 matrix[0][4]=q_real.x;
    matrix[1][4]=q_real.y;
173 matrix[2][4]=q_real.z;

175
    // Gauss-Jordan-ALGORITHM
177
    printf("\n");
179
    j=1;
181 for (i=0; i<3; i++)
    {
183   if (matrix[i][j]==0)
      {
185     if(matrix[i+1][j]!=0)
        {
187       for (count=0; count<5; count++)
          {
189         change = matrix[i][count];
            matrix[i][count] = matrix[i+1][count];
191         matrix[i+1][count] = change;
          }
193     }
        else
195     {
          for (count=0; count<5; count++)
197       {
            change = matrix[i][count];
199         matrix[i][count] = matrix[i+2][count];
            matrix[i+2][count] = change;
201       }
        }
203   }

205   value = matrix[i][j];
      for (l=1; l<5; l++)
207   {
        matrix[i][l]/=value;
209   }
      for (k=i+1; k<3; k++)
211   {
        value = matrix[k][j];
213     for (l=1; l<5; l++)
```

```
      {
215     (matrix[k][l])-=value*(matrix[i][l]);
      }
217   }
    j++;
219 }

221 // CALCULATE q_rec (QSPIRAL)

223 q_rec.z = matrix[2][4];
  q_rec.y = matrix[1][4]-q_rec.z*matrix[1][3];
225 q_rec.x = matrix[0][4]-q_rec.z*matrix[0][3]-q_rec.y*matrix[0][2];

227 printf("#######################################################\n");
  printf("#                                                     #\n");
229 printf("#               Q S P I R A L                         #\n");
  printf("#                                                     #\n");
231 printf("#  %12.8lf %12.8lf %12.8lf  #\n", q_rec.x, q_rec.y, q_rec.z);
  printf("#                                                     #\n");
233 printf("#######################################################\n");

235 return 0;
}
```

Listing 6.2: Source code of the C program QSPIRAL.

6.4 Job File for Spin Spiral Calculations

As discussed in [18] calculations at host systems are performed according to a respective job file. These job files contain the tasks the host system shall perform.
The calculation of spin spirals using the VASP program is a little bit tricky, especially if the system that is investigated has more than one atom in its basis, as it has been discussed above. In this case it is necessary to initialize the magnetic moments. Spin spiral calculations, as they have been practiced throughout the course of this work, are fully selfconsistent calculations for different lengths of the spin spiral wave vector $\boldsymbol{q}$. Therefore the calculations are carried out within a loop, where $\boldsymbol{q}$ is rescaled in every step. Of course the initial values of the magnetic moments have to be modified throughout the steps of the loop as well. As job files grow confusing soon, an example job file for a spin spiral calculation in $LaMnO_3$ along the crystallographic [001] axis at the host system helios will be discussed in this section.

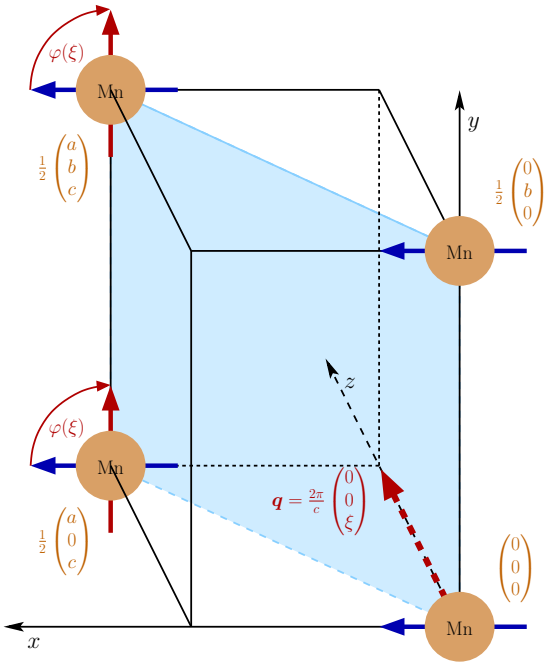

Figure 6.5: Magnetic structure of orthorhombic $LaMnO_3$, $\boldsymbol{q} = \left(0, 0, \frac{2\pi\xi}{c}\right)$, $0 \leq \xi \leq \frac{1}{2}$.

6.4.1 The Magnetic Structure of $LaMnO_3$

Without going into details of the compound, which is investigated in this example, it seems to be important to present the magnetic structure of the material for $\boldsymbol{q} = (0, 0, 0)$ and how this structure changes throughout the calculation. $LaMnO_3$ is an insulator with strongly localized magnetic moments, which arise from the Mn $3d$ electrons. In the case where the spin spiral wave vector's length is zero the system is assumed to be ferromagnetically ordered, with all magnetic moments being parallel to the x-axis. As it is shown in figure 6.5 the magnetic moments in the $z = \frac{c}{2}$-plane start to rotate for nonvanishing values of $\boldsymbol{q}$ until a global collinear antiferromagnetic ordering is reached for $\boldsymbol{q} = \left(0, 0, \frac{2\pi}{c}\right)$.

6.4.2 Job File: $LaMnO_3$ [001]

Listing 6.3 shows how the job file for the above discussed spin spiral calculation in $LaMnO_3$ has been set up. This example can be taken as a draft for future spin spiral calculations. In contrast to usual job files it contains a lot of calculations which are carried out using the bash basic calculator, bc.

```
#$ -N LaMnO3_001
#$ -q para1.q
```

```
#$ -pe orte* 8
#
INDIR=$SGE_CWD_PATH
VASP_DIR=$HOME/VASP_IB/
WORKDIR=$TMP
#
echo $WORKDIR >> $INDIR/WHERE
cp -p $VASP_DIR/vasp-5.2.11_noncoll $WORKDIR/vasp
#
cp -p $INDIR/KPOINTS $WORKDIR/KPOINTS
cp -p $INDIR/POTCAR $WORKDIR/POTCAR
cp -p $INDIR/POSCAR $WORKDIR/POSCAR
#
cd $WORKDIR
ls -l
#
#
# define pi
#
pi=`echo "4*a(1)" | bc -l`
#
#
# define lattice constant (use POSCAR data)
#
a0=5.537
#
#
# define Bravais vectors a_i (use POSCAR data)
#
a1_x=`echo "scale=8; $a0*1.0112572882555606" | bc -l`
a1_y=`echo "scale=8; $a0*0.0" | bc -l`
a1_z=`echo "scale=8; $a0*0.0" | bc -l`
#
a2_x=`echo "scale=8; $a0*0.0" | bc -l`
a2_y=`echo "scale=8; $a0*1.4223363084734302" | bc -l`
a2_z=`echo "scale=8; $a0*0.0" | bc -l`
#
a3_x=`echo "scale=8; $a0*0.0" | bc -l`
a3_y=`echo "scale=8; $a0*0.0" | bc -l`
a3_z=`echo "scale=8; $a0*1.0036666341794538" | bc -l`
#
#
# define q in Cartesian coordinates (use QSPIRAL program)
#
qc_x=0.0
qc_y=0.0
qc_z=1.130618
#
#
# define QSPIRAL (use QSPIRAL program)
#
QSPIRAL_x=0.00
QSPIRAL_y=0.00
QSPIRAL_z=1.00
#
```

```
#
# define lattice positions of magnetic ions in Direct coordinates (use POSCAR data)
#
Rd1_x=0.0
Rd1_y=0.0
Rd1_z=0.0
#
Rd2_x=0.5
Rd2_y=0.0
Rd2_z=0.5
#
Rd3_x=0.0
Rd3_y=0.5
Rd3_z=0.0
#
Rd4_x=0.5
Rd4_y=0.5
Rd4_z=0.5
#
#
# define modulus of magnetic moment M
#
M=4.0
#
#
# calculate lattice positions of magnetic ions in Cartesian coordinates
#
R1_x=`echo "scale=8; $Rd1_x*$a1_x+$Rd1_y*$a2_x+$Rd1_z*$a3_x" | bc -l `
R1_y=`echo "scale=8; $Rd1_x*$a1_y+$Rd1_y*$a2_y+$Rd1_z*$a3_y" | bc -l `
R1_z=`echo "scale=8; $Rd1_x*$a1_z+$Rd1_y*$a2_z+$Rd1_z*$a3_z" | bc -l `
#
R2_x=`echo "scale=8; $Rd2_x*$a1_x+$Rd2_y*$a2_x+$Rd2_z*$a3_x" | bc -l `
R2_y=`echo "scale=8; $Rd2_x*$a1_y+$Rd2_y*$a2_y+$Rd2_z*$a3_y" | bc -l `
R2_z=`echo "scale=8; $Rd2_x*$a1_z+$Rd2_y*$a2_z+$Rd2_z*$a3_z" | bc -l `
#
R3_x=`echo "scale=8; $Rd3_x*$a1_x+$Rd3_y*$a2_x+$Rd3_z*$a3_x" | bc -l `
R3_y=`echo "scale=8; $Rd3_x*$a1_y+$Rd3_y*$a2_y+$Rd3_z*$a3_y" | bc -l `
R3_z=`echo "scale=8; $Rd3_x*$a1_z+$Rd3_y*$a2_z+$Rd3_z*$a3_z" | bc -l `
#
R4_x=`echo "scale=8; $Rd4_x*$a1_x+$Rd4_y*$a2_x+$Rd4_z*$a3_x" | bc -l `
R4_y=`echo "scale=8; $Rd4_x*$a1_y+$Rd4_y*$a2_y+$Rd4_z*$a3_y" | bc -l `
R4_z=`echo "scale=8; $Rd4_x*$a1_z+$Rd4_y*$a2_z+$Rd4_z*$a3_z" | bc -l `
#
echo "------------------------------------------------------------"
#
echo "R1 = [ $R1_x, $R1_y, $R1_z ]"
echo "R2 = [ $R2_x, $R2_y, $R2_z ]"
echo "R3 = [ $R3_x, $R3_y, $R3_z ]"
echo "R4 = [ $R4_x, $R4_y, $R4_z ]"
#
echo "------------------------------------------------------------"
#
#
#
# ++++++++++++++++++++++++++++++++++++++++++++++++++++++++++++++++
```

```
# spin spiral loop
# ++++++++++++++++++++++++++++++++++++++++++++++++++++++++++++++++
#
for i in `seq 0.00 0.05 1.00`
do
#
#
echo " "
echo "------------------------------------------------------------"
echo "QSPIRAL = $i"
echo "------------------------------------------------------------"
echo " "
#
#
# calculate q*xi, xi=$i, in Cartesian coordinates
#
q_x=`echo "scale=8; $qc_x*$i" | bc -l`
q_y=`echo "scale=8; $qc_y*$i" | bc -l`
q_z=`echo "scale=8; $qc_z*$i" | bc -l`
#
echo "q = [ $q_x, $q_y, $q_z ]"
#
#
# calculate angles phi_i = q*Ri (radian, degree)
#
qR1=`echo "$q_x*$R1_x+$q_y*$R1_y+$q_z*$R1_z" | bc -l`
qR1_deg=`echo "scale=5; $qR1*(180.0/$pi)" | bc -l`
#
qR2=`echo "$q_x*$R2_x+$q_y*$R2_y+$q_z*$R2_z" | bc -l`
qR2_deg=`echo "scale=5; $qR2*(180.0/$pi)" | bc -l`
#
qR3=`echo "$q_x*$R3_x+$q_y*$R3_y+$q_z*$R3_z" | bc -l`
qR3_deg=`echo "scale=5; $qR3*(180.0/$pi)" | bc -l`
#
qR4=`echo "$q_x*$R4_x+$q_y*$R4_y+$q_z*$R4_z" | bc -l`
qR4_deg=`echo "scale=5; $qR4*(180.0/$pi)" | bc -l`
#
echo "q*R1 = $qR1_deg deg"
echo "q*R2 = $qR2_deg deg"
echo "q*R3 = $qR3_deg deg"
echo "q*R4 = $qR4_deg deg"
#
#
# calculate initial magnetic moments for MAGMOM-tag
#
M_R1_x=`echo "scale=8; $M*c($qR1)" | bc -l`
M_R1_y=`echo "scale=8; $M*s($qR1)" | bc -l`
M_R1_z=0.0
#
M_R2_x=`echo "scale=8; $M*c($qR2)" | bc -l`
M_R2_y=`echo "scale=8; $M*s($qR2)" | bc -l`
M_R2_z=0.0
#
M_R3_x=`echo "scale=8; $M*c($qR3)" | bc -l`
M_R3_y=`echo "scale=8; $M*s($qR3)" | bc -l`
```

```
M_R3_z=0.0
#
M_R4_x=`echo "scale=8; $M*c($qR4)" | bc -l`
M_R4_y=`echo "scale=8; $M*s($qR4)" | bc -l`
M_R4_z=0.0
#
#
# calculate QSPIRAL
#
qsp_x=`echo "scale=4; $i*$QSPIRAL_x" | bc -l`
qsp_y=`echo "scale=4; $i*$QSPIRAL_y" | bc -l`
qsp_z=`echo "scale=4; $i*$QSPIRAL_z" | bc -l`
#
# write INCAR file and run calculation
#
cat >INCAR <<!
SYSTEM = LaMnO3
NELM = 500
ALGO = Conjugate
ISTART = 0
ISMEAR = 0
SIGMA = 0.05
LDAU = .TRUE.
LDAUTYPE = 2
LDAUL = -1 2 -1
LDAUU = 0 2.0 0
LDAUJ = 0 0 0
LDAUPRINT = 1
RWIGS = 2.17 0.69 1.47
I_CONSTRAINED_M = 1
LAMBDA = 0
M_CONSTR = 16*0 16*0 16*0 1 0 0 1 0 0 1 0 0 1 0 0
MAGMOM = 16*0 16*0 16*0 $M_R1_x $M_R1_y $M_R1_z $M_R2_x $M_R2_y $M_R2_z $M_R3_x
    $M_R3_y $M_R3_z $M_R4_x $M_R4_y $M_R4_z
ENINI = 400
ENCUT = 700
EDIFF = 1E-4
ISYM = 0
LREAL = Auto
LNONCOLLINEAR = .TRUE.
LASPH = .TRUE.
LSPIRAL = .TRUE.
LZEROZ = .TRUE.
QSPIRAL = $qsp_x $qsp_y $qsp_z
NPAR = 1
!
#
echo "------------------------------------------------------------"
cat INCAR
echo "------------------------------------------------------------"
#
mpirun -hostfile /tmp/hostfile_plain_${JOB_ID} -n 8 ./vasp
E=`grep "E0" OSZICAR | tail -1`
echo -e "QSPIRAL =$i\t$E" >> SUMMARY
#
```

```
222 mkdir $INDIR/QSPIRAL_$i
    OUTDIR=$INDIR/QSPIRAL_$i
224 #
    gzip CHGCAR DOSCAR EIGENVAL IBZKPT OSZICAR OUTCAR PROCAR XDATCAR vasprun.xml
226  mv CHGCAR.gz $OUTDIR/.
     mv CONTCAR $OUTDIR/.
228  mv DOSCAR.gz $OUTDIR/.
     mv EIGENVAL.gz $OUTDIR/.
230  mv IBZKPT.gz $OUTDIR/.
     mv OSZICAR.gz $OUTDIR/.
232  mv OUTCAR.gz $OUTDIR/.
     mv PROCAR.gz $OUTDIR/.
234  mv XDATCAR.gz $OUTDIR/.
     mv vasprun.xml.gz $OUTDIR/.
236 #
    #
238 done
    #
240 # ++++++++++++++++++++++++++++++++++++++++++++++++++++++++++++++++++++
    # end of spin spiral loop
242 # ++++++++++++++++++++++++++++++++++++++++++++++++++++++++++++++++++++
    #
244 cp -p SUMMARY $INDIR/SUMMARY
    #
246 #
    exit
```

Listing 6.3: Job file for a spin spiral calculation in $LaMnO_3$.

This job file can be divided into different sections:

- Job parameters for the host system and file operations, lines 1-19.
- Definitions (Bravais lattice, spin spiral wave vector $\boldsymbol{q}$, ...), lines 20-82.
- Calculation of parameters for the INCAR file, lines 83-183.
- Writing the INCAR file and executing the actual calculation at the host system, lines 184-221.
- File operations, lines 222-246.

Discussion

Due to the way spin spirals are treated by VASP it is necessary to initialize the direction of the magnetic moments. This is done by specifying the MAGMOM-tag. It has already been mentioned that in a spin spiral structure the angle φ_i for the rotation of a magnetic moment of an atom $\boldsymbol{R}_i$ is given by $\varphi_i(\xi) = \boldsymbol{q}(\xi) \cdot \boldsymbol{R}_i$.
For the unit circle the relations $x = \cos\varphi$ and $y = \sin\varphi$ are well known, see figure 6.6.

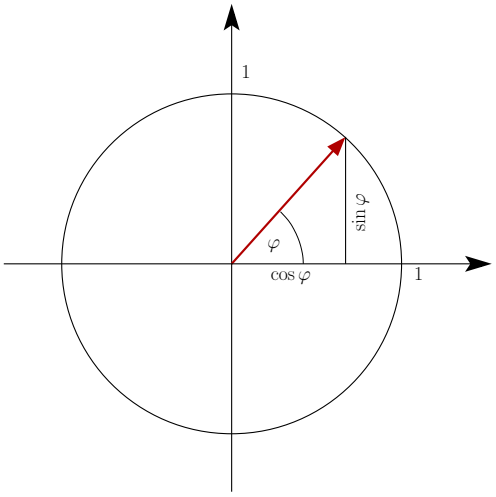

Figure 6.6: Trigonometric relations at the unit circle.

Consequently the direction of the magnetic moments can be derived by calculating the inner product $\boldsymbol{q} \cdot \boldsymbol{R}_i$. In the job file, listing 6.3, this product is calculated in Cartesian coordinates.
The experienced VASP user knows that the first lines of the POSCAR file contain the scaling factor, which is the lattice constant in cubic structures, and the three Bravais vectors divided by this factor. As a consequence the scaling factor and the three Bravais vectors are defined in the job file in lines 25-44.
The spin spiral wave vector $\boldsymbol{q}$ in Cartesian coordinates can be calculated by hand or by using the QSPIRAL program. Its components are defined in the job file in lines 45-49. Moreover $\boldsymbol{q}$ has to be defined in reciprocal coordinates which is done in lines 52-56.
The positions of the magnetic ions $\boldsymbol{R}_i$ are defined in direct coordinates in lines 59-75. In lines 78-82 the modulus of the ions' magnetic moment is defined.
The magnetic ions' lattice positions in Cartesian coordinates are calculated automatically in lines 83-111.
The spin spiral loop's counter variable i is used as the spin spiral wave vector's parameter of dilation ξ, $\boldsymbol{q} = \boldsymbol{q}(\xi)$. The actual value of $\boldsymbol{q}$ is calculated in lines 127-135 and the resulting angles $\varphi_i(\xi)$ are calculated in lines 136-155. Using these angles the magnetic moments are initialized in lines 156-174.

Although the job file in listing 6.3 is quite long and it takes some time to set up such a file but it is worth while the effort. This is because usually spin spiral calculations are carried out into different crystallographic directions. A job file as it is shown

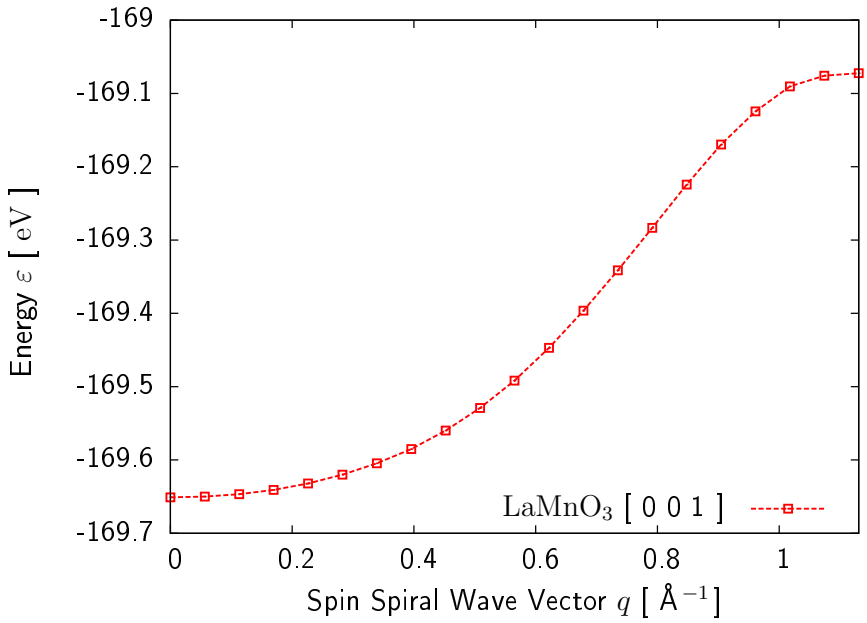

Figure 6.7: Spin spiral calculation for FM $LaMnO_3$, [001].

in listing 6.3 can be modified in an easy way just by changing some of the definitions. Another advantage is that the amount of possible mistakes is reduced.

6.4.3 Dispersion of a [001] Spin Spiral in $LaMnO_3$

Figure 6.7 shows the dispersion relation $E(\boldsymbol{q})$ for $LaMnO_3$, where $\boldsymbol{q}$ is given by

$$\boldsymbol{q}(\xi) = \frac{2\pi}{c} \begin{pmatrix} 0 \\ 0 \\ \xi \end{pmatrix} , \tag{6.22}$$

which has been gained by using the job file in listing 6.3.

7 Examples for Spin Spiral Calculations

After the introduction to spin spiral calculations in the context of density functional theory which has been given throughout the last chapters, some examples for spin spiral calculations as well as applications of these are presented in this chapter.

7.1 Spin Spirals in bcc Fe

The α-phase of iron, which has a body centered cubic crystal structure, is stable below 1185 K. Above its Curie temperature of 1043 K α-Fe is paramagnetic. Below the Curie temperature α-Fe is ferromagnetic with a ground state magnetic moment of 2.2 μ_B per atom [7]. The crystal structure data that has been used for the following calculations is found in [25]. The respective lattice parameter is 2.8608 Å.

7.1.1 Estimation of the Spin Wave Stiffness Constant D

As it has been shown in chapter 5 the magnon dispersion for a ferromagnetic material with a cubic Bravais lattice is given by

$$\omega_{\boldsymbol{k}} = g_j \mu_B H_{ext} + Dk^2 \tag{7.1}$$

in the limit of long wavelengths, where D is called spin wave stiffness constant. This constant can be measured by inelastic neutron scattering. As a consequence spin spiral calculations for low excitation energies can be used to compare the underlying physical model to experimental data.
This is done by applying a quadratic fit to the dispersion obtained by the spin spiral calculation. The spin spiral calculation starts with the ferromagnetic state and ends in an antiferromagnetic state as shown in figure 7.1. The calculation is based on mesh of $16 \times 16 \times 16$ k-points. The initial energy cutoff is set to 267.7 eV while the ENCUT tag is defined as 500 eV. The choosen smearing method is the tetrahedron method with Blöchl corrections. Moreover parallelization is avoided by NPAR = 1 in order to obtain the respective densities of states.

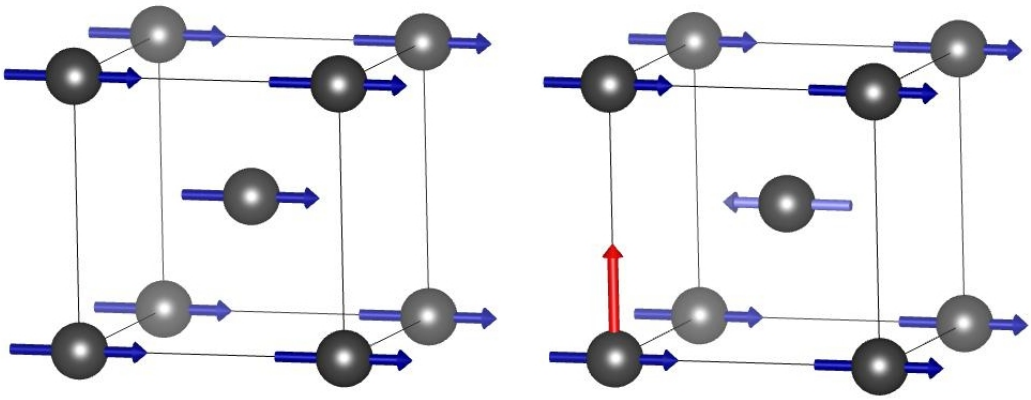

(a) $\boldsymbol{q} = 0$ (b) $\boldsymbol{q} = \boldsymbol{q}_{max}$

Figure 7.1: Magnetic structure of bcc Fe for a spin spiral calculation in [001] direction (red arrow).

The wavelength λ_{max} of the spin spiral leading to the antiferromagnetic state, figure 7.3b, is a_0. Figure 7.2 shows the result of the spin spiral calculation and the respective quadratic fit. The fit curve is based on spin spiral wave vectors with modulus lower than 5% of $|\boldsymbol{q}_{max}|$. The calculation yields a ferromagnetic groundstate as expected. The spin stiffness constant D turns out to be 316 meVÅ^2. In comparsion to experimental data this is an overestimation of about 11 %.

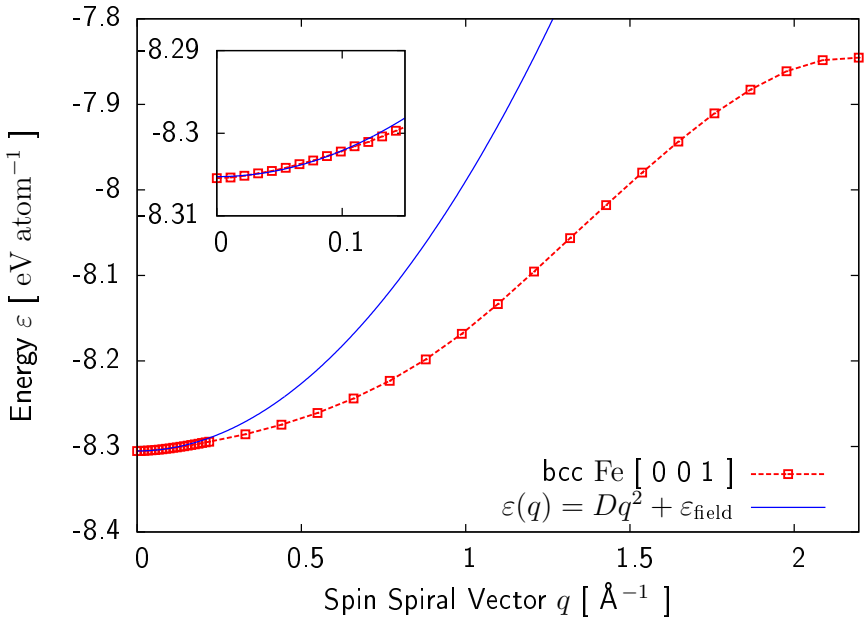

Figure 7.2: [001] spin spiral calculation for bcc Fe.

Figure 7.3 shows the non spin split densities of states for $\boldsymbol{q} = 0$ and $\boldsymbol{q} = \boldsymbol{q}_{max}$. The

increased number of states at the Fermi level for $\boldsymbol{q} = \boldsymbol{q}_{max}$ can be understood in terms of molecular orbitals. The interaction of electrons with like spin leads to the largest energy difference between bonding and antibonding states. As a consequence the bandwidth is reduced in the antiferromagnetic case leading to higher electron densities.

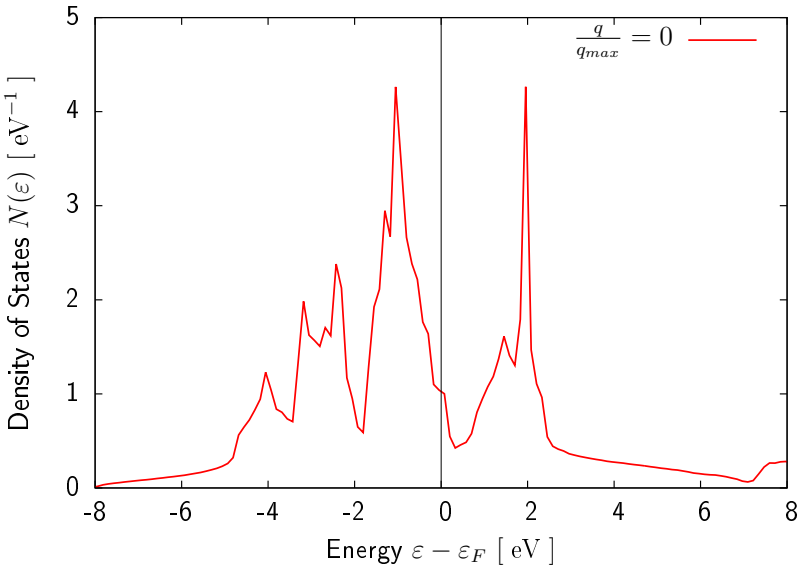

(a) $\boldsymbol{q} = 0$

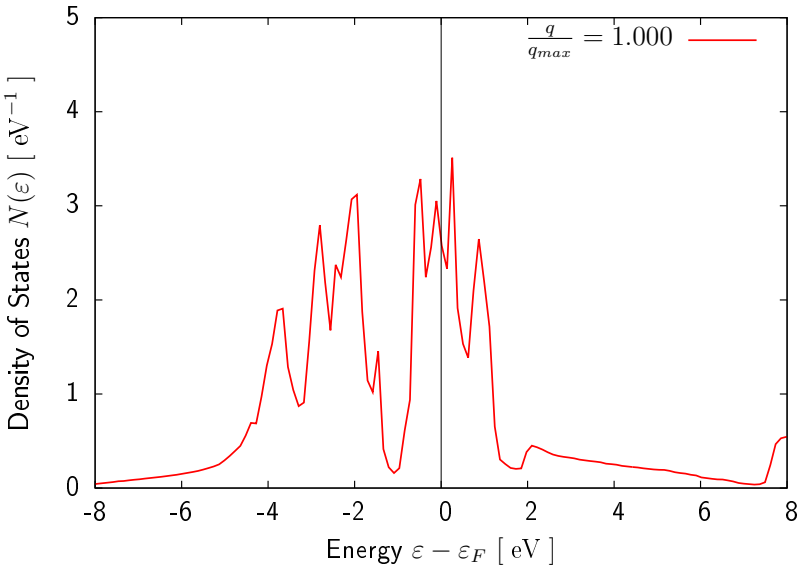

(b) $\boldsymbol{q} = \boldsymbol{q}_{max}$

Figure 7.3: Comparsion of the densities of states for $\boldsymbol{q} = 0$ and $\boldsymbol{q} = \boldsymbol{q}_{max}$ in bcc Fe.

7.2 Spin Spirals in hcp Co

Below a temperature of 673 K the most stable phase of pure cobalt is the Co-α phase, which has a hexagonal close packed crystal structure with two atoms in its basis. The lattice parameters are found to be $a = b = 2.5071$ Å, $c = 4.0686$ Å [26].

7.2.1 Estimation of the Spin Wave Stiffness Constant D

As in the last section the spin stiffness constant D shall be determined by a quadratic fit of the dispersion gained by a [001] spin spiral calculation in hcp Co. Figure 7.4 illustrates the magnetic structures for $\boldsymbol{q} = 0$ and $\boldsymbol{q} = \boldsymbol{q}_{max}$, where $\lambda_{max} = c$. The

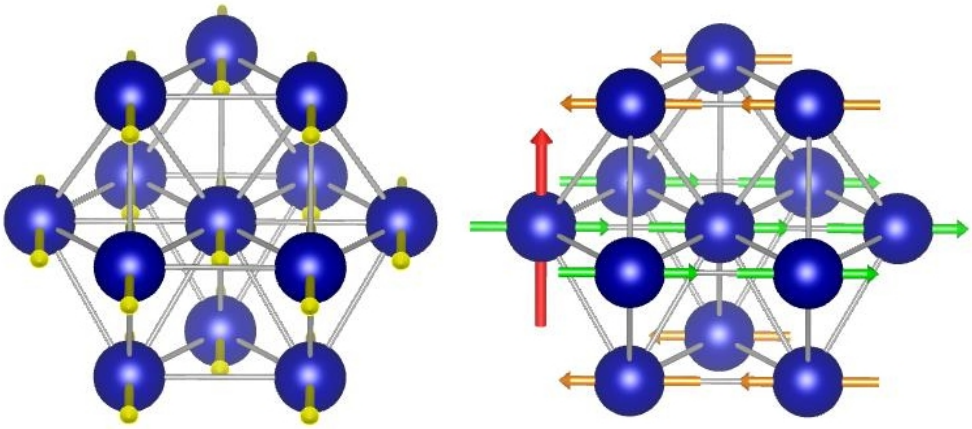

(a) $\boldsymbol{q} = 0$ (b) $\boldsymbol{q} = \boldsymbol{q}_{max}$

Figure 7.4: Magnetic structure of hcp Co for [001] spin spiral. $\boldsymbol{q} = 0$ and $\boldsymbol{q} = \boldsymbol{q}_{max}$ (red arrow).

k-mesh, which has been used for the calculations consisits of $12 \times 12 \times 12$ points. Equivalent to the spin spiral calculation in bcc Fe the tetrahedron method with Blöchl correction has been used. The initial cutoff energy is set to 400 eV while the ENCUT tag is set to 600 eV. Due to the fact that the cell contains two atoms, the magnetic moments have to be initalized properly. Therefore a job file similar to listing 6.3 has been set up.

Figure 7.5 shows the result of the spin spiral calculation as well as the quadratic fit. Again the fit is based on spin spiral vectors with modulus less than 5% of $|\boldsymbol{q}_{max}|$.

The spin wave stiffness constant D is obtained as 420 meVÅ^2, which is an underestimation of the experimental value by about 18%.

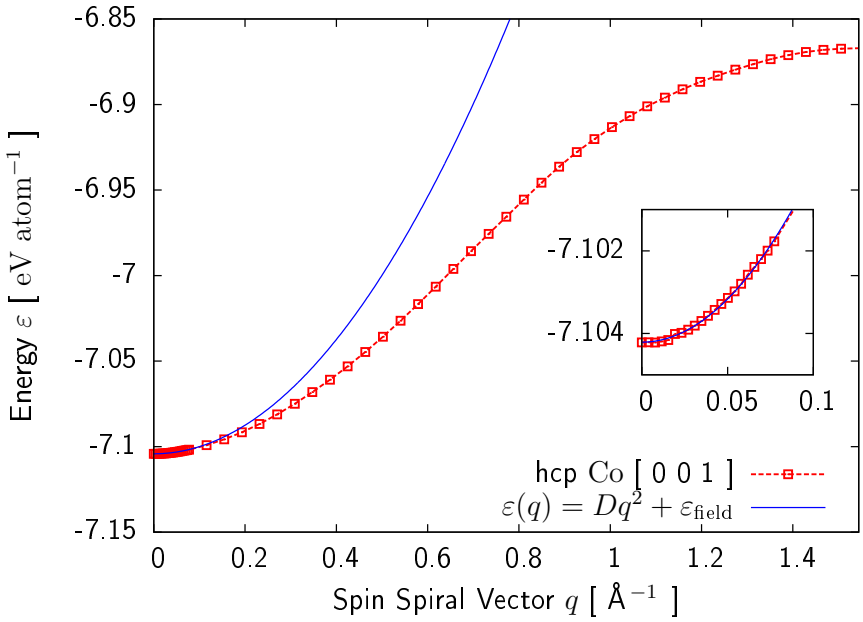

Figure 7.5: [001] spin spiral calculation for hcp Co.

7.3 Spin Spirals in MnO

7.3.1 The Crystal Structure

Manganese oxide MnO has the NaCl, rock salt structure. This structure is a face centered cubic lattice with a basis of two atoms, one manganese and one oxygen atom. The structural data as for instance the lattice constant of 4.408 Å, which leads to a cell volume of about 85.6 $Å^3$, is taken from [27]. This crystal structure is shown in figure 7.6. The structural relaxation increases the volume by 3.6% to 88.8 $Å^3$. This

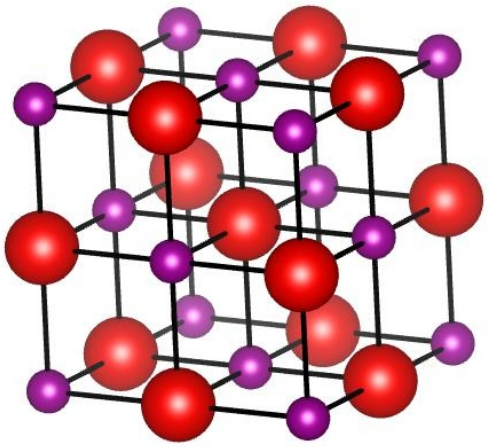

Figure 7.6: Crystal structure of MnO (Mn violet, O red).

increase is caused by a growth of the lattice constant by 1.2 %. The lattice constant of the relaxed structure is given by $a_0 \approx 4.461$ Å.

7.3.2 Static PBE- and HSE-Calculations

As a first step the electronic structure of MnO is determined in a spin polarized GGA calculation using the PBE functional. Therefore a Γ-centered k-mesh of $10 \times 10 \times 10$ points is used. Moreover Gaussian smearing and a SIGMA value of 0.05 are applied. The GGA calculation leads to a metallic state with a magnetic moment per cell of about $4.8\,\mu_B$. Figure 7.7 shows the total density of states that has been gained by this calculation. The electronc structure, which is obtained by the GGA calculation does not show the experimentally found insulating behaviour. As a consequence hybrid functionals have to be applied to the structure. The respective density of states has an energy gap of about 2.0 eV. Therefore it is about 0.6 eV to small in comparison to experimental data from transport measurements [28]. This underestimation of the energy gap by the HSE functional is a well known problem. In Figure 7.8 the total

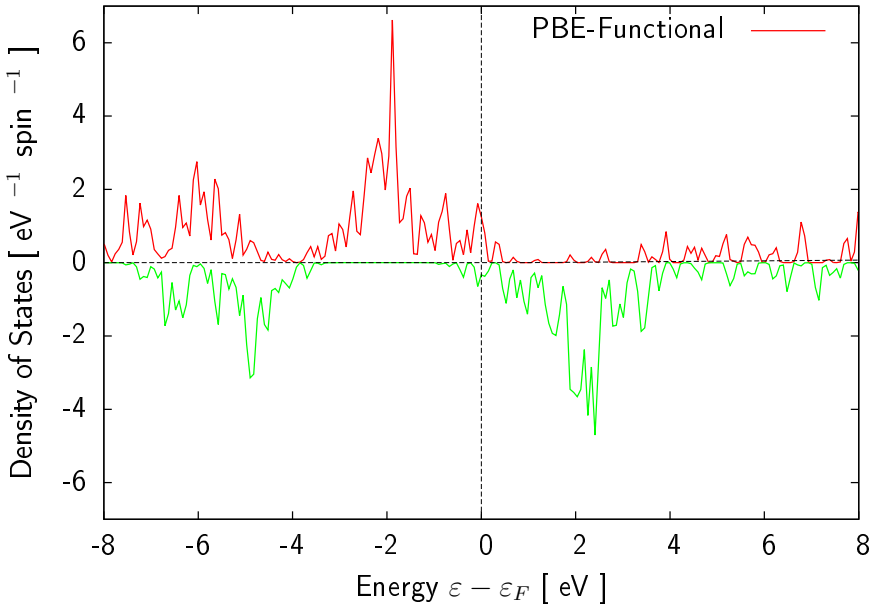

Figure 7.7: Total density of states of MnO in PBE calculation.

density of states gained by the usage of the HSE functional is presented.

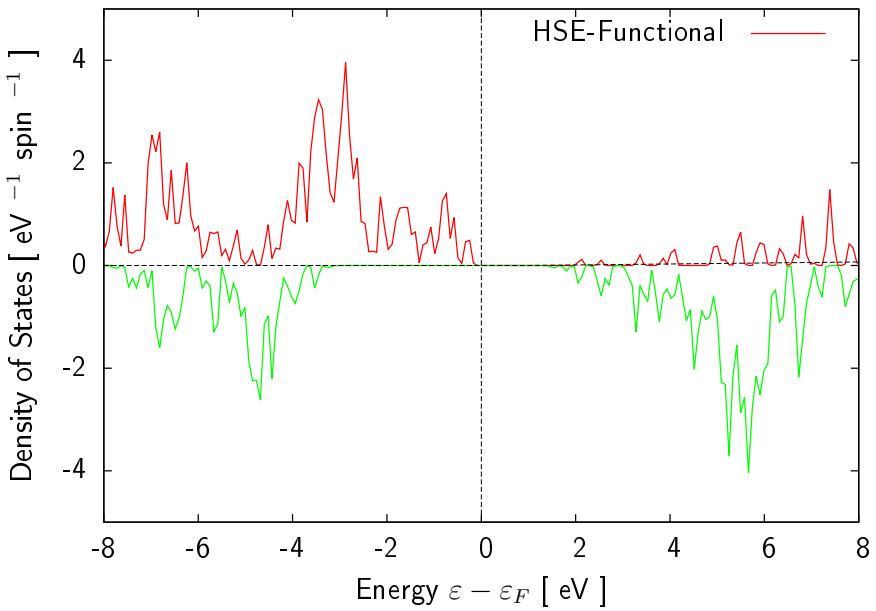

Figure 7.8: Total density of states of MnO using the HSE hybrid functional.

The magnetic moment per cell reveals to be 5.0 μ_B. This is the value one expects from Hund's rules in the limit of pure ionic bonding. As an atom Mn has an [Ar]$3d^5 4s^2$ electron configuration. In the case of pure ionic bonding it is expected to be in a Mn^{2+}

state. The oxygen is expected to be in a O^{2-} state. According to Hund's rules the spin momentum is then given by $S = \frac{5}{2}$ and the orbital angular momentum L vanishes. This causes a magnetic moment of $5\,\mu_B$.

7.3.3 PBE+U Calculations, Optimizing the U-Parameter

Due to the fact that one cannot use the HSE hybrid functional in the context of spin spiral calculations one has to switch to PBE+U calculations. As a consequence an onsite correction parameter U has to be determined first. There are two criteria that have to be fulfilled by an electronic structure, which has been modellized by using a parameter U. The energy gap as well as the overall shape of the electronic structure shall fit best to a reference structure. Here the HSE calculation's result is taken as a reference. The search procedure for the U parameter has been carried out within a range of 0 to 10 eV.
It is found that an onsite correction parameter $U = 5$ eV, which acts on the Mn $3d$-electrons gives the best result. Figure 7.9 shows the result of the onsite corrected GGA calculation. In comparsion to the density of states gained by the HSE functional, see figure 7.8, the peak positions are slightly moved. The energy gap, which is obtained by this calculation, is about 1.9 eV. Consequently the energy gap gained by using the HSE hybrid functional is underestimated by 0.1 eV. The electronic structure that has been obtained by applying the PBE functional with an onsite correction of $U = 5$ eV is shown in figure 7.9.

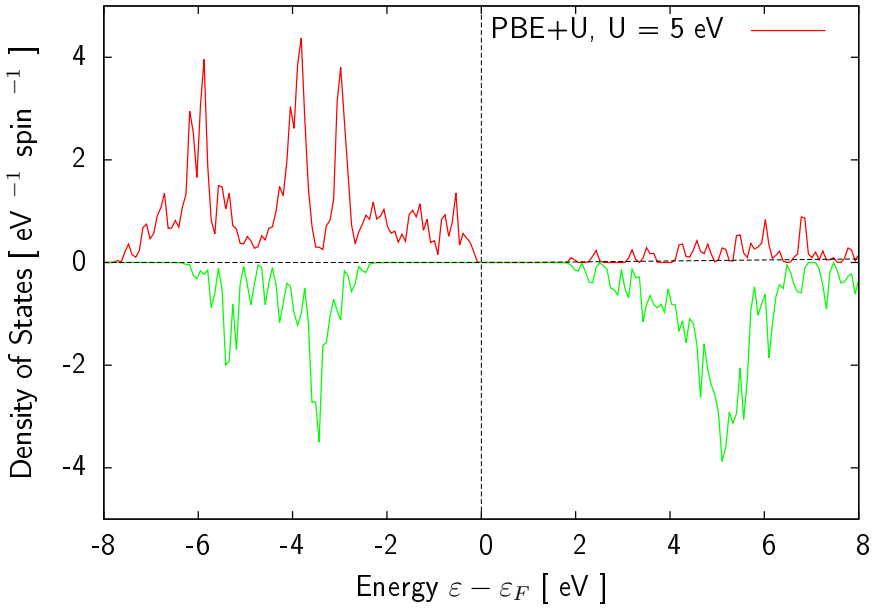

Figure 7.9: MnO PBE+U calculation using $U = 5$ eV.

7.3.4 PBE+U Spin Spiral Calculations

In this section the results of the spin spiral calculations in MnO are presented. Calculations have been performed for three different lattice directions, which are [001], [110] and [111]. Due to the fact that the cell is not distorted calculations as for instance a [100] spin spiral yield no new information.
The spin spiral calculations have been carried out using a mesh of $12 \times 12 \times 12$ k-points. In accordance with the static, spin polarized calculations in the sections above Gaussian smearing has been used together with a SIGMA value of 0.05. The initial cutoff energy ENINI is set to 600 eV, while the ENCUT tag is defined as 800 eV.

[001] - Spin Spiral Calculation

Given that the wavelength λ_{max} that leads to a collinear antiferromagnetic ordering along the c-axis, see figure 7.10, is related to the modulus of the respective spin spiral wave vector $\boldsymbol{q}_{max}$ via

$$|\boldsymbol{q}_{max}| = \frac{2\pi}{\lambda_{max}} \,, \tag{7.2}$$

$\lambda_{max} = a_0$, where a_0 is the lattice constant. Figure 7.11 shows the dispersion for the

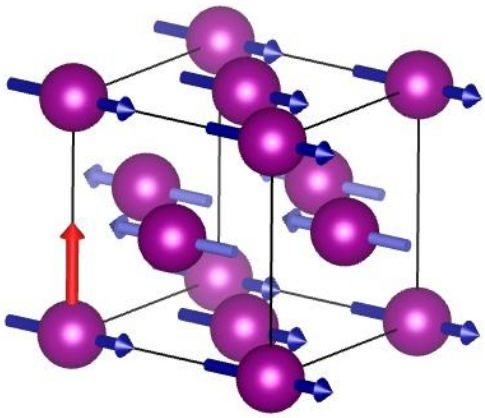

Figure 7.10: Magnetic structure of MnO for $\boldsymbol{q}_{max}$, [001] direction (red arrow).

spin spiral calculation along the [001] axis. The spin spiral calculation starts with the collinear ferromagnetic state, which has been obtained by the PBE+U calculation in section 7.3.3. As the spin spiral wave vector is increased the energy decreases. For the collinear antiferromagnetic case, where the magnetic moments are ferromagnetically ordered in the a-b plane and antiferromagnetically coupled to the neighbouring c planes the dispersion shows a minimum.

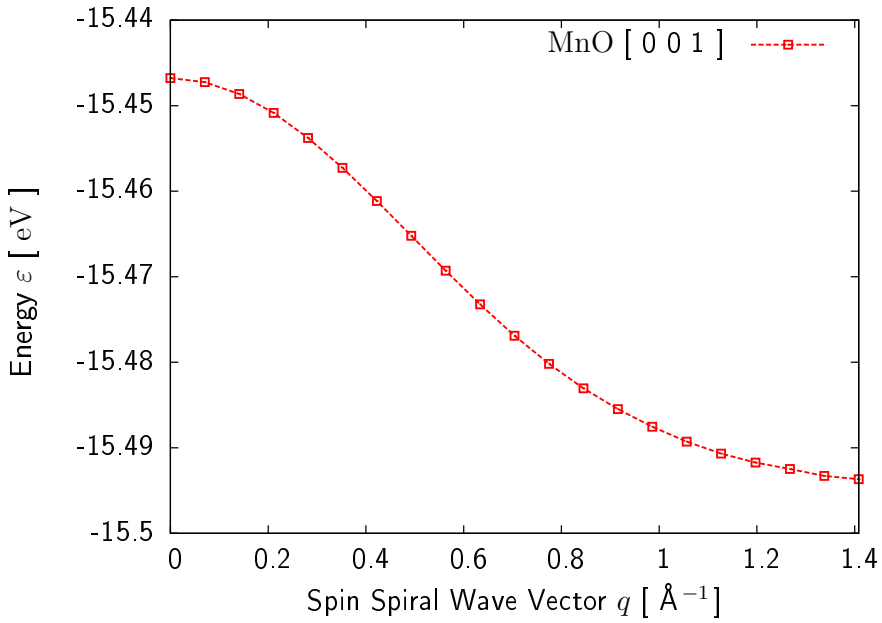

Figure 7.11: MnO spin spiral along the [001] direction.

[110] - Spin Spiral Calculation

Now a spin spiral calculation along the crystallographic [110] axis is carried out. The result is shown in figure 7.12. The collinear antiferromagnetic magnetic state, which

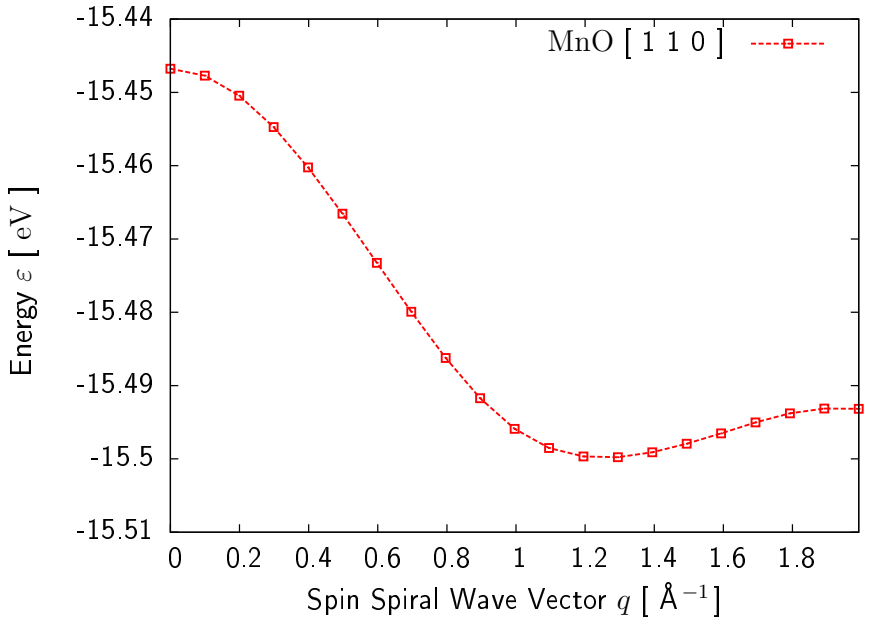

Figure 7.12: MnO spin spiral along the [110] direction.

is found to minimize the energy for spin spiral structures along the [001] direction, is

obtained for the spin spiral wave vector $\boldsymbol{q}_{max}$ in this case. The wavelength of this spin spiral wave vector is given by $\lambda_{max} = \frac{a_0}{\sqrt{2}}$. In figure 7.13a this collinear state, which is obtained by a [110] spin spiral with wavelength λ_{max} is shown. As can be seen in figure 7.12 this state does not lead to a minimum in the dispersion.

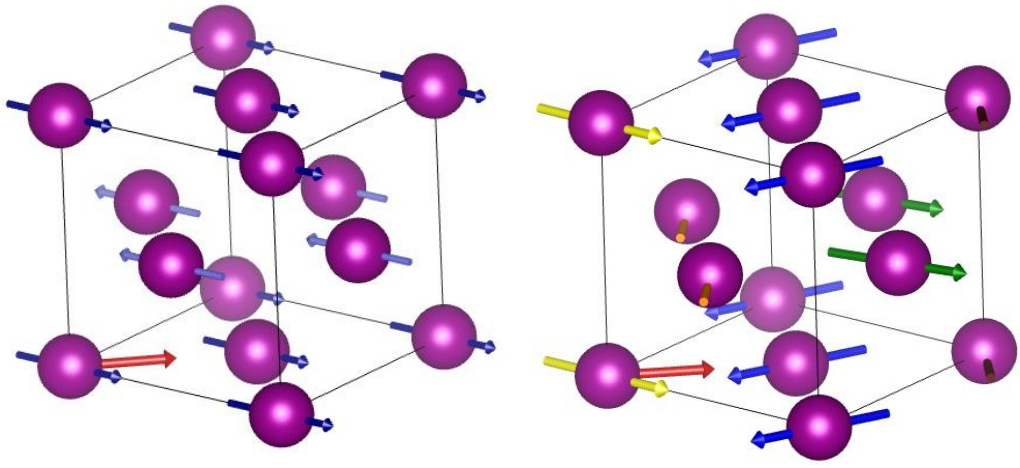

(a) $\boldsymbol{q} = \boldsymbol{q}_{max}$ (b) $\boldsymbol{q} = \boldsymbol{q}_{sp}$

Figure 7.13: Magnetic structure of MnO for $\boldsymbol{q}$ in [110] direction (red arrow).

Figure 7.12 reveals that the energy is lowered to a minimum by an antiferromagnetic spin spiral state. This state is obtained if the spin spiral wave vector $\boldsymbol{q}_{sp} = 0.65 \times \boldsymbol{q}_{max}$. The respective wavelength is given by $\lambda_{sp} \approx 4.61$ Å. In this complex magnetic structure the magnetic moments in neighbouring phase planes differ by an angle of $\Delta\varphi = 123.22°$, see figure 7.13b.

[111] - Spin Spiral Calculation

Finally a spin spiral in the crystallographic [111] direction is investigated. Figure 7.14 shows the result. The energy minimum is found to be a collinear antiferromagnetic state with wave vector $\boldsymbol{q}_{max}$ and wavelenght $\frac{2a_0}{\sqrt{3}}$. The respective magnetic structure is illustrated in figure 7.15.
In this structure the magnetic moments are ferromagnetically coupled inside the phase planes while neighbouring phase planes are coupled antiferromagnetically.

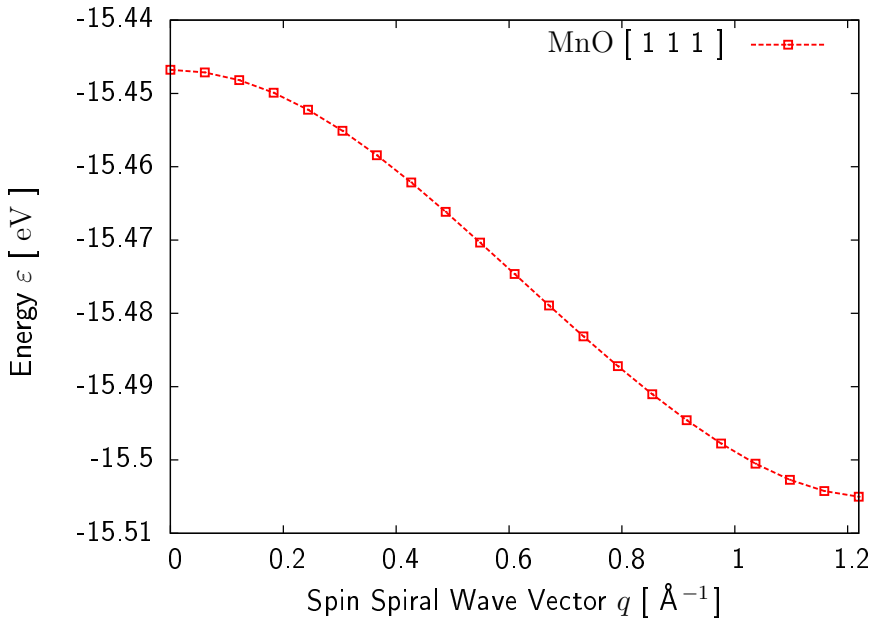

Figure 7.14: MnO spin spiral along the [110] direction.

Discussion

In order to find out, which magnetic structure is the magnetic groundstate of MnO, the different dispersions are compared in figure 7.16.
As one can see from this plot the magnetic groundstate is a collinear antiferromagnetic ordering in the [111] direction. This magnetic structure has been verified experimentally by Shull et al. in 1951 [29].
The theory of spin wave excitations in antiferromagnets predicts a dispersion that is linear in $|\boldsymbol{q}|$ in the limit of long wavelengths [6]. This behaviour has not been proved

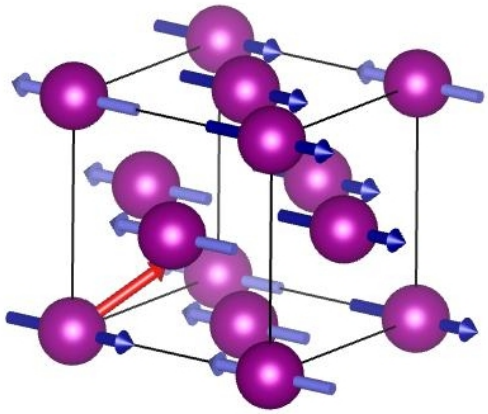

Figure 7.15: Magnetic structure of MnO for $\boldsymbol{q}_{max}$, [111] direction (red arrow).

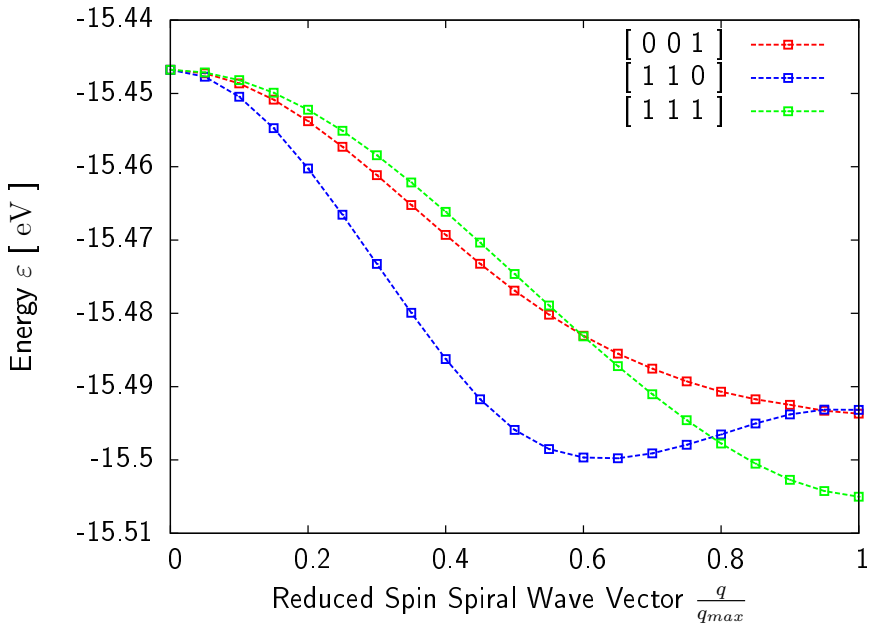

Figure 7.16: Comparison of spin spiral calculations in MnO.

by these calculations. A reason why it has not been possible to show the linear $|\boldsymbol{q}|$ dependence of the excitation energies may be that the cell's magnetic moment did not stay constant throughout the calculations. This is shown in figure 7.17.

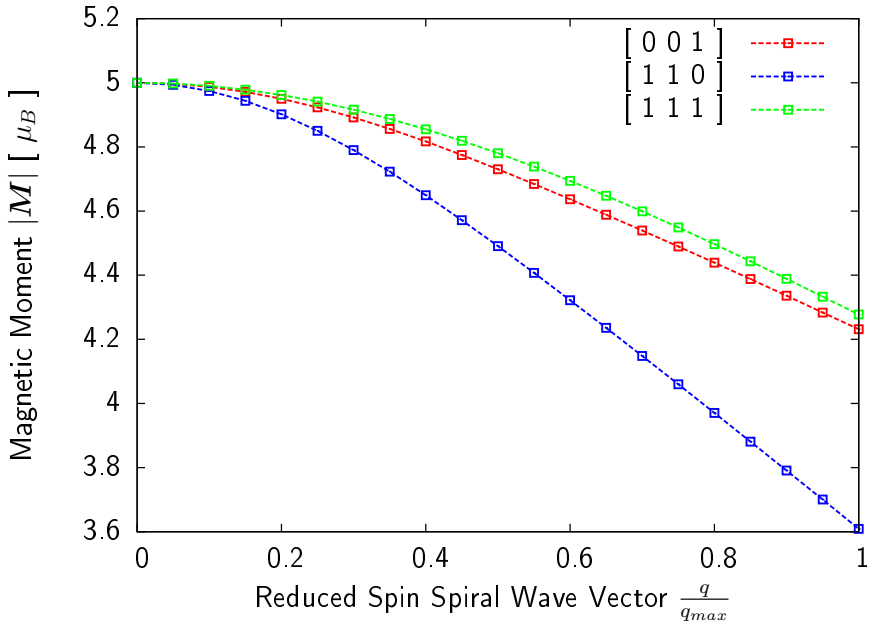

Figure 7.17: Magnetic moment of the investigated MnO cell.

7.3.5 Estimation of the Nèel Temperature T_N

The data which has been gained by the spin spiral calculations in the last sections will now be used to determine the exchange constants and the Nèel temperature of MnO. This estimation is based on a publication by Kübler et al. [30].
As the Mn moments are localized, the coupling of different Mn atoms can be described by the Heisenberg Hamiltonian

$$\mathbf{H} = -\sum_{i,j} J_{ij} \mathbf{S}_i \mathbf{S}_j \tag{7.3}$$

with exchange constants J_{ij}, where $J_{ii} = 0$. In the ferromagnetic groundstate at $T = 0$ the exchange energy is

$$E_0 = -S^2 \sum_i z_i J_i \tag{7.4}$$

where z_i are the coordination numbers of the lattice. Due to the fact that antiferromagnetic states are not eigenstates of the Heisenberg Hamiltonian it is only possible to write down variational estimates of their exchange energies and subtract them from (7.4). The result for such an exchange energy difference is

$$\Delta E = -4S^2 \sum_i z_i^{00} J_i \tag{7.5}$$

where z_i^{00} gives the coordination number for oppositely ordered moments. For an antiferromagnetic arrangement as it has been gained by the spin spiral calculation in [001] direction, see figure 7.10, these numbers are

$$z_i^{00} = 8,\ 0,\ 16,\ 0,\ 16,\ 0,\ 36\ . \tag{7.6}$$

For the antiferromagnetic arrangement which has been gained by the [111] spin spiral calculation, see figure 7.15, the coordination numbers z_i^{00} for oppositely ordered moments are

$$z_i^{00} = 6,\ 6,\ 12,\ 0,\ 12,\ 8,\ 24\ . \tag{7.7}$$

Now the energy differences between the ferromagnetic and the antiferromagnetic state for the spin spiral in [001] direction ΔE_I and the spin spiral in [111] direction ΔE_{II} can be used to determine the exchange constants and the Nèel temperature of MnO. Therefore all exchange constants except for those between nearest neighbours and next

nearest neighbours J_1 and J_2 have to be ignored. According to (7.5) ΔE_I accounts to

$$\Delta E_I = -4S^2 (8J_1 + 0J_2) = -32S^2 J_1 \tag{7.8}$$

and ΔE_{II} is obtained as

$$\Delta E_{II} = -4S^2 (6J_1 + 6J_2) = -24S^2 (J_1 + J_2) \ . \tag{7.9}$$

For the calculation of the Nèel temperature the relation

$$k_B T_N = -4S (S + 1) J_2 \tag{7.10}$$

where k_B is the Boltzmann constant, is used. In the case of a ferromagnetic material the formula

$$k_B \Theta = -4S (S + 1) (J_1 + J_2) \tag{7.11}$$

has to be applied in order to obtain a result for the paramagnetic Curie temperature Θ.

As $\Delta E_I \approx 57.6$ meV and $S = \frac{5}{2}$ the nearest neighbour exchange constant J_1 is calculated as -0.29 meV. Using $\Delta E_{II} \approx 76.6$ meV the next nearest neighbour exchange constant J_2 is obtained to be -0.22 meV. Inserting J_2 into (7.11) the Nèel temperature of MnO is given by 90.4 K. In comparison to the experimental data of 122 K [6] the critical temperature is underestimated by about 26 % by this approach. The reason for this underestimation is probably due to the sole use of first nearest neighbour interactions. Considering second and third neighbour shells would certainly increase the value for T_N, in particular since magnetic interactions decay only slightly stronger than $\frac{1}{r}$. Moreover the cell's magnetic moment changed in the course of the calculation from $5\mu_B$ to about $4.3\mu_B$ causing smaller energy differences ΔE_I and ΔE_{II}. These smaller values lead to an underestimation of the exchange constants and thereby to an underestimation of the critical temperature.

7.4 Spin Spirals in $LaMnO_3$

The famous material $LaMnO_3$ is known to be an insulating A-type antiferromagnet. Nevertheless the calculations, which are presented here treat $LaMnO_3$ as a halfmetallic ferromagnet. It would therefore be an interesting task to calculate the electronic structure for the insulating antiferromagnetic structure in future.

7.4.1 The Crystal Structure

The $LaMnO_3$ cell, which is investigated in the following sections is a distorted perovskite structure $a \approx c \neq b$. The orthorhombic cell contains four formula units. The central Mn atom is surrounded by a distorted octahedron of oxygen atoms. The crystal structure data is taken from [31] for 293 K. The cell, which has a volume of about 244.68 $Å^3$ is illustrated in figure 7.18.

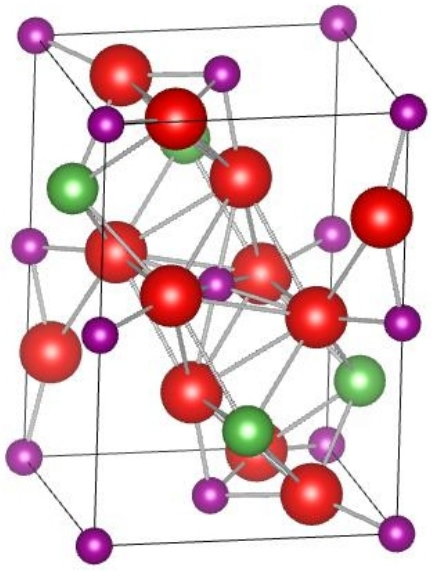

Figure 7.18: Crystal Structure of orthorhombic $LaMnO_3$.

In a first step the crystal structure is relaxed using the PBE functional. This structural relaxation leads to a decrease of the cell volume by 2.6%.

7.4.2 Static PBE- and HSE-Calculations

After having relaxed the structure a static GGA calculation using the PBE functional is carried out. The result of this calculation is shown in figure 7.19. The electronic

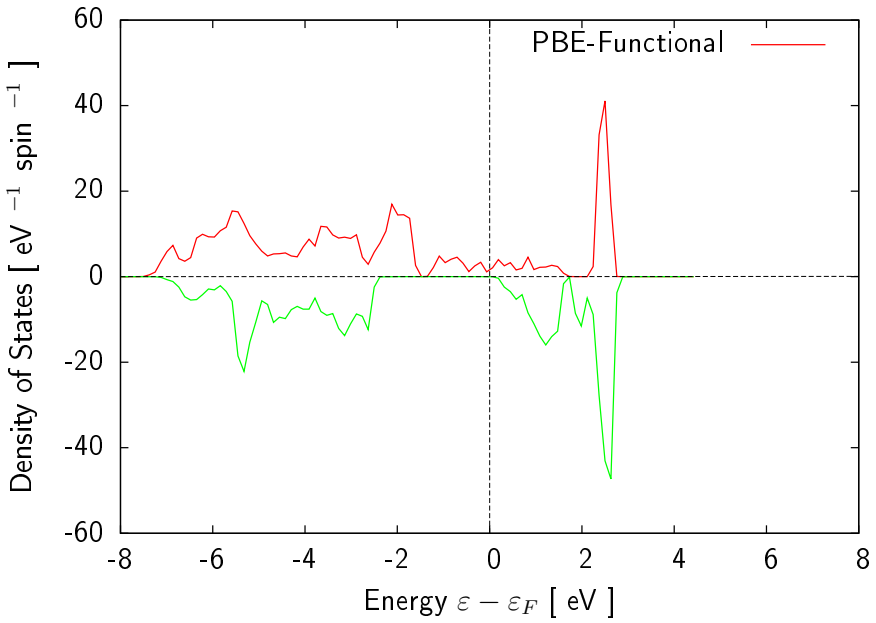

Figure 7.19: Electronic structure of ferromagnetic $LaMnO_3$ using the PBE functional.

structure whis is obtained by applying the PBE functional shows halfmetallic ferromagnetic behaviour. As experimental data suggests the material to be an antiferromagnetic insulator the HSE hybrid functional is applied to the structure in the next step.

Against all odds the calculation using the HSE hybrid functional does not lead to an energy gap. As it is shown in figure 7.20 Mn $3d$ electrons lead to finite electric conductivity at $T = 0$. The magnetic moment per cell occurs to be $15.4\mu_B$. The magnetic moment per Mn atom accounts to $3.9\mu_B$.

If one treats the compound in a pure ionic picture, where the oxygen forms a O^{2-} ion and lanthanum is in a La^{3+} state, Mn is expected to be in a Mn^{3+} state. According to the atomic electron configuration of Mn which is $[Ar]3d^5 4s^2$, the $3d$ metal is supposed to have a magnetic spin moment of $4\mu_B$. This is an indicator that the magnetic moments are strongly localized in this material.

Due to the strong crystal field effects in these ionic compounds the orbital moments are quenched. As a consequence ***LS***-coupling can be neglected and the generalized Bloch theorem can be applied.

7.4.3 PBE+U Calculations, Optimizing the U-Parameter

Although the calculation using the HSE hybrid functional did not lead to an energy gap for the spin up electrons, it has been switched to a description utilizing the PBE+U

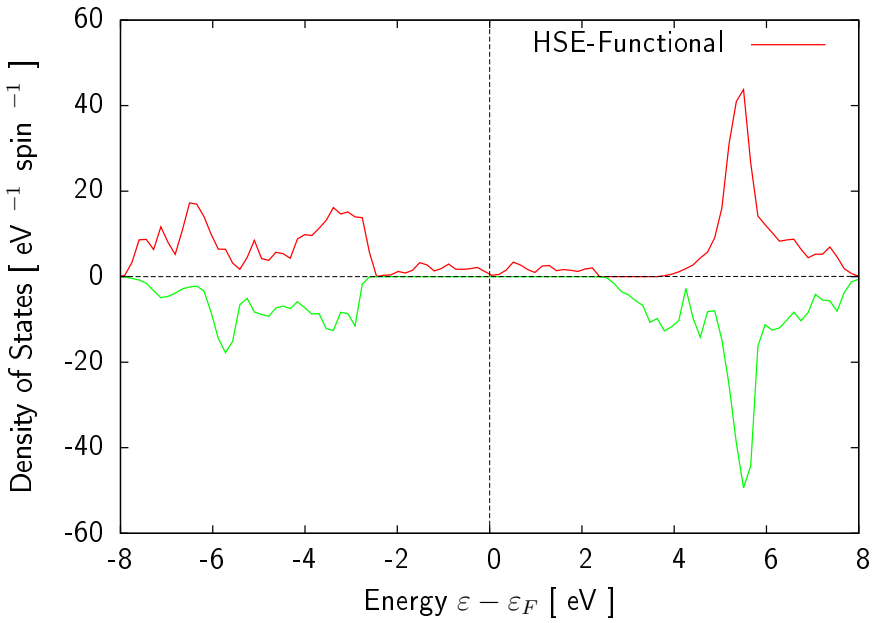

Figure 7.20: Electronic structure of ferromagnetic $LaMnO_3$ using the HSE functional.

approach for the spin spiral calculations. This has been done in order to give a better description of the gap for the spin down electrons. Moreover the shape of the dispersions gained by the spin spiral calculations get smoother if this gap is reproduced best.
Therefore a parameter U that fits to the HSE result best has been searched. This parameter turns out to be $U = 2$ eV. Figure 7.21 shows the total density of states gained by the PBE+U calculation.

7.4.4 PBE+U Spin Spiral Calculations

The spin spiral calculations on $LaMnO_3$ are performed using a mesh of $6 \times 6 \times 6$ k-points. Gaussian smearing is used and SIGMA is set to 0.05. Moreover the conjugate gradient algorithm is applied. The initial energy cutoff is defined as 400 eV, while the ENCUT tag is set to 700 eV. It should be noted that these calculations have been carried out under the use of parallelization. Therefore only the calculated energies are obtained.

Spin Spiral Calculations in [001], [010] and [100] direction

As a first step spin spiral calculations are carried out along the axes of the crystal. Figure 7.22 shows the magnetic structures for different spin spiral wave vectors $\boldsymbol{q}$. As

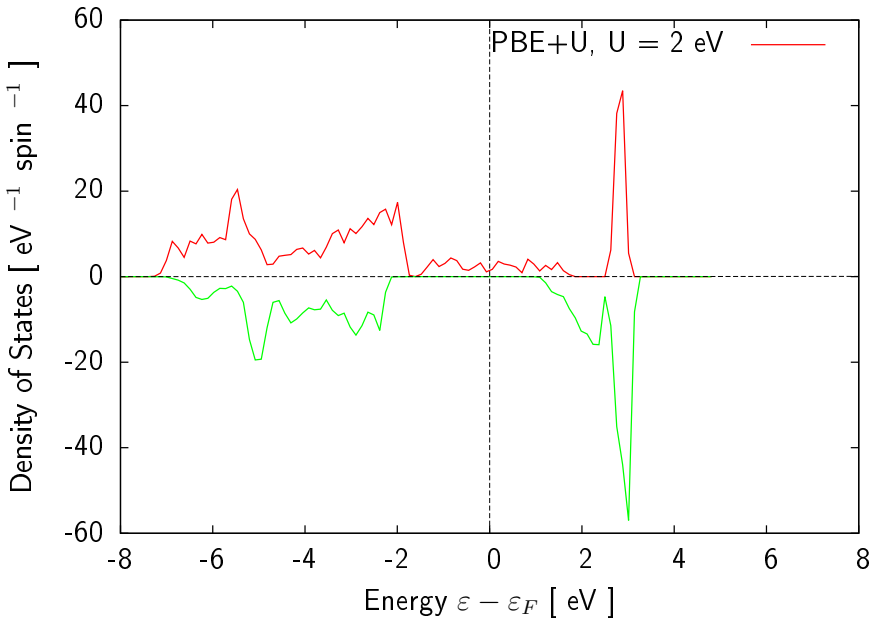

Figure 7.21: Electronic structure of ferromagnetic $LaMnO_3$ obtained by a PBE+U calculation using an onsite correction parameter $U = 2$ eV.

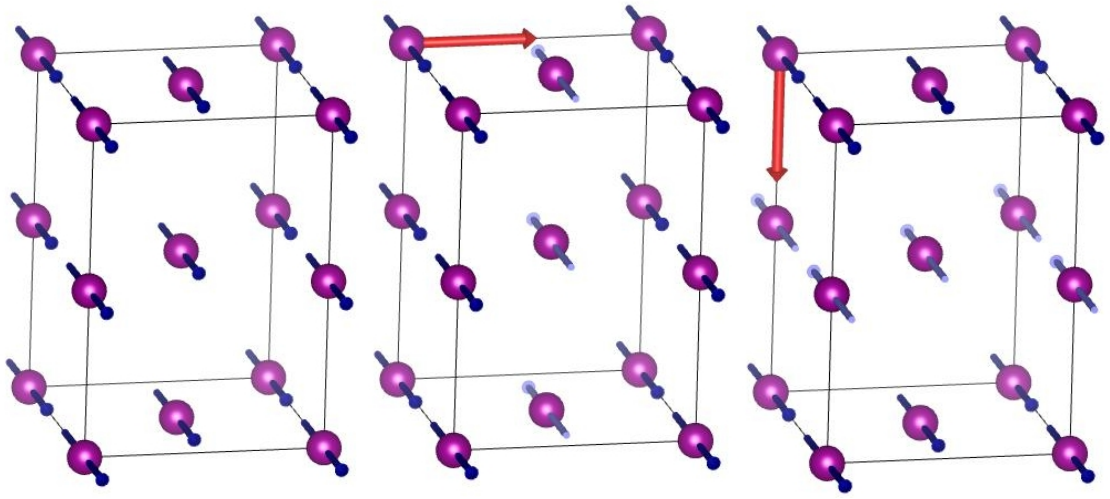

(a) $\boldsymbol{q} = 0$ (b) $\boldsymbol{q} = \boldsymbol{q}_{max}$ (c) $\boldsymbol{q} = \boldsymbol{q}_{max}$

Figure 7.22: Magnetic structure of $LaMnO_3$ for $\boldsymbol{q} = 0$ (a) and $\boldsymbol{q} = \boldsymbol{q}_{max}$ for [001] (b) and [010] direction (c).

one might expect, the wavelengths λ_{max} that lead to the final states illustrated in

figure 7.22 are given as

$$\begin{aligned} [001]: &\quad \lambda_{max} = c, \\ [010]: &\quad \lambda_{max} = b, \\ [100]: &\quad \lambda_{max} = a. \end{aligned}$$

In figure 7.23 a comparsion of the spin spiral dispersions along the different crystal axes can be seen.

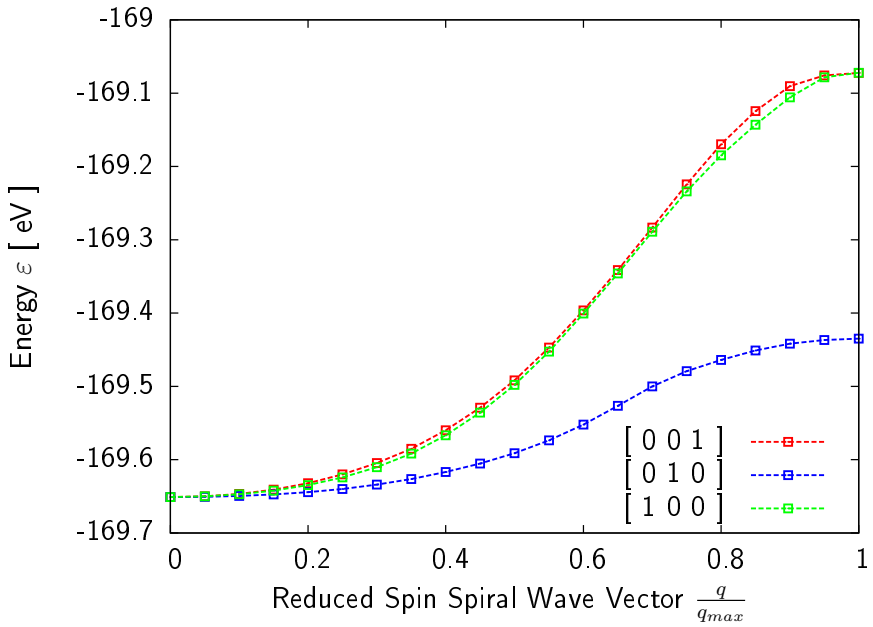

Figure 7.23: Comparison of spin spiral calculations in [001], [010] and [100] direction.

By these dispersions the distortion along the ***b***-axis is verified. The dilation along this axis leads to a weaker interaction of the localized magnetic moments and therefore the energetical response to changes in the magnetic structure is smaller. Moreover the ferromagnetic state occurs to be the magnetic groundstate.

Spin Spiral Calculations in [110], [101] and [011] direction

In this section the results of spin spiral calculations for spin spirals which propagate across the planes built by the lattice vectors are investigated. As an example how the magnetic structure changes throughout such a spin spiral the magnetic structure for $\boldsymbol{q} = 0$ and $\boldsymbol{q} = \boldsymbol{q}_{max}$ are illustrated for a [101] spin spiral calculation in figure 7.24. In this special case the wavelength λ_{max} is given by $\sqrt{a^2 + c^2}$. Figure 7.25 shows a comparison of the different spin spiral calculations. Again the distortion of

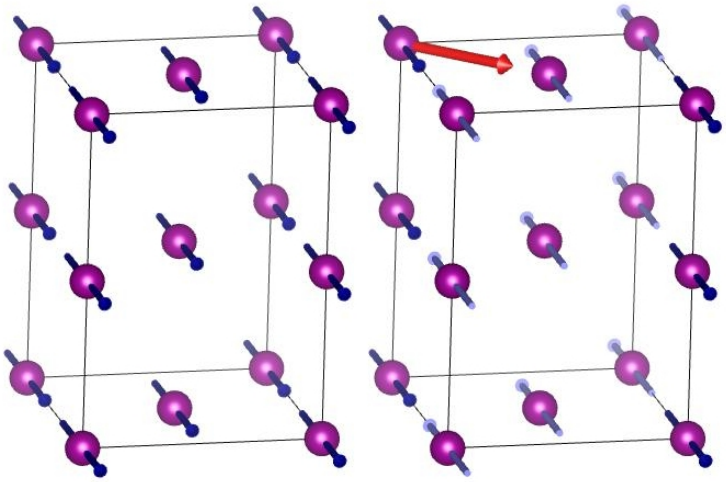

(a) $\boldsymbol{q} = 0$ (b) $\boldsymbol{q} = \boldsymbol{q}_{max}$

Figure 7.24: Magnetic structure of $LaMnO_3$ for a [101] spin spiral.

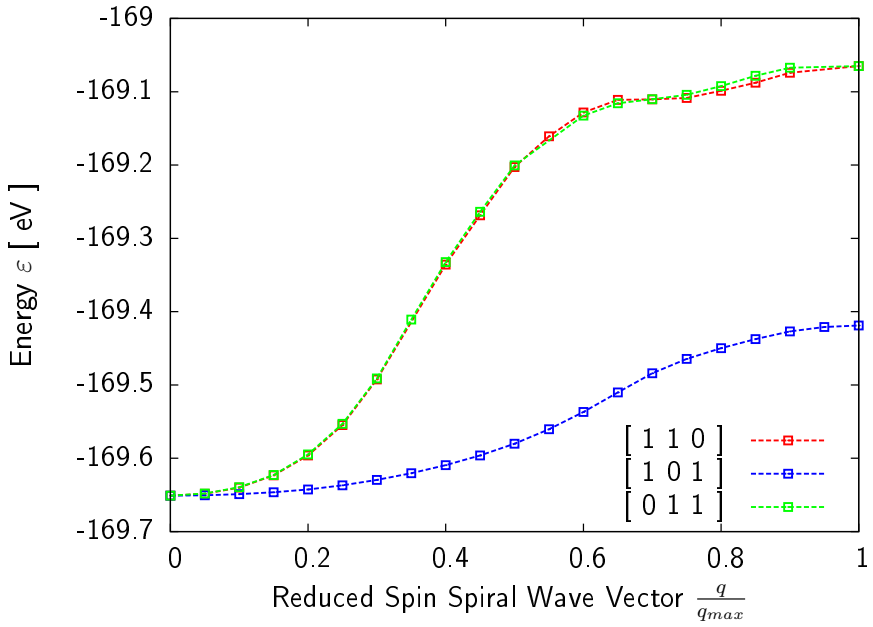

Figure 7.25: Comparison of spin spiral calculations in [110], [101] and [011] direction.

the cell is verified by these dispersions. The magnetic groundstate remains to be the ferromagnetic state for $\boldsymbol{q} = 0$.

Spin Spiral Calculations in [111] direction

In figure 7.26a the dispersion of the spin spiral calculation in the [111] direction is shown. In figure 7.26b a comparsion of spin spirals in different lattice directions is

given.

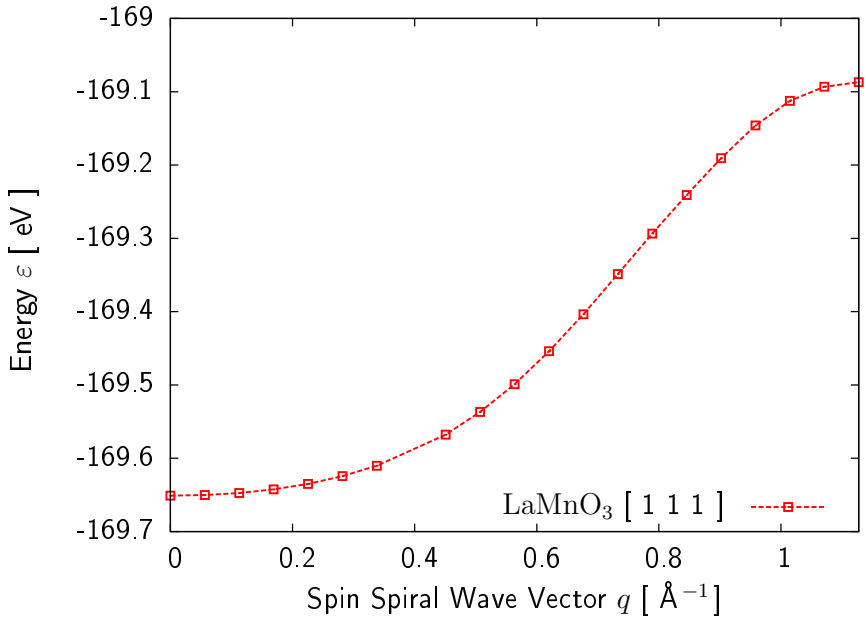

(a) Spin spiral dispersion.

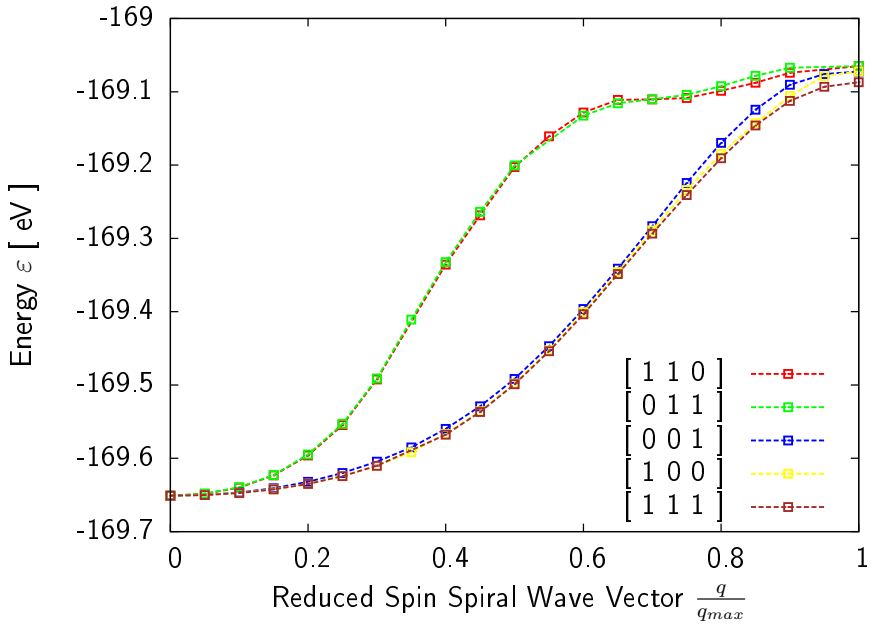

(b) Comparison of different directions.

Figure 7.26: Spin spiral calculations for $LaMnO_3$.

8 Conclusion and Outlook

In the course of this work it has been shown that VASP consistently calculates flat spin spirals as long as the magnetic moments are initialized and the spin spiral wave vector is defined properly. The necessary reciprocal coordinates of the spin spiral wave vector to a given magnetic structure can be calculated using the program that has been introduced in this thesis. Moreover it is recommended to use job files similar to the one that has been presented in this thesis as it saves a lot of work if spin spiral calculations have to be carried out into different directions.
The calculation of conical spin spirals should be avoided. Hybrid functionals cannot be used in the context of spin spiral calculations. As a consequence one has to switch to the L(S)DA+U approach. The information about the magnetic moments is lost as soon as the spin spiral tag is set to be true. In order to gain this information anyway the constrained moment routines have to be switched on and the information about the magnetic moments will be written to the OSZICAR file.
In the last chapter examples for spin spiral calculations have been given. It has been shown how spin stiffness constants, exchange constants and Curie temperatures can be derived from spin spiral calculations.
Although the restriction to flat spin spirals is a drawback if one aims to map the spin spiral dispersions to a Heisenberg model, spin spiral calculations in VASP are quite useful to determine the magnetic groundstate of a material.
As long as the cells do not contain too many atoms and one abstains from calculating densities of states spin spiral calculations can be carried out in a reasonable time via parallelization.
Based on the knowledge gained in the course of this work on spin spiral calculations in VASP it should be possible to calculate the magnetic groundstates of complex magnetic structures in future.

List of Figures

List of Listings

Bibliography

[1] N. G. Nereson, C. E. Olsen, and G. P. Arnold, Phys. Rev. **135** A176, 1964.

[2] G. Venturini et al., J. Alloys Compounds **210** 213, 1994.

[3] J. Hemberger et al. The multiferroic phases of (Eu:Y)MnO3. `http://arxiv.org/cond-mat/0603258`, 2006.

[4] M. Marsmann, J. Hafner. *Broken symmetries in the crystalline and magnetic structures of γ-iron. Phys. Rev. B*, **66** 224409, 2002.

[5] J. Kübler, V. Eyert. *Electronic structure calculations.* In *Electronic and magnetic properties of metals and ceramics* (ed. K.H.J. Buschow). VCH Verlagsgesellschaft, Weinheim, 1992.

[6] N. W. Ashcroft, D. Mermin. *Festkörperphysik.* Oldenbourg, 2007.

[7] P. Mohn. *Magnetism in the Solid State, An Introduction.* Springer, 2$^{\text{nd}}$ printing, 2006.

[8] F. Schwabl. *Quantenmechanik.*, Springer, 6$^{\text{th}}$ printing, 2005.

[9] H. Leeb, M. Faber. *Atom- und Molekülphysik.* Lecture notes, TU Vienna, 2007.

[10] K. Held, L. Leber, S. Danner, A. Girschik. *Quantentheorie II.* Lecture notes, TU Vienna, 2009.

[11] W. Heitler, F. London. *Wechselwirkung neutraler Atome und homöopolare Bindung nach der Quantenmechanik.* Zeitschrift für Physik, **44** 455-472, 1927.

[12] S. Bühler-Paschen, P. Mohn. *Festkörperphysik II.* Lecture notes, TU Vienna, 2009.

[13] P. Hohenberg, W. Kohn. *Inhomogeneous Electron Gas. Phys. Rev.*, **136** B864, 1964.

[14] W. Kohn, L. J. Sham. *Self-Consistent Equations Including Exchange and Correlation Effects. Phys. Rev.*, **140** A1133, 1965.

[15] J. Kübler. *Theory of Itinerant Electron Magnetism.* Oxford University Press, 2000.

[16] U. v. Barth, L. Hedin. *A local exchange-correlation potential for the spin polarized case: I. J. Phys. C: Solid State Phys.* **5**, 1972.

[17] R. Zeller. *Spin-Polarized DFT Calculations and Magnetism.* In *Computational Nanoscience: Do it Yourself!* (ed. J. Grotendorst, S. Blügel, D. Marx). NIC Series **31**, ISBN 3-00-017350-1, pp. 419-445, 2006.

[18] S. Danner. *The Electronic Structure of* $BaMF_4$ *(*$M = Mg, Cr, Mn, Fe, Co, Ni$*) using Hybrid Functionals.* Project Work, TU Vienna, 2011.

[19] J. P. Perdew, K. Burke, M. Ernzerhof. *Erratum: Generalized gradient approximation made simple. Phys. Rev. Lett.*, 78:1396, 1997.

[20] K. Held et al. *The LDA+DMFT Approach to Materials with Strong Electronic Correlations.* In *Quantum Simulations of Complex Many-Body Systems: From Theory to Algorithms.* NIC Series **10**, pp. 175-209, 2002.

[21] S. L. Dudarev et al. *Electron-energy-loss spectra and the structural stability of nickel oxide: An LSDA+U study. Phys. Rev. B*, **57** 3, 1998.

[22] J. Heyd, G. E. Scuseria, M. Ernzerhof. *Hybrid functionals based on a screened coulomb potential. J. Chem. Phys.*, 118(18):8207, 2003.

[23] C. Herring. *Magnetism IV: Exchange Interactions among Itinerant Electrons.* In *Magnetism* (ed. G. T. Rado, H. Suhl), Academic Press, 1966.

[24] `www.vasp.at`

[25] E. A. Owen, G. I. Williams. Journal of Scientific Instruments **31**:49-54, 1954.

[26] R. W. G. Wyckoff.*Hexagonal closed packed, hcp, structure*, 2nd edititon, Interscience Publishers, New York, 1963.

[27] C. Fontana, *Struttura dell'ossido manganoso*, Gazzetta Chimica Italiana, 56:396-397, 1926.

[28] M. Ali, M. Fridman, M. Denayer, P. Nagels. Phys. Status Solidi **28**:193, 1968.

[29] C. G. Shull, W. A. Strauser, E. O. Wollan. *Neutron Diffraction by Paramagnetic and Antiferromagnetic Substances.* Phys. Rev. **83**, 333, 1951.

[30] J. Kübler, A. R. Williams, C. B. Sommers. *Formation and coupling of magnetic moments in Heusler alloys*. Phys. Rev. B, **28**, 4, 1983.

[31] J. B. A. A. Elemans, B. van Laar, K. R. van der Veen, B. O. Loopstra. *The Crystallographic and Magnetic Structures of* $La_{1-x}Ba_xMn_{1-x}Me_xO_3$ *(*Me = Mn *or* Ti*)*. Journal of Solid State Chemistry **3**, 238-242, 1971.

Acknowledgements

At this point I would like to thank my advisor Peter Mohn for his guidance and the great working atmosphere he offers. Moreover I have to express my gratitude to Sepp Redinger for various discussions and his support in software questions.
I give Christoph Gruber props for months of ups and downs in the context of our work on spin spiral calculations as well as the friendship that has developed. I thank Robert Hammerling for various discussions on different physical problems and his support.
I want to thank my collegues Pedro Bedolla-Velàzquez, Andreas Garhofer, Michael Wolloch and Gregor Feldbauer for the great time we spent together.

An dieser Stelle möchte ich mich bei meinen Eltern bedanken, die bei meiner Einschulung vor 19 Jahren wohl nicht gedacht hätten, dass ich nicht zuletzt durch ihre Unterstützung einst eine derartige Arbeit verfassen würde.

Besonderer Dank gilt meiner Freundin Laura die mich durch das Studium begleitet hat und mir in schwierigen Stunden stets zur Seite stand.

This work has been supported by the "Spezialforschungsbereich Vienna Computational Materials Laboratory", SFB ViCoM.

Stefan Danner February, 2012